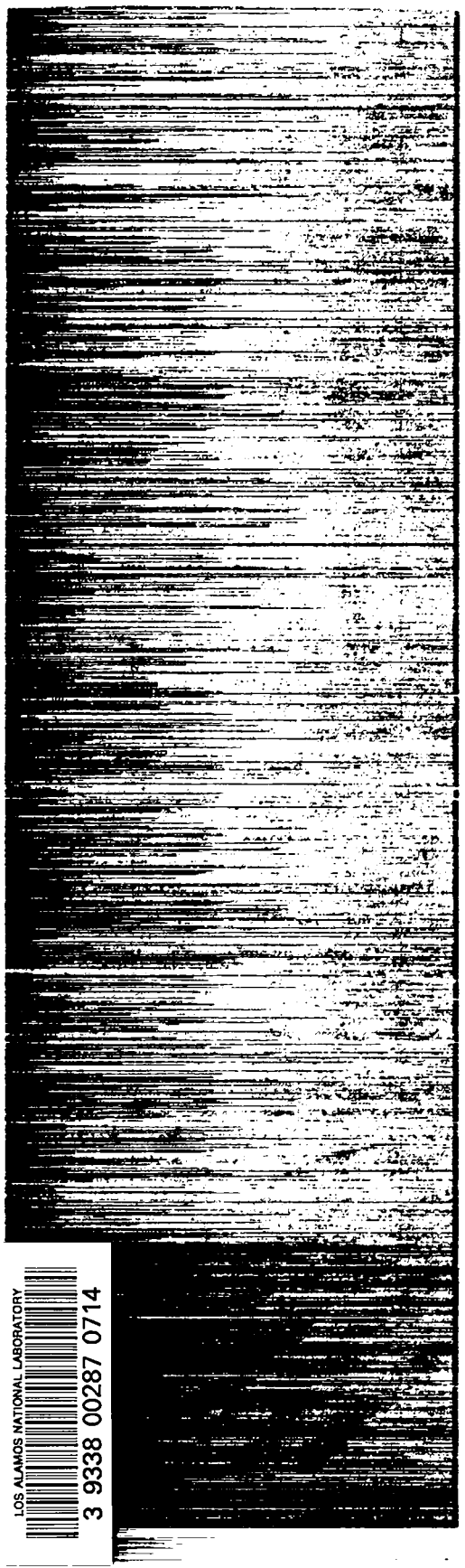

Benchmark Analysis of MCNP™ ENDF/B-VI Iron

Los Alamos
NATIONAL LABORATORY

Los Alamos National Laboratory is operated by the University of California for the United States Department of Energy under contract W-7405-ENG-36.

Edited by Patricia W. Mendius, Group CIC-1
Prepared by Ann Nagy, Group X-6

An Affirmative Action/Equal Opportunity Employer

LA-12884

UC-700
Issued: December 1994

Benchmark Analysis of MCNP™ ENDF/B-VI Iron

John D. Court
John S. Hendricks

Los Alamos
NATIONAL LABORATORY
Los Alamos, New Mexico 87545

BENCHMARK ANALYSIS OF MCNP™ ENDF/B-VI IRON

by

John D. Court and John S. Hendricks

ABSTRACT

The MCNP ENDF/B-VI iron cross-section data was subjected to four benchmark studies as part of the Hiroshima/Nagasaki dose re-evaluation for the National Academy of Science and the Defense Nuclear Agency. The four benchmark studies were:

- **the iron sphere benchmarks from the Lawrence Livermore Pulsed Spheres**
- **the Oak Ridge National Laboratory Fusion Reactor Shielding Benchmark**
- **a 76-cm diameter iron sphere benchmark done at the University of Illinois**
- **the Oak Ridge National Laboratory Benchmark for Neutron Transport through Iron**

MCNP4A was used to model each benchmark and computational results from the ENDF/B-VI iron evaluations were compared to ENDF/B–IV, ENDF/B–V, the MCNP Recommended Data Set (which includes Los Alamos National Laboratory Group T–2 evaluations), and experimental data. The results show that the ENDF/B-VI iron evaluations are as good as, or better than, previous data sets.

MCNP is a trademark of the Regents of the University of California, Los Alamos National Laboratory.

I. INTRODUCTION

The discrepancy between the calculated and in situ measurements of the thermal neutron activation doses at both Hiroshima and Nagasaki have been recognized since the final report describing the 1986 Dose System, DS-86.[1] With the release of the new MCNP4A[2] ENDF/B-VI[3,4] evaluation for iron, it is hoped that this new data will provide better calculational matches to the integral experiments, warranting a new evaluation of the Hiroshima source spectrum.[5]

In this report, we compare four iron neutron data libraries: ENDF/B-V, ENDF/B-VI, the MCNP Recommended Library containing T-2 evaluations, and in some cases, ENDF/B-IV. In general, the MCNP Recommended Library appears best, but the difference between the results from the different libraries is, on the most part, small. The MCNP Recommended iron cross section, also referred to as the T-2 iron evaluation, has MCNP ZAID identification 26000.55c and is a special iron evaluation developed for the Fusion Materials Irradiation Facility (FMIT) in Hanford, Washington.[6] A major improvement to the iron cross-section data set in ENDF/B-VI is the addition of isotopic cross sections. Whereas ENDF/B-IV, ENDF/B-V, and the MCNP Recommended Libraries have an elemental iron cross-section data file, ENDF/B-VI contains the four naturally occurring isotopes of iron. Table I shows the different iron compositions of the four data sets.

MCNP, a general-purpose Monte Carlo N-Particle code, can be used for neutron, photon, electron, or coupled neutron/photon/electron transport and includes the ability to calculate eigenvalues for critical systems. The neutron cross-section data are pointwise continuous, and all reactions given in a particular cross-section evaluation are accounted for. Thermal neutrons are described by both the free gas and S(α,β) models. MCNP4A is the most recent version which includes ENDF/B-VI physics, among other new features. An assortment of variance reduction techniques enables MCNP4A to tackle deep penetration and streaming problems with reduced computational loads. Of particular importance to this study, the ENDF/B-VI iron evaluation includes the new Kalbach-87 formalism (File 6–Law 1–Lang 2), which has coupled energy-angle scattering.

TABLE I. **Iron Data Set Comparisons.**

ENDF/B-IV		ENDF/B-V		MCNP Rec.		ENDF/B-VI	
Zaid	At %	Zaid	At %	Zaid	At %	Zaid	At %
26000.11c	100	26000.50c	100	26000.55c	100	26054.60c	5.90
						26056.60c	91.72
						26057.60c	2.10
						26058.60c	0.28

The four benchmark experiments chosen for this study consisted of an assortment of geometries composed of iron or high-carbon steel. Several source spectra were also used to adequately cover the full neutron energy range. The Lawrence Livermore Pulsed Sphere experiments[7] included two iron spheres of 0.9 and 4.8 mean free paths, containing a 14-MeV pulsed D-T neutron source in the center. The second benchmark calculation was the Oak Ridge National Laboratory Fusion Shielding Benchmark,[8,9] consisting of a monodirectional 14 MeV D-T neutron source incident on various laminated slab shields composed of SS-304 and borated polyethylene. The third benchmark model was a 76-cm diameter iron sphere[10,11] containing a 15.3-cm diameter void with D-T and ^{252}Cf spectra for separate neutron source calculations. We were unable to locate experimental data for this benchmark, but all four iron libraries were compared. The last benchmark was an Oak Ridge fission benchmark through iron and steel.[12] A beam of neutrons from a reactor was incident on four iron slabs of increasing thickness, and three different Bonner Ball measurements were taken at three different angles. Although experimental data for this benchmark was available, our interpretation of the problem specification is apparently inadequate, so only the comparisons between the four libraries are meaningful.

II. LAWRENCE LIVERMORE PULSED SPHERES

A. Experimental Setup

In the 1960's, the Lawrence Livermore Laboratory instituted an extensive pulsed sphere program to measure, with relatively good resolution, the neutron spectra from spherical targets bombarded with 14 MeV neutrons in order to provide benchmark data for neutron transport codes and nuclear cross sections.[13] Two of the three iron spheres were modeled using MCNP. Figure 1 shows the geometry of the iron spheres.[13] The opening into the sphere is to accommodate a low mass target assembly containing a thin tritiated titanium disk, which utilized the T(d,n)^{4}He reaction when bombarded with a 400 keV D^+ ion beam. The result was a nearly isotropic source of 14 MeV neutrons.

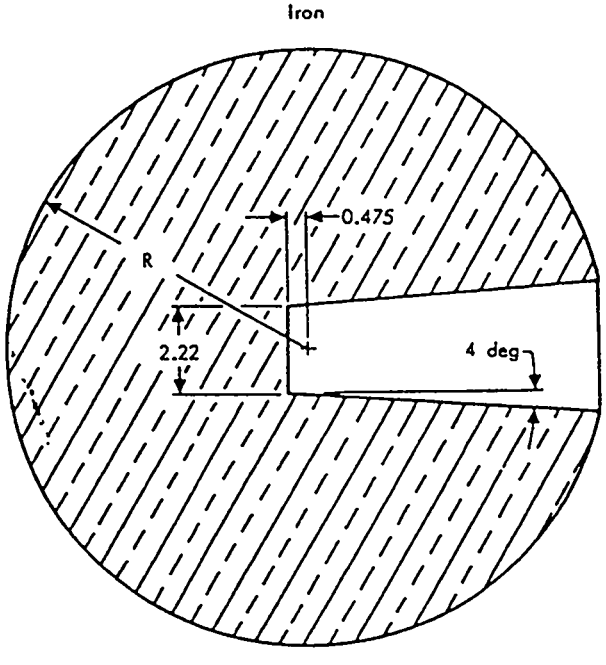

λ	R
0.9	4.46
4.8	22.40

All dimensions in centimeters

Fig. 1. Geometry of the spherical iron targets.

The 0.9 mfp sphere was fabricated from Armco Ingot Iron. The 4.8 mfp sphere was fabricated from ASTM-A7 iron. The elemental composition of the MCNP model is shown in Table II. Further details of the problem setup can be found in the MCNP input deck found in Table A.1 in the appendix.

B. Results and Discussion

The time of flight spectrum of the neutrons leaving each sphere was measured. The results were integrated in two different time bins. The time bins were chosen to correspond roughly to the amount of time that a particle of the given energy would take to travel from the center of the sphere to the detector without collision. The neutron detectors were not located at the same distance from the center of the sphere for each experiment. The comparisons between ENDF/B-V, MCNP Recommended, and ENDF/B-VI are contained in Table III. Figures 2 through 5 show the measured spectra plotted against the calculated spectra for the 0.9 mfp iron sphere. Figures 6 through 9 are the spectra for the 4.8 mfp iron sphere.

In all cases, ENDF/B-VI appears somewhat better than ENDF/B-V, but not quite as good as the MCNP Recommended Library, which is a modified ENDF/B-V set with a LANL group T-2 evaluation, 26000.55c.

TABLE II. **Elemental Composition of the Iron Spheres.**

Element	Atom %
Fe	97.0
C	1.2
Mn	1.0
P	0.7
S	0.1
ρ	7.85 g/cm^3

TABLE III. **Ratio of Calculated to Experimental Values for the Livermore Pulsed Spheres.**

Radius (mfp)	Data Set	12-16 MeV	2-16 MeV
0.9	ENDF/B-V	0.989	0.984
	MCNP Rec.	1.001	1.007
	ENDF/B-VI	0.999	1.006
4.8	ENDF/B-V	0.866	0.834
	MCNP Rec.	0.934	0.946
	ENDF/B-VI	0.903	0.952

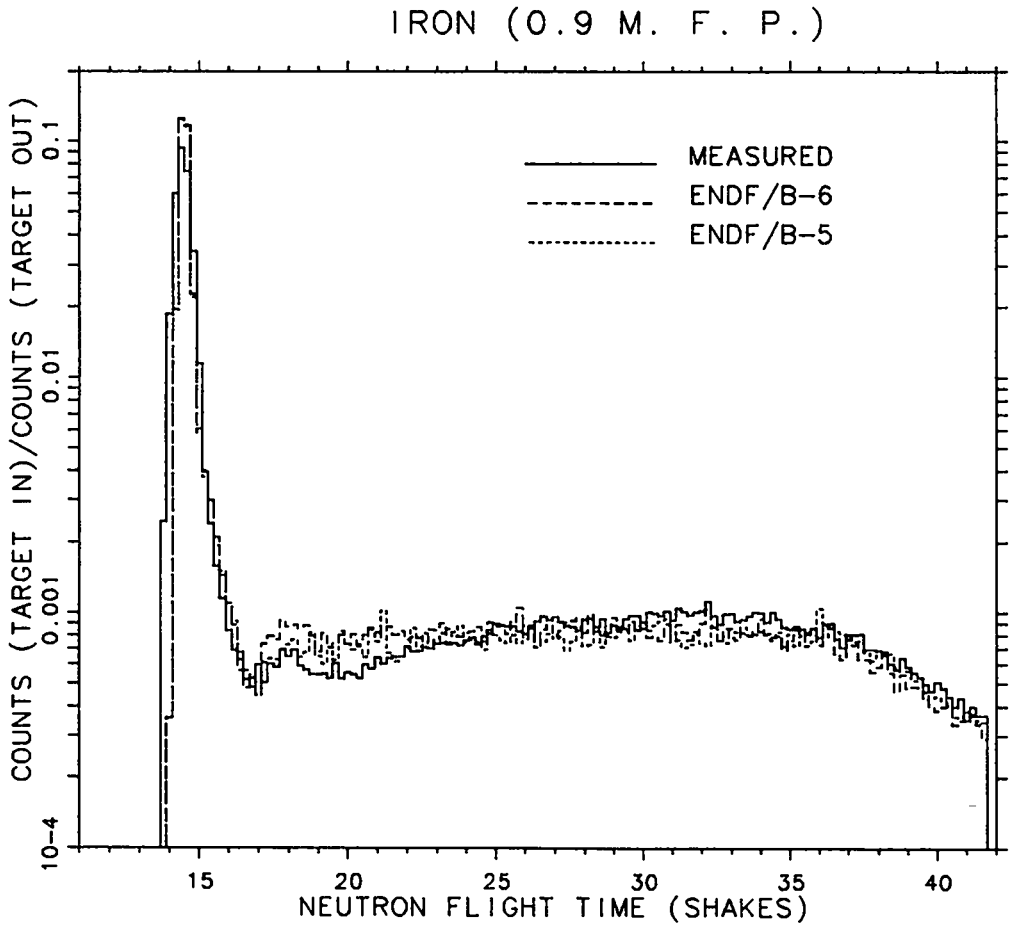

Fig. 2. Plot of experimental and calculated count rates as a function of time for an iron sphere with 0.9 mean free path radius. The detector was located 766.0 cm from the center of the sphere at 30 degrees with respect to the deuteron beam. (1 shake = 10 ns)

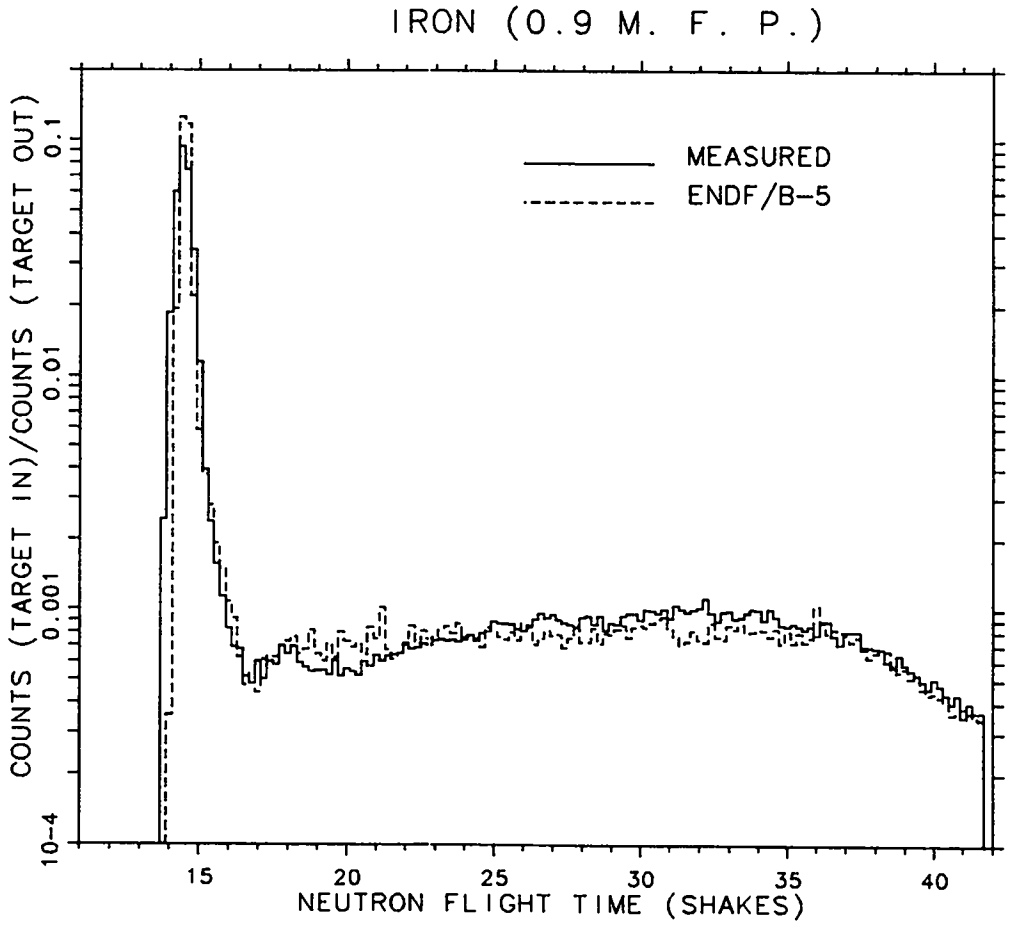

Fig. 3. Plot of experimental and ENDF/B-V calculated count rates for the iron sphere of 0.9 mean free path radius.

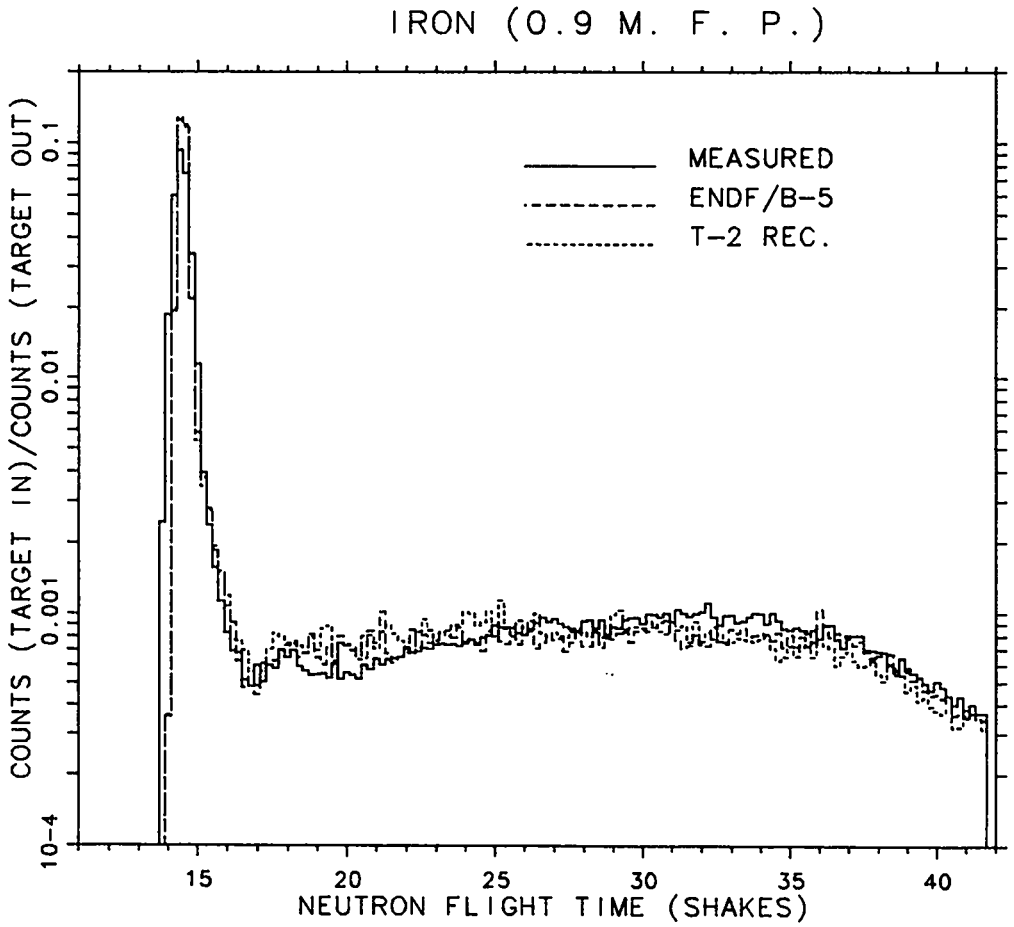

Fig. 4. Plot of experimental, ENDF/B-V, and MCNP Recommended calculated rates for the iron sphere with 0.9 mean free path radius.

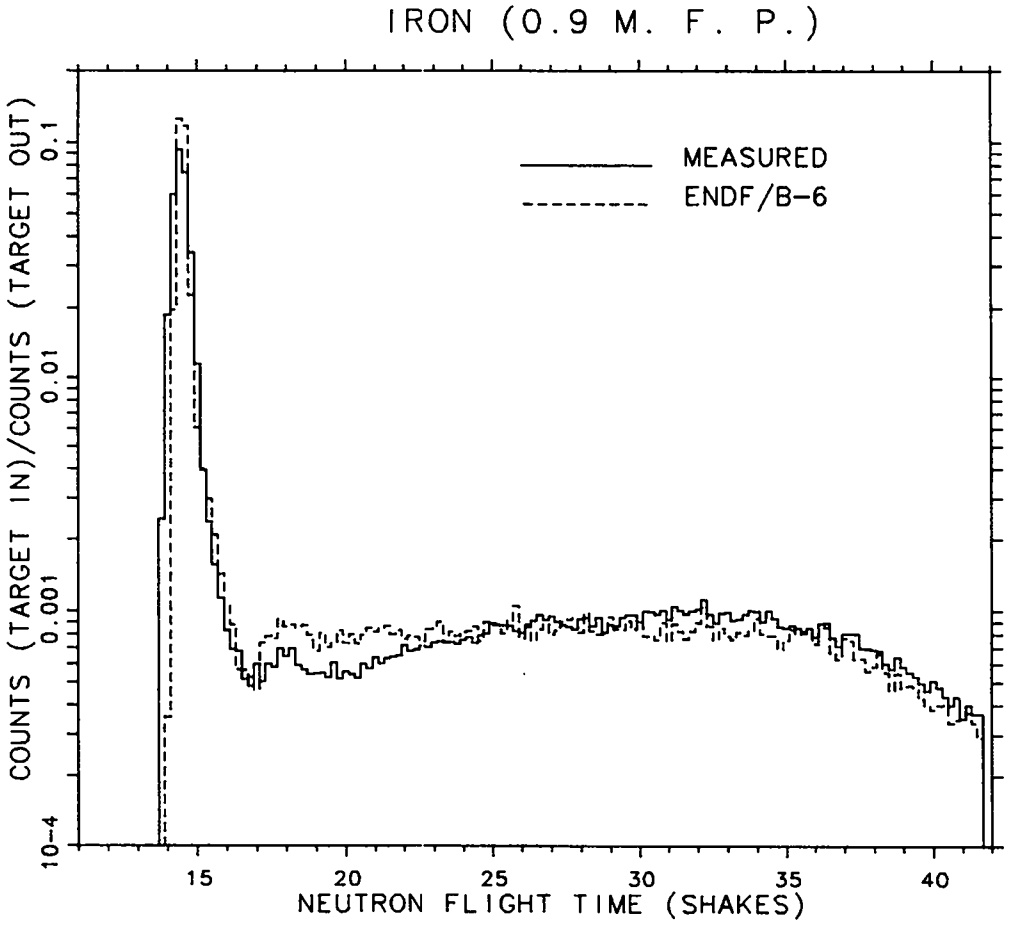

Fig. 5. Plot of experimental and ENDF/B-VI calculated count rates for the iron sphere of 0.9 mean free path radius.

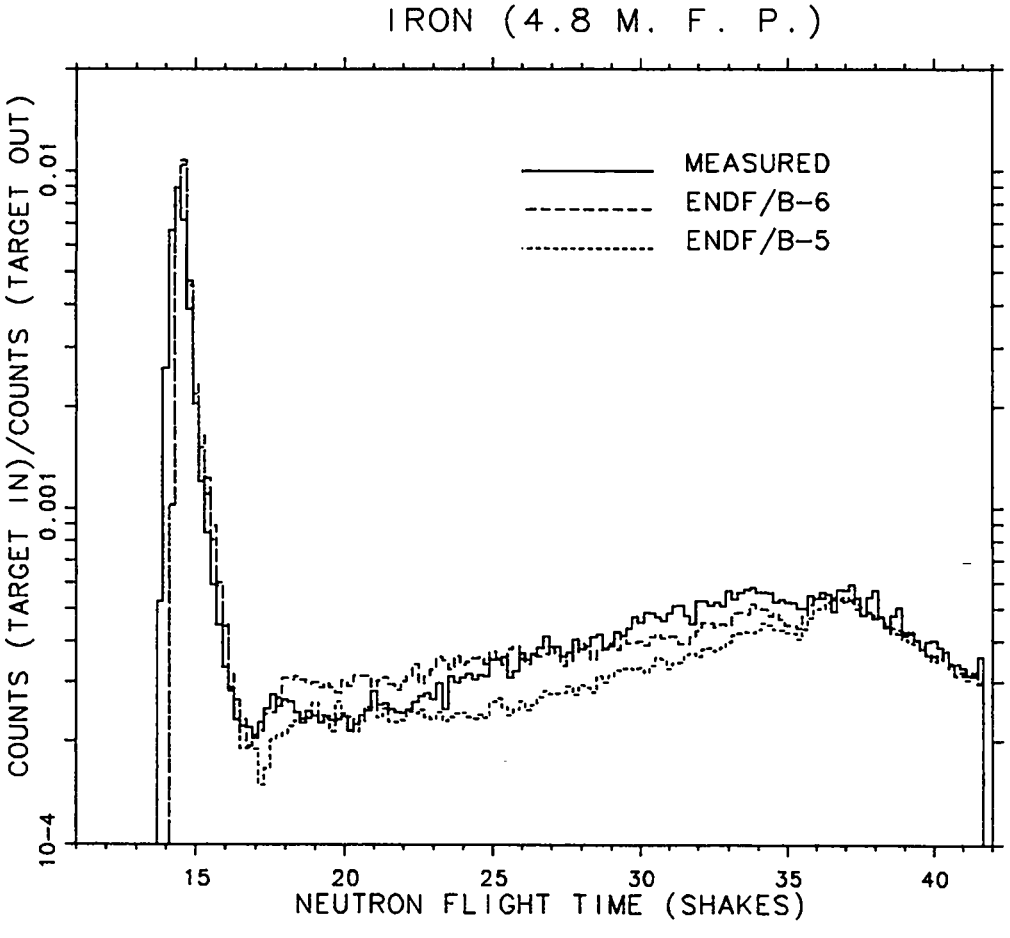

Fig. 6. Plot of experimental and calculated count rates as a function of time for an iron sphere with 4.8 mean free path radius. The detector was located 766.0 cm from the center of the sphere at 30 degrees with respect to the deuteron beam. (1 shake = 10 ns)

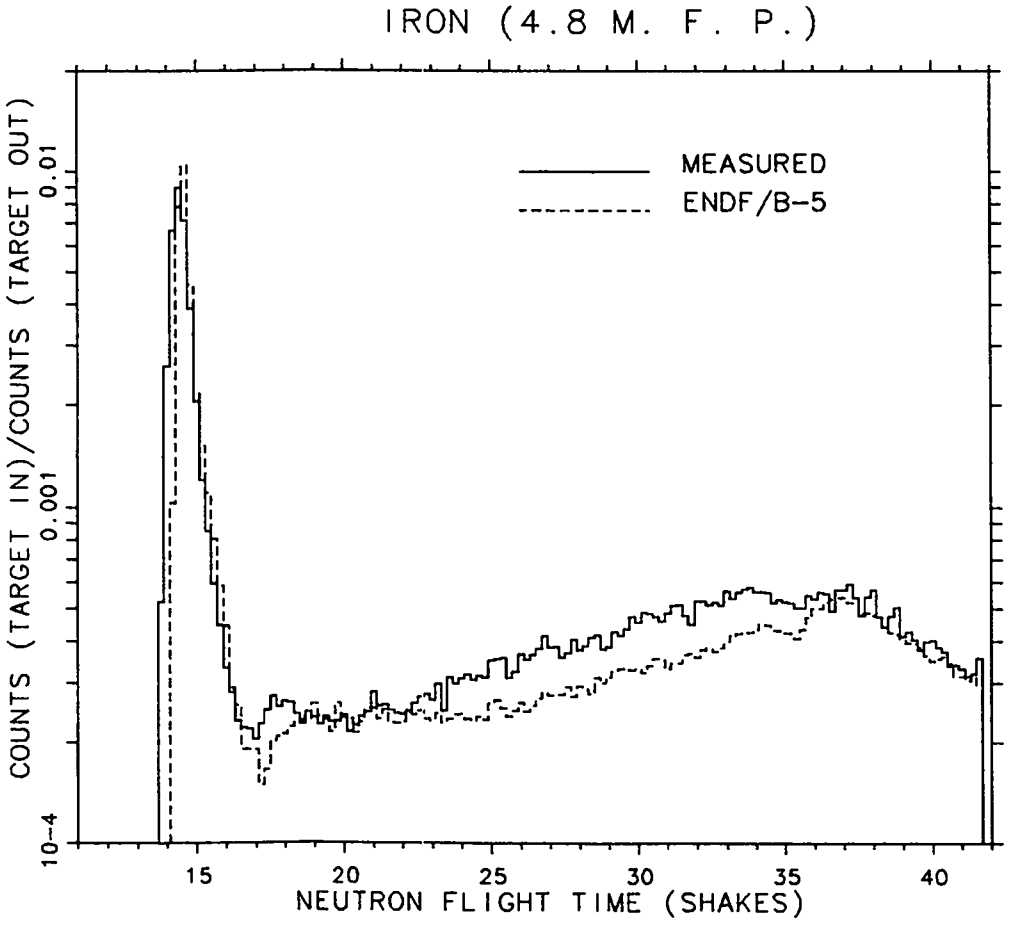

Fig. 7. Plot of experimental and ENDF/B-V calculated count rates for the iron sphere of 4.8 mean free path radius.

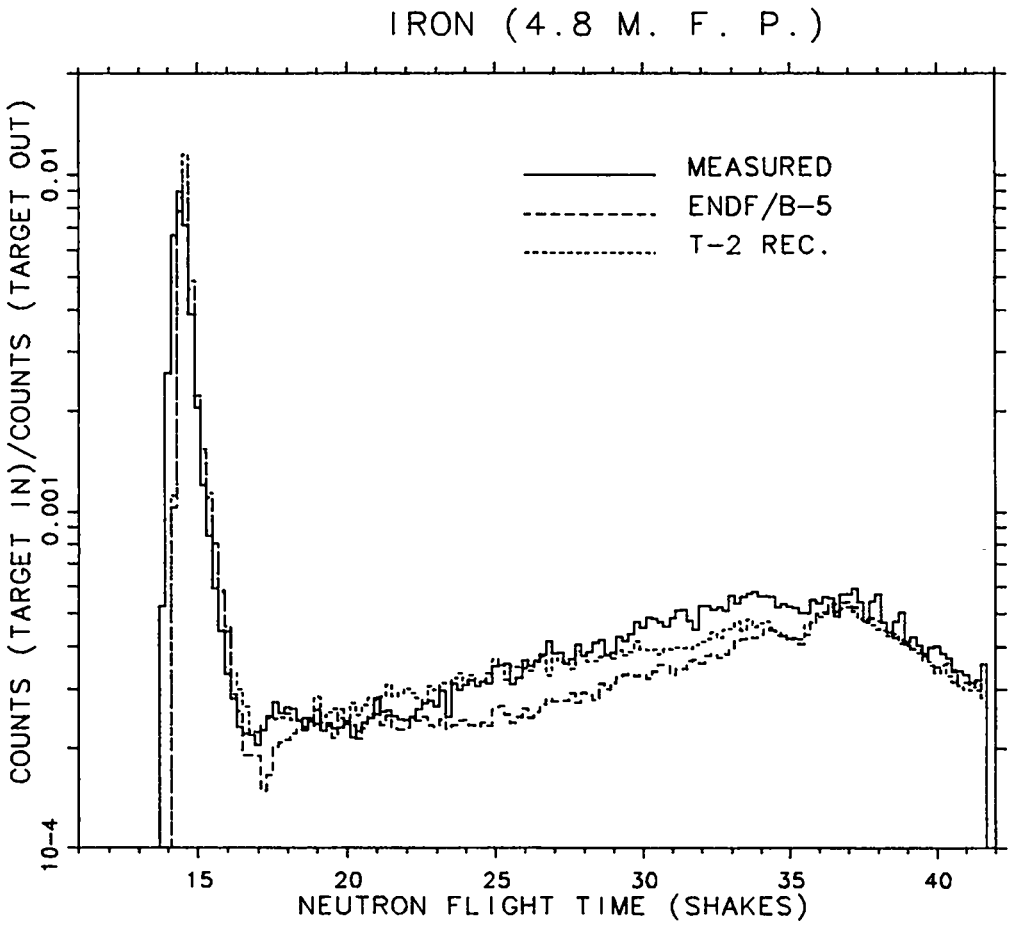

Fig. 8. Plot of experimental, ENDF/B-V, and MCNP Recommended calculated rates for the iron sphere with 4.8 mean free path radius.

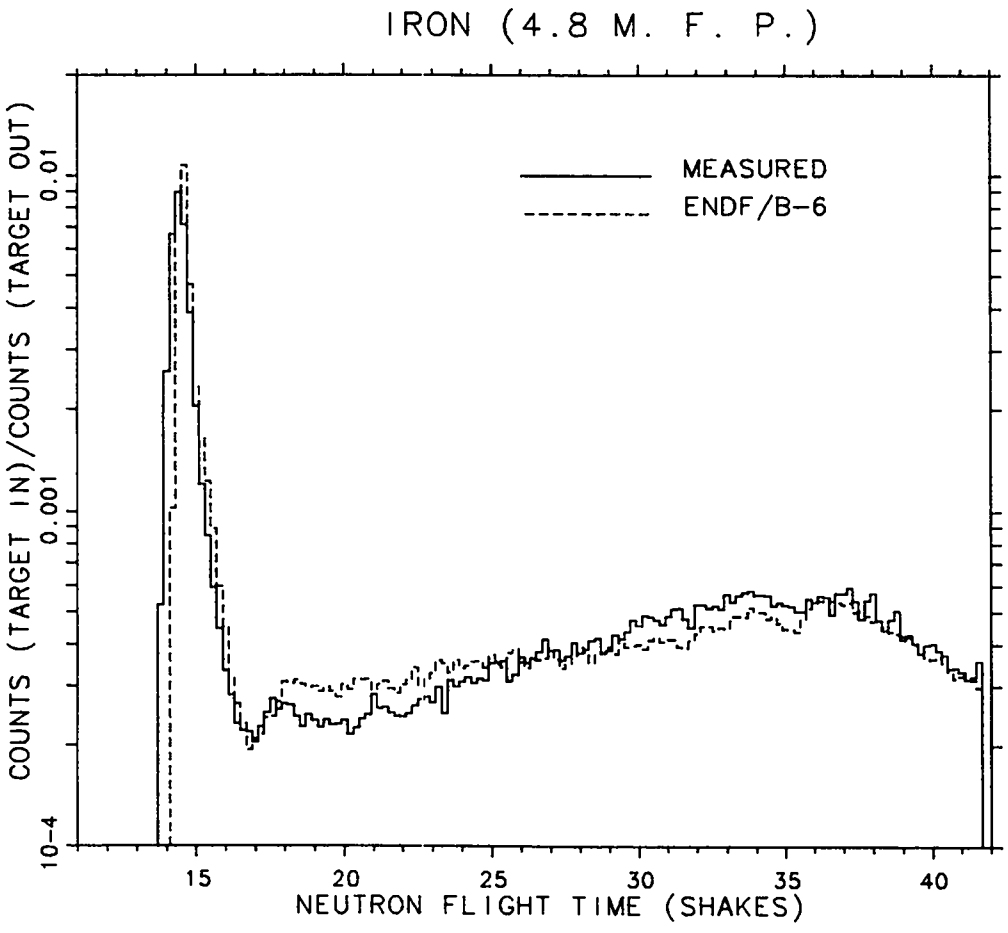

Fig. 9. Plot of experimental and ENDF/B-VI calculated count rates for the iron sphere of 4.8 mean free path radius.

III. FUSION REACTOR SHIELDING BENCHMARK

A. Experimental Setup

A benchmark experiment was conducted at Oak Ridge National Laboratory in 1980 in order to simulate the radiation exposure that would be present at the first wall of a fusion reactor. Again, the T(d,n)^{4}He reaction was utilized by bombarding a tritiated target with a deuteron beam, resulting in a nearly-isotropic source of 14 MeV neutrons. The tritiated titanium target was imbedded inside an iron cavity liner which served as a spectrum modifier and made the neutron spectrum incident on the experimental shield configuration similar to the spectrum incident on the first wall of a fusion reactor. Figure 10 is a sketch of the experimental layout.[8]

The 14 MeV neutrons passed through several different configurations of laminated slabs composed of SS-304 and borated polyethylene. Table IV shows the shielding configuration compositions. The composition of the materials used in the benchmark is shown in Table V. The neutron and photon energy spectra were measured by detectors placed both on- and off-axis beyond the laminated shielding. An example MCNP input deck for this problem can be found in Table A.2 in the appendix.

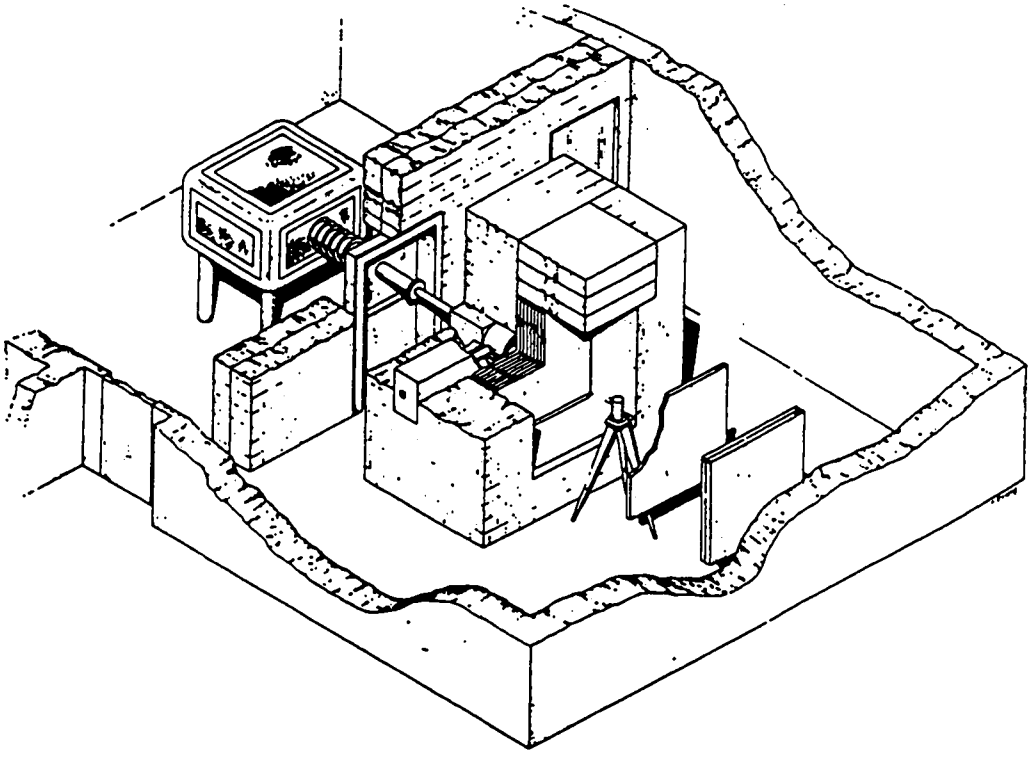

Fig. 10. Fusion Shielding Benchmark Experimental Layout.

TABLE IV. **Composition and Thickness of SS-304 and Borated Polyethylene Slabs**

Configuration	Composition						Total Slab Thickness (cm)
	SS-304[a]	SS-304	BP[b]	SS-304	BP	SS-304	
	Slab Thickness (cm)						
1	0						0
2	15.24						15.24
3	30.48						30.48
4	30.48	5.08	5.08				40.64
5	30.48	5.08	5.08	5.08			45.72
6	30.48	5.08	5.08	5.08	5.08		50.80
7	30.49	5.08	5.08	5.08	5.08	5.08	55.88

[a]Stainless Steel Type 304 [b]Borated Polyethylene

TABLE V. **Fusion Shielding Benchmark Material Composition.**

Number Density (atom/cm Barn)						
Element	Concrete	Air	Iron	SS-304	BP[a]	LP[b]
^{1}H	7.86×10^{-3}				7.13×10^{-2}	5.926×10^{-2}
^{10}B					4.87×10^{-4}	
^{11}B					1.97×10^{-3}	
C					3.41×10^{-2}	3.338×10^{-2}
^{14}N		3.64×10^{-5}				
^{16}O	4.39×10^{-2}	9.74×10^{-6}			3.64×10^{-3}	1.125×10^{-2}
^{23}Na	1.05×10^{-3}					
Mg	1.40×10^{-4}					
^{27}Al	2.39×10^{-3}					
Si	1.58×10^{-2}					
K	6.90×10^{-4}					
Ca	2.92×10^{-3}					
Cr				1.77×10^{-2}		
^{55}Mn				1.77×10^{-3}		
Fe	3.10×10^{-4}		8.48×10^{-2}	6.02×10^{-2}		
Ni				7.83×10^{-3}		
^{6}Li						5.565×10^{-4}
^{7}Li						6.944×10^{-3}

[a]Borated Polyethylene [b]Lithiated Paraffin

B. Results and Discussion

Four configurations were modeled in MCNP, configurations 1, 2, 3, and 7. Table VI gives the positions of the detectors relative to the neutron source in the MCNP reference coordinate system for the four configurations.[14] The detector coordinates in the MCNP input files are relative to the reference coordinate system. Only neutron flux tallies have been reported in this publication.

The calculated results were integrated over five different energy ranges and compared to the experimental confidence levels. These results, presented in Table VII, indicate that the integration is above the upper limit with a value greater than one, below the lower limit by a value less than one, and within the experimental limits by a value equal to one.

In these integral results, the recommended MCNP data library and ENDF/B-VI returned much the same results, which are better than the ENDF/B-V results.

Experimental data was taken in the form of experimental upper and experimental lower bounds. Each configuration and detector position was modeled in MCNP and plotted against the experimental upper and lower bounds in Figures 11 through 34.

Again, ENDF/B-VI and the MCNP Recommended Library results appear better than the ENDF/B-V results, especially for Configuration 7.

TABLE VI. **MCNP Detector Tally Positions**

Shielding Configuration	Coordinates (cm)
1	on axis: (0, 154.5, 0)
2	on axis: (0, 154.5, 0)
3	on axis: (0, 154.5, 0) off axis: (-100, 159.2, 0)
7	on axis: (0, 154.5,0) off axis: (46, 154.5, 0)

TABLE VII. **Fusion Reactor Shielding Integrated Energy Group Comparisons**

Configuration	Detector Position	Energy Group (MeV)	ENDF/B-V	T-2 Rec.	ENDF/B-VI
1	On	0–2	1.249	1.157	1.164
		2–5	1.140	1.143	1.140
		5–10	1.000	1.000	1.000
		10–13	0.934	0.955	1.109
		> 13	1.116	1.100	0.949
2	On	0–2	1.003	0.997	0.982
		2–5	0.981	1.000	1.012
		5–10	0.865	1.000	1.000
		10–13	1.000	1.056	1.054
		> 13	1.035	1.085	1.043
3	On	0–2	0.979	1.000	0.970
		2–5	0.875	0.999	1.000
		5–10	0.770	0.970	1.000
		10–13	0.949	1.000	1.000
		> 13	0.953	1.039	0.972
	Off	0–2	1.258	1.301	1.255
		2–5	1.000	1.145	1.127
		5–10	0.869	1.000	1.018
		10–13	0.910	1.000	1.000
		> 13	1.170	1.356	1.217
7	On	0–2	0.798	0.901	0.842
		2–5	0.823	0.997	0.961
		5–10	0.848	1.000	1.000
		10–13	0.910	1.000	1.000
		> 13	1.000	1.097	1.038
	Off	0–2	0.736	0.822	0.793
		2–5	0.757	0.948	0.921
		5–10	0.765	0.951	1.000
		10–13	0.870	1.000	1.000
		> 13	0.907	1.016	0.977

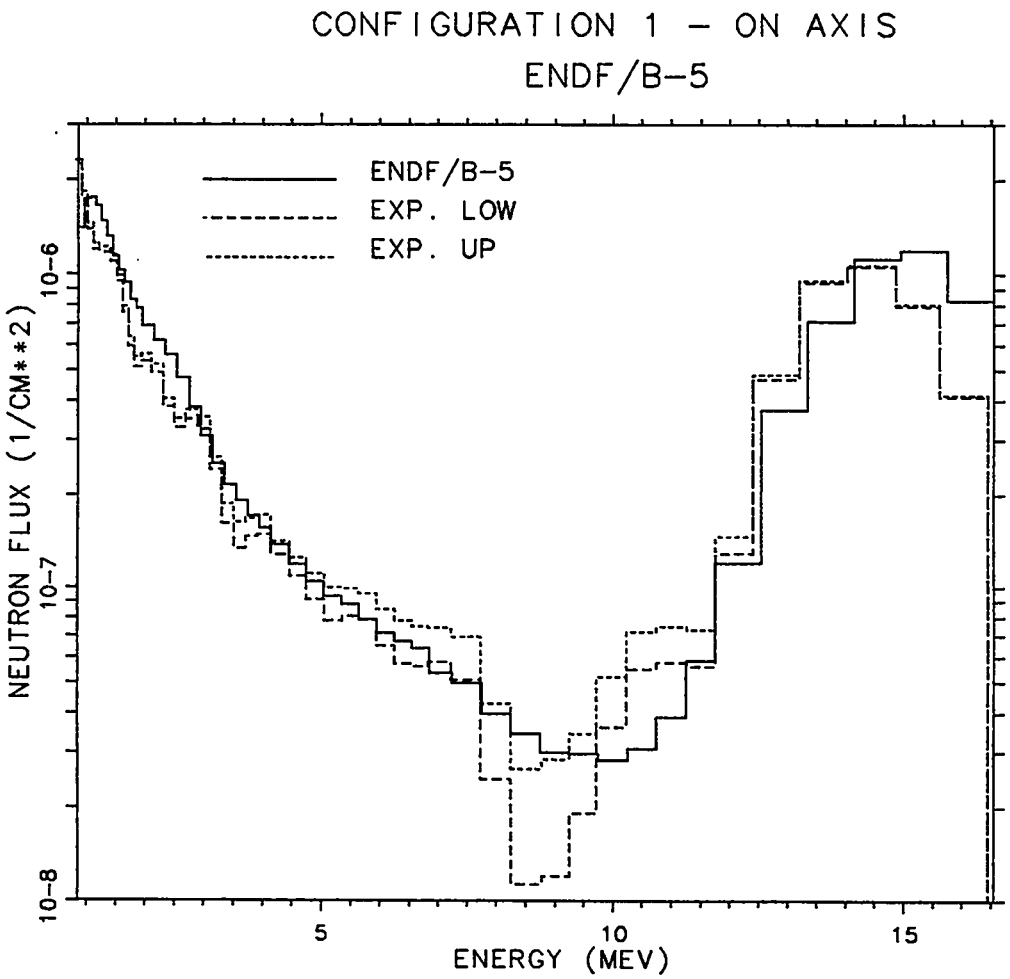

Fig. 11. Plot of ENDF/B-V calculated and experimental upper and lower confidence levels for configuration 1 with the detector on axis.

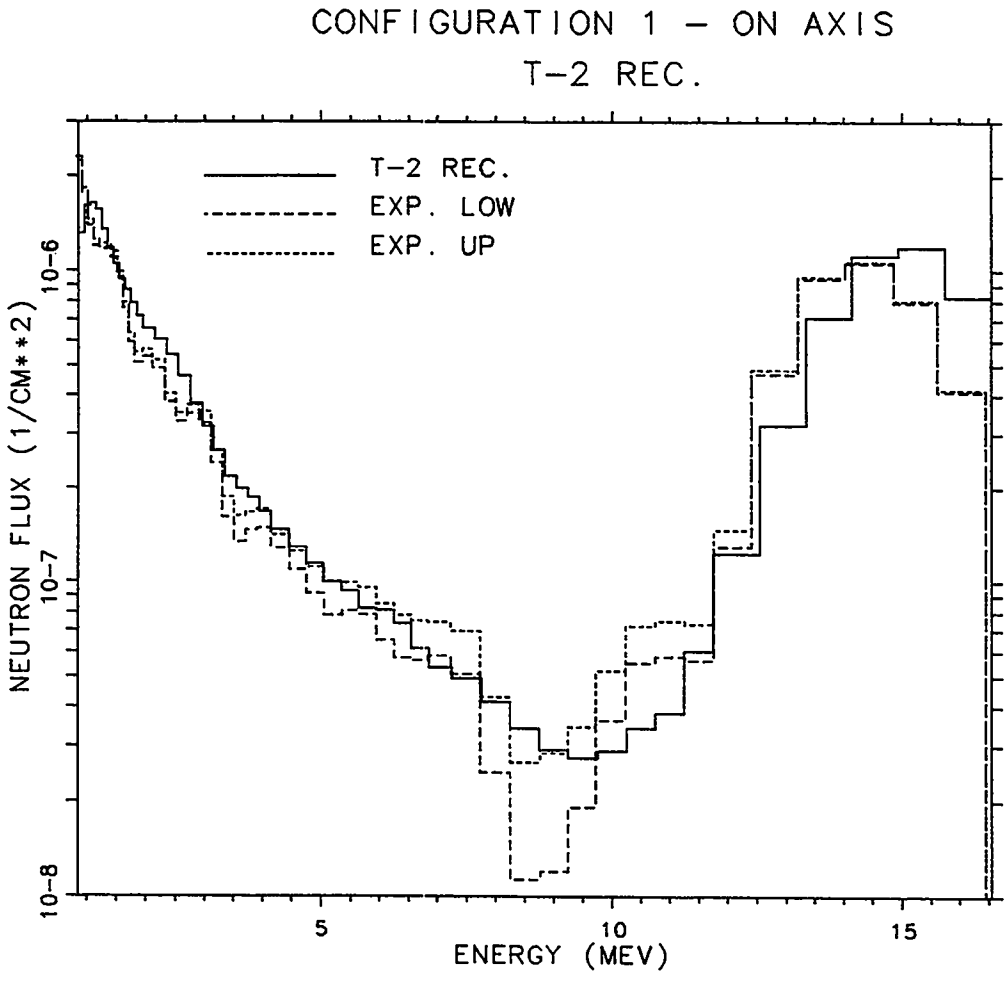

Fig. 12. Plot of MCNP Recommended calculated and experimental upper and lower confidence levels for configuration 1 with the detector on axis.

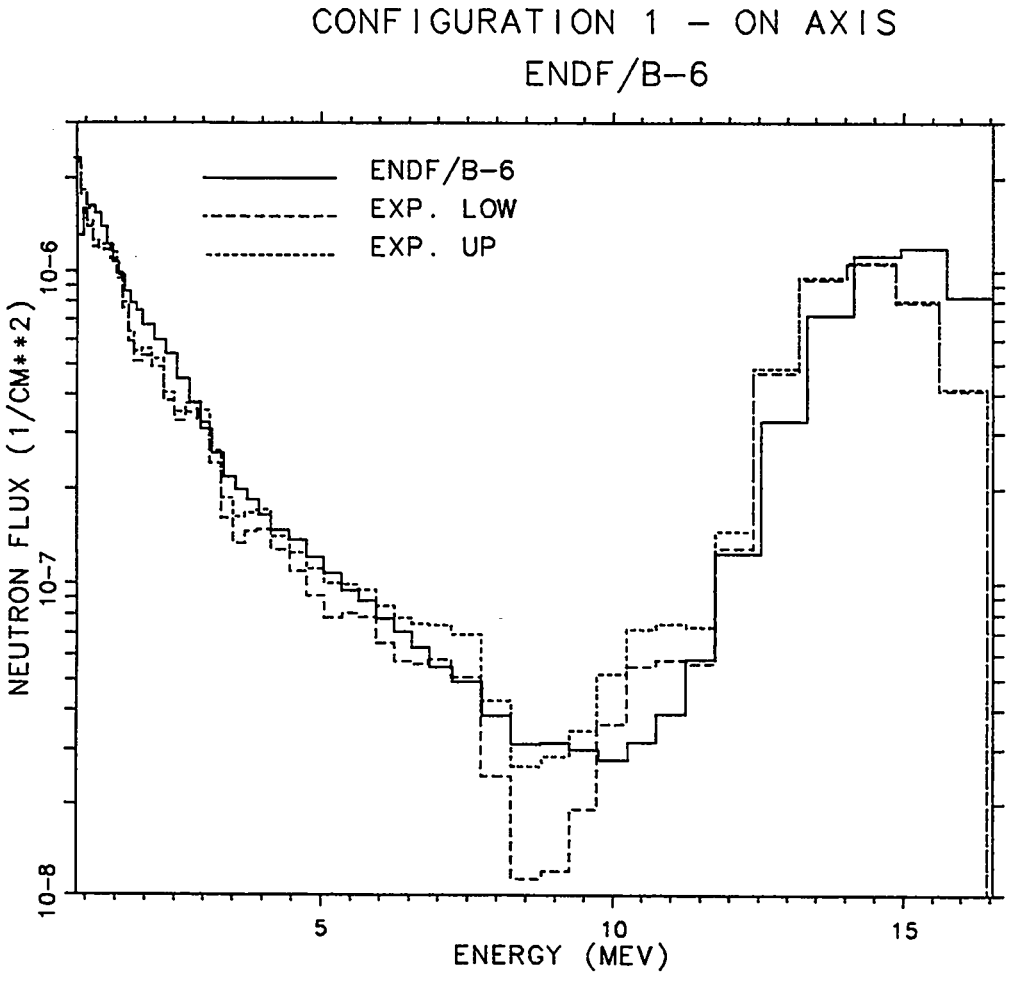

Fig. 13. Plot of ENDF/B-VI calculated and experimental upper and lower confidence levels for configuration 1 with the detector on axis.

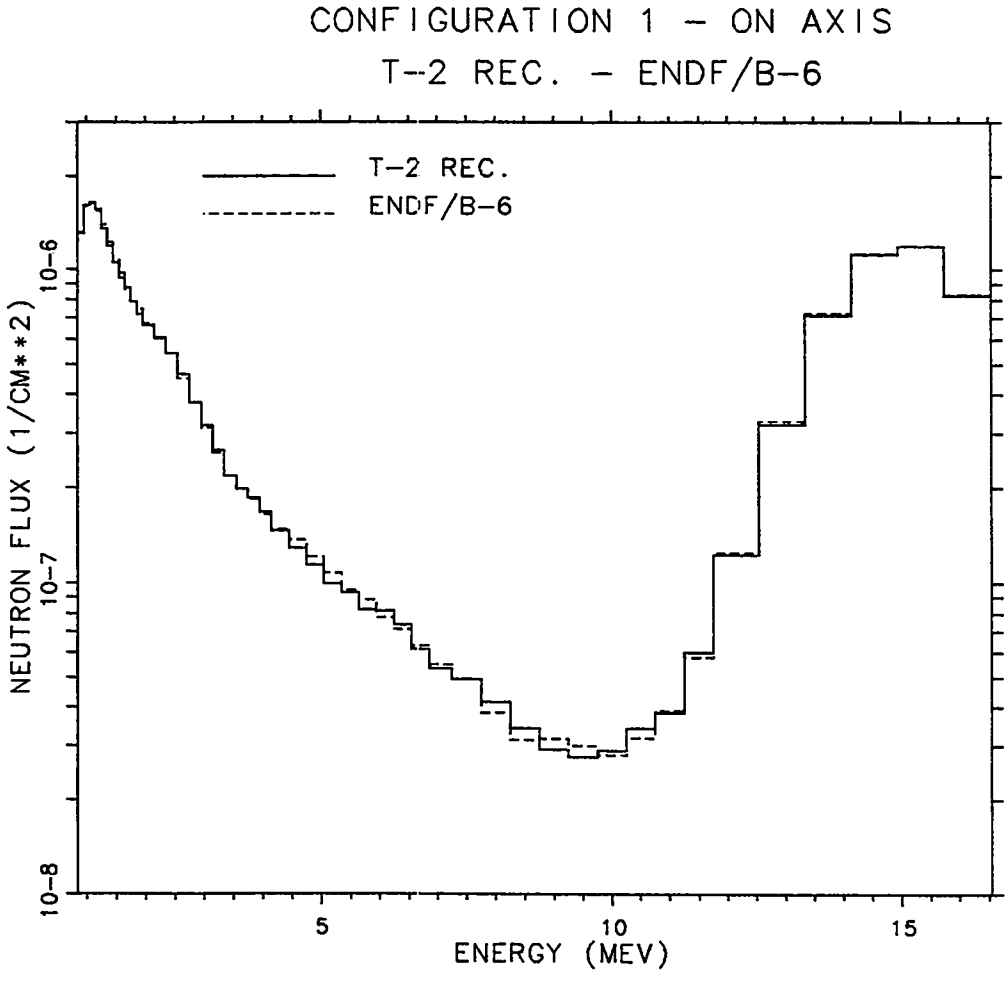

Fig. 14. Plot of MCNP Recommended and ENDF/B-VI calculated for configuration 1 with the detector on axis.

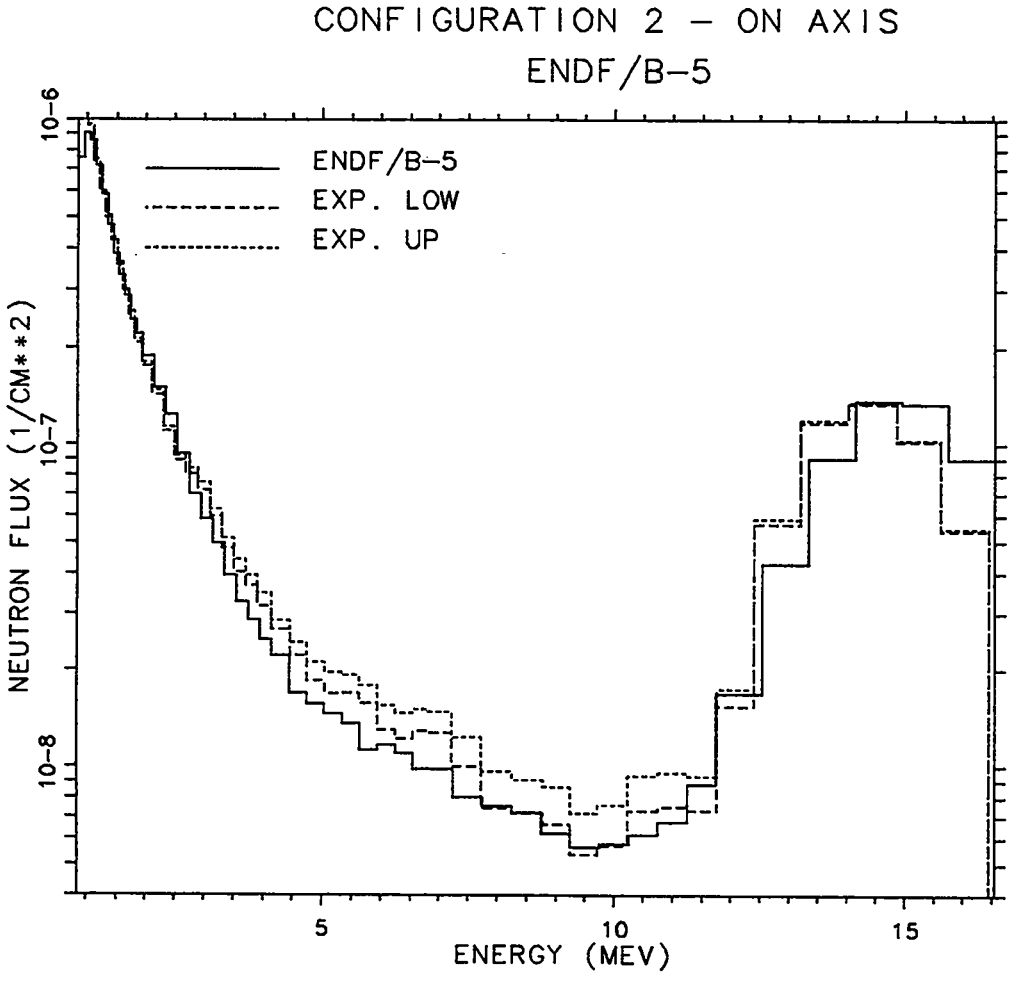

Fig. 15. Plot of ENDF/B-V calculated and experimental upper and lower confidence levels for configuration 2 with the detector on axis.

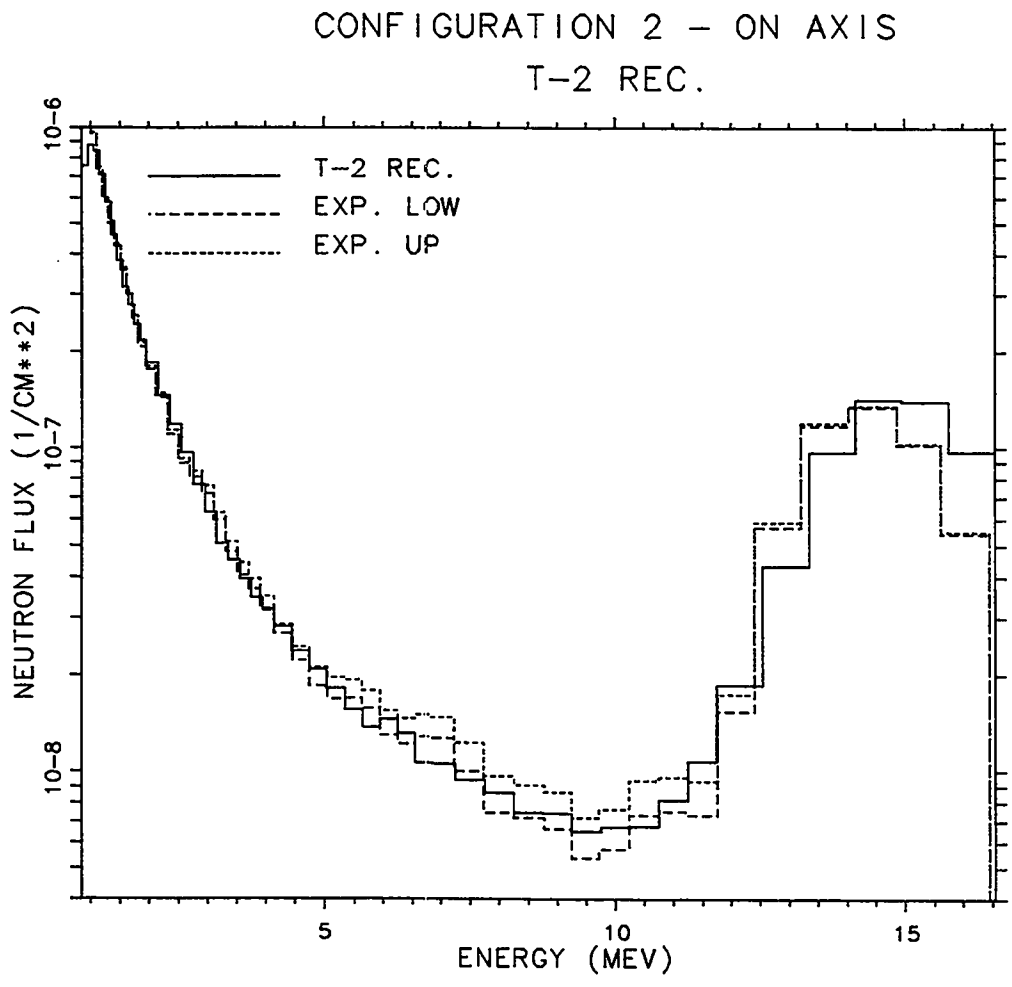

Fig. 16. Plot of MCNP Recommended calculated and experimental upper and lower confidence levels for configuration 2 with the detector on axis.

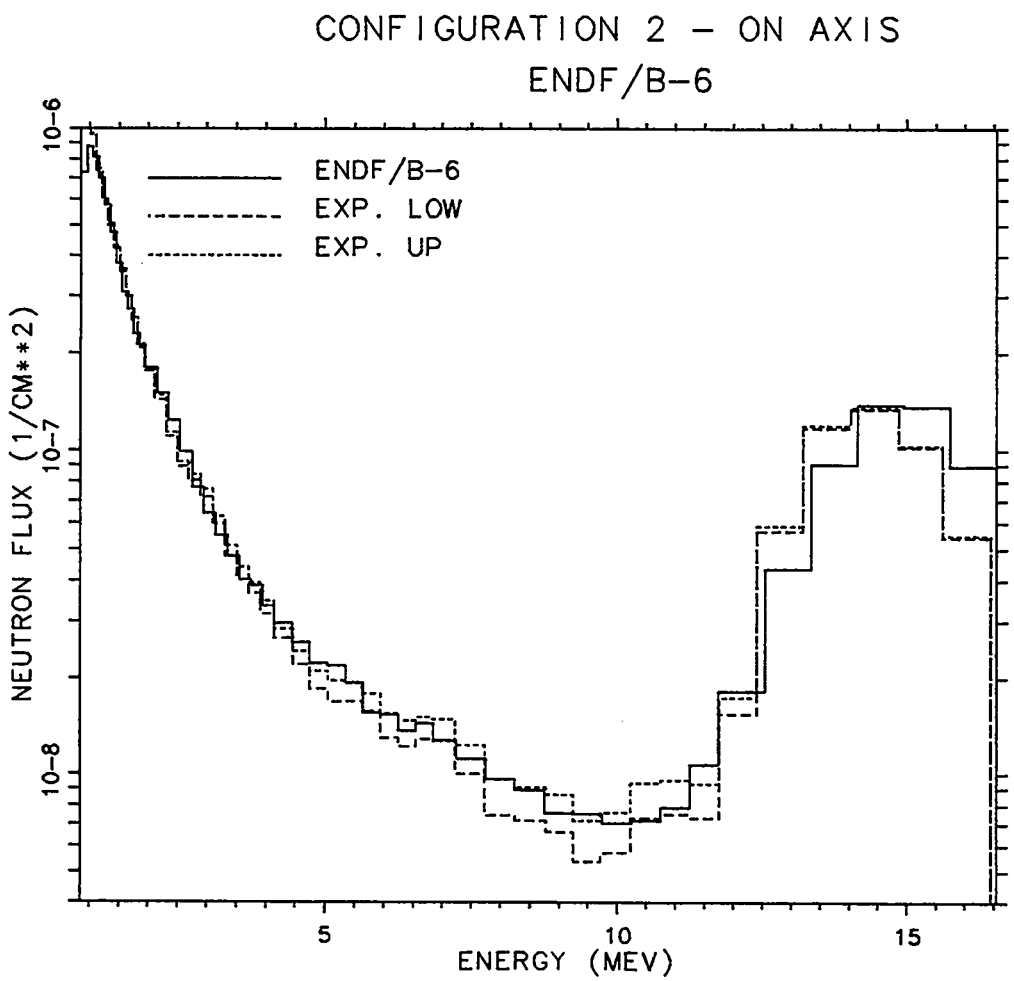

Fig. 17. Plot of ENDF/B-VI calculated and experimental upper and lower confidence levels for configuration 2 with the detector on axis.

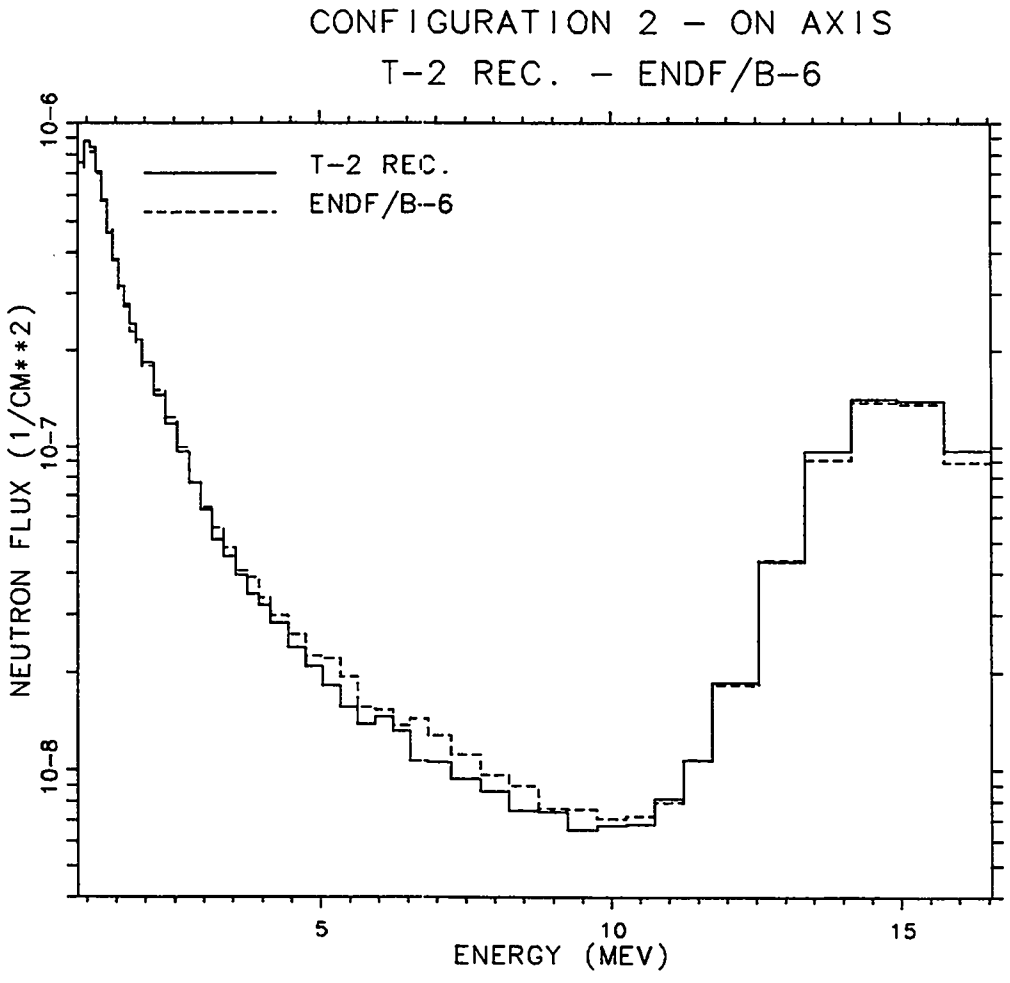

Fig. 18. Plot of MCNP Recommended and ENDF/B-VI calculated for configuration 2 with the detector on axis.

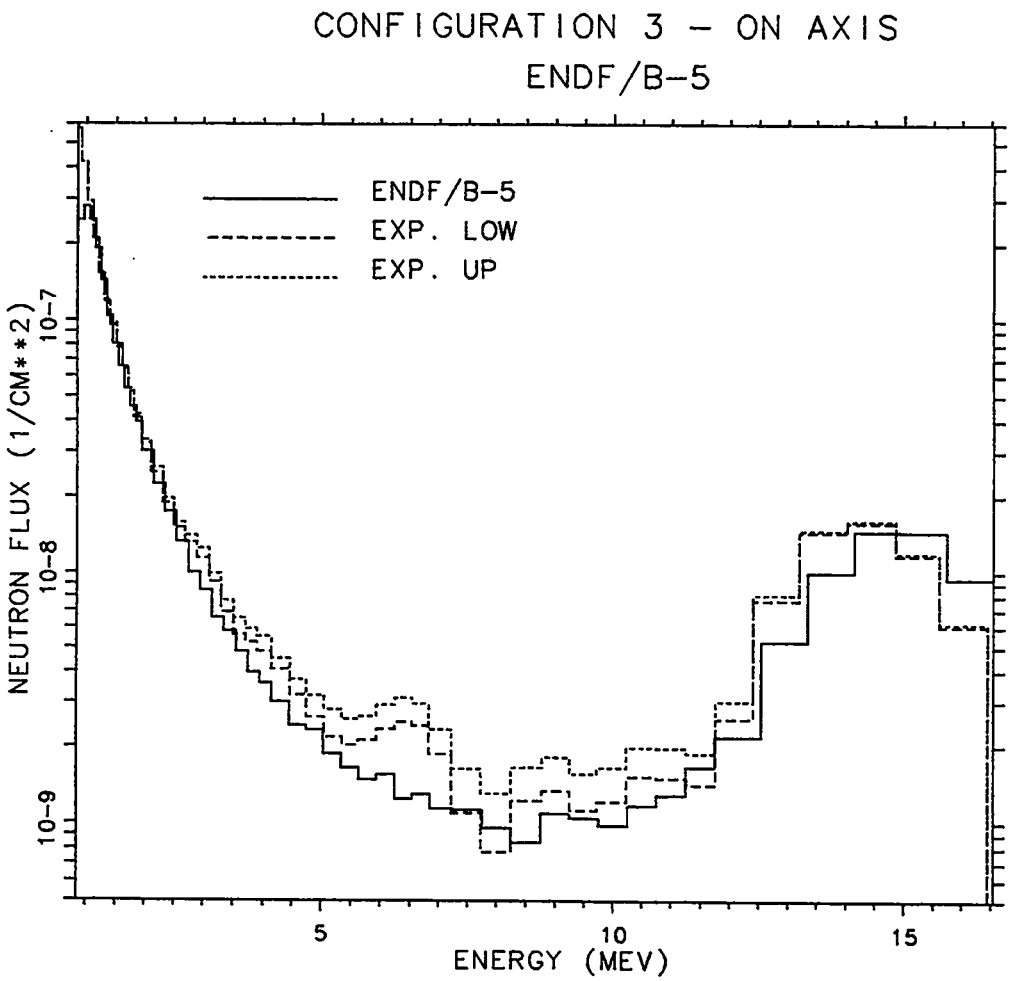

Fig. 19. Plot of ENDF/B-V calculated and experimental upper and lower confidence levels for configuration 3 with the detector on axis.

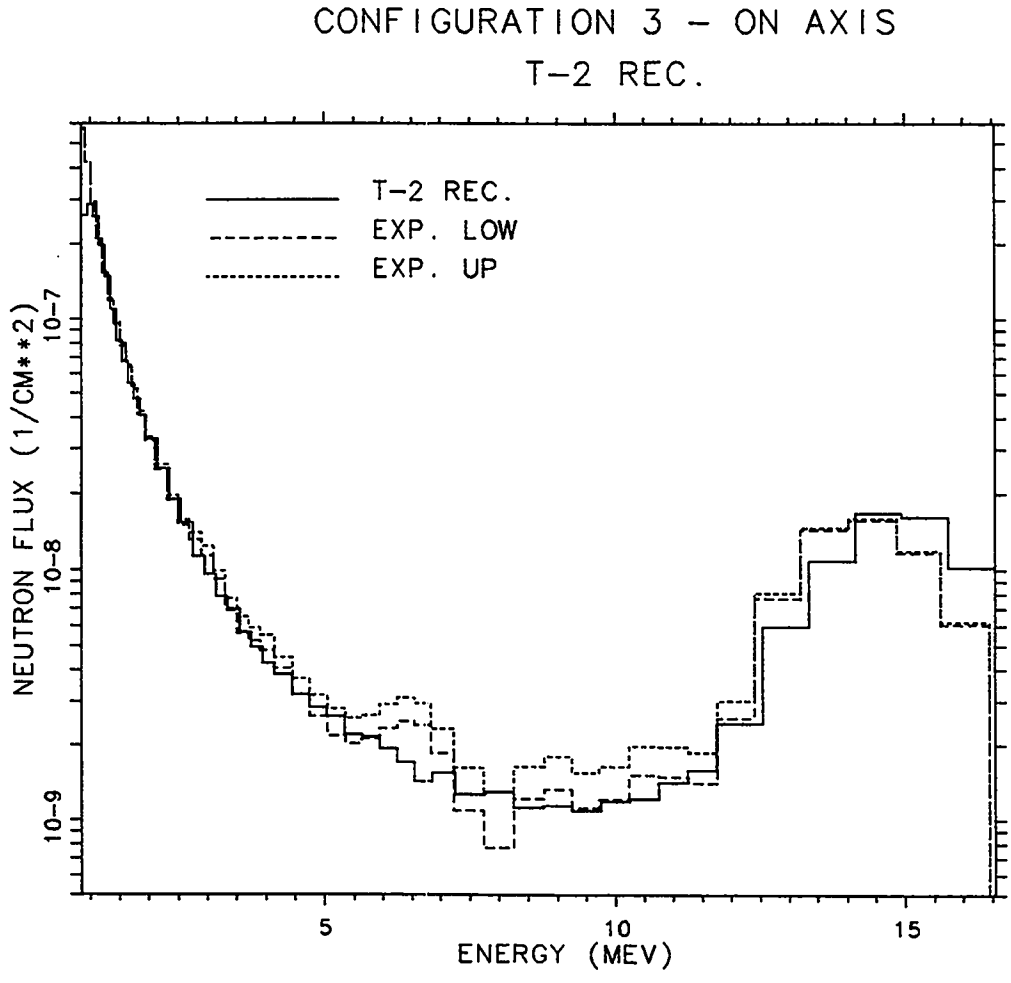

Fig. 20. Plot of MCNP Recommended calculated and experimental upper and lower confidence levels for configuration 3 with the detector on axis.

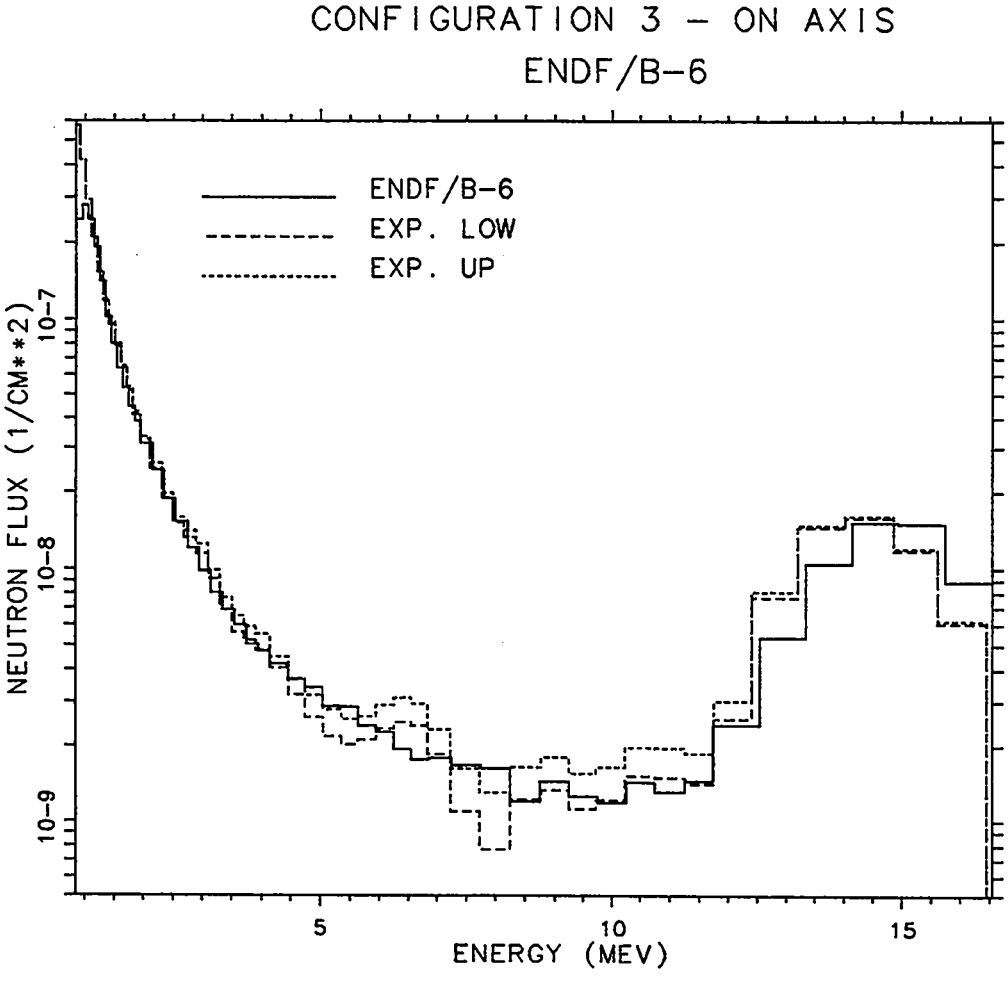

Fig. 21. Plot of ENDF/B-VI calculated and experimental upper and lower confidence levels for configuration 3 with the detector on axis.

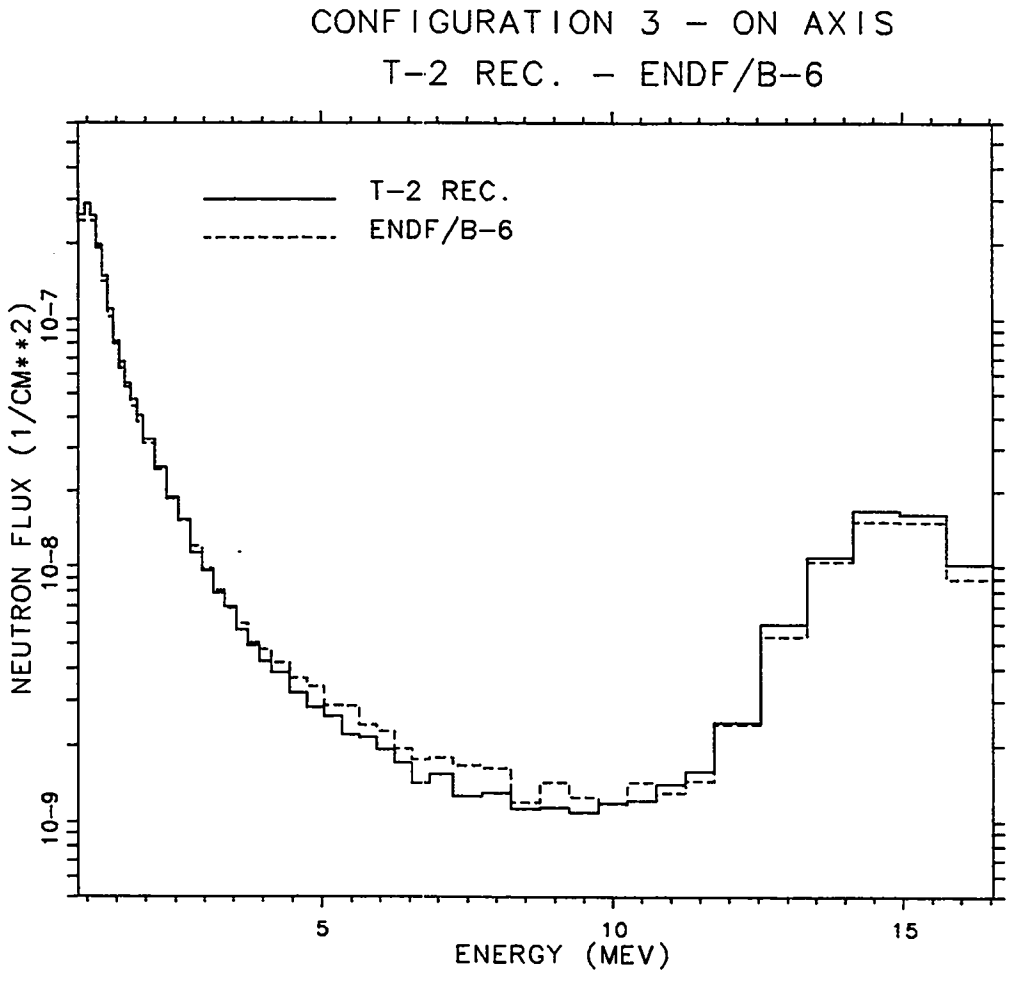

Fig. 22. Plot of MCNP Recommended and ENDF/B-VI calculated for configuration 3 with the detector on axis.

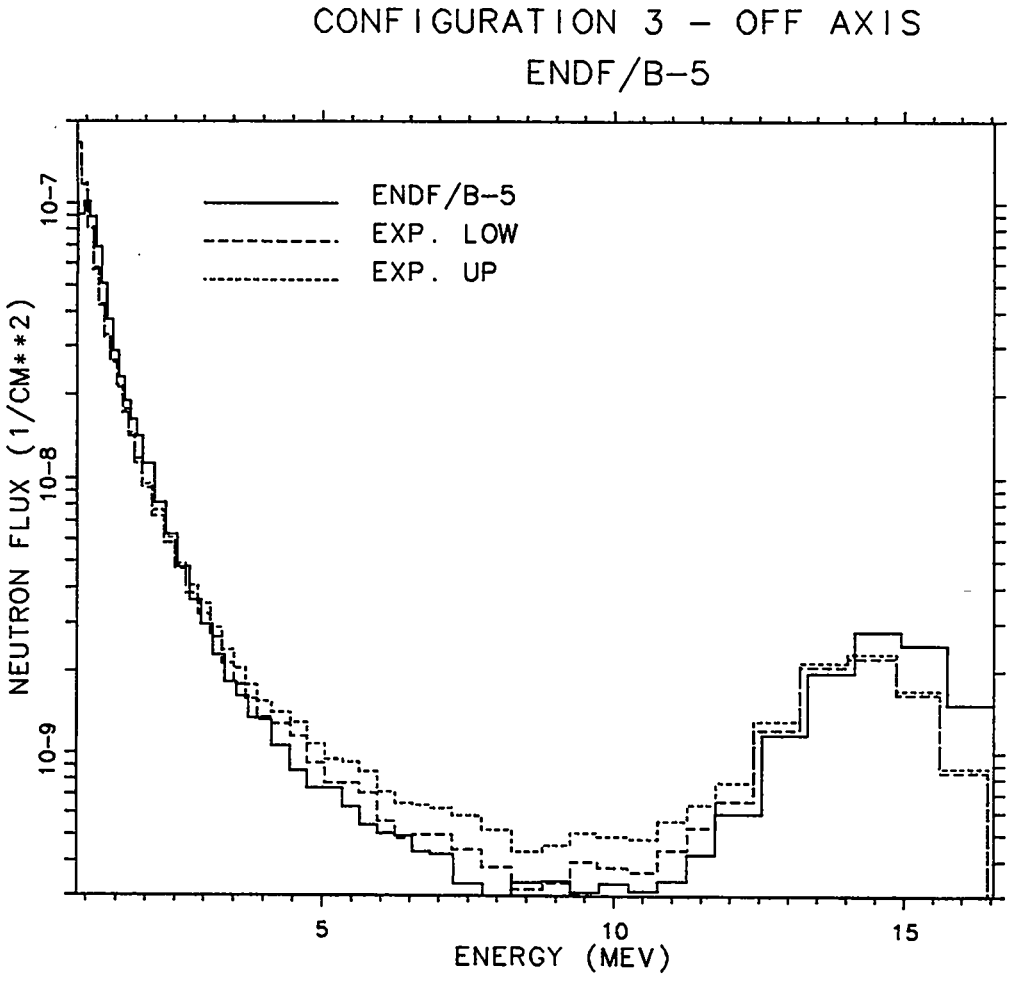

Fig. 23. Plot of ENDF/B-V calculated and experimental upper and lower confidence levels for configuration 3 with the detector off axis.

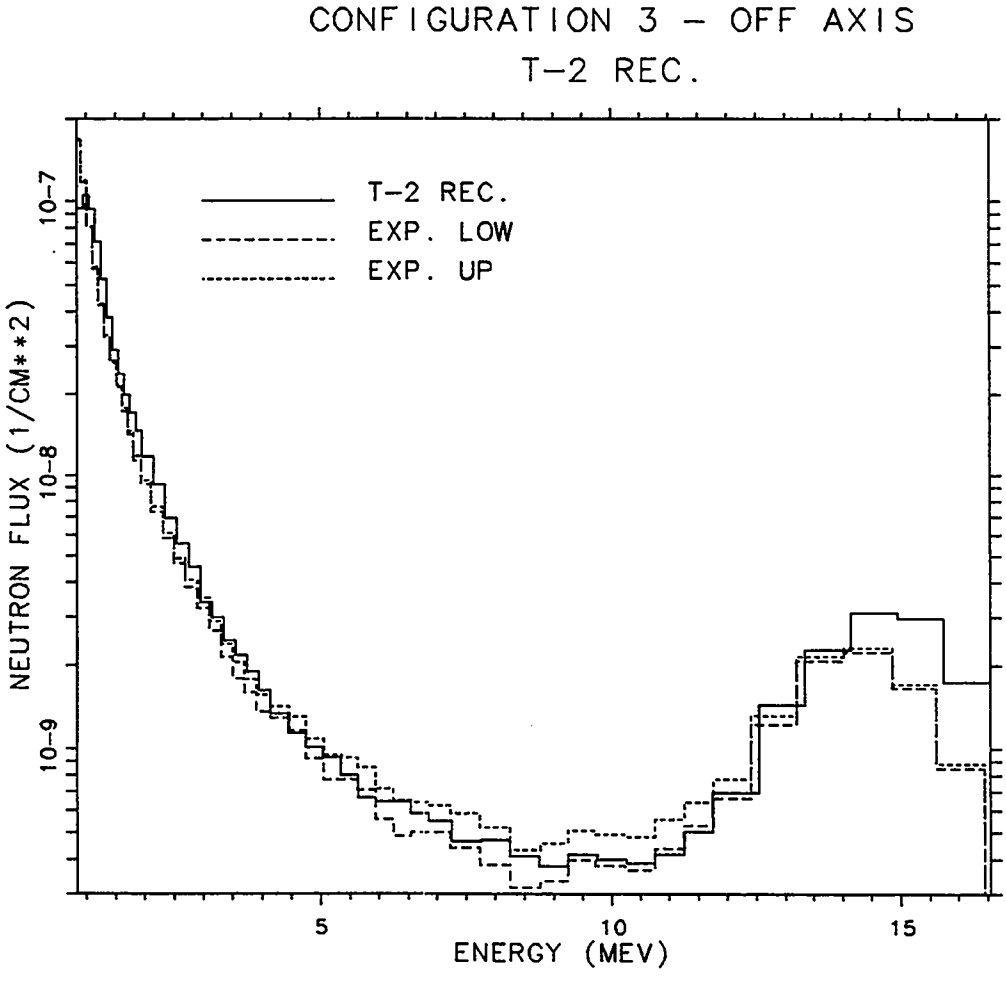

Fig. 24. Plot of MCNP Recommended calculated and experimental upper and lower confidence levels for configuration 3 with the detector off axis.

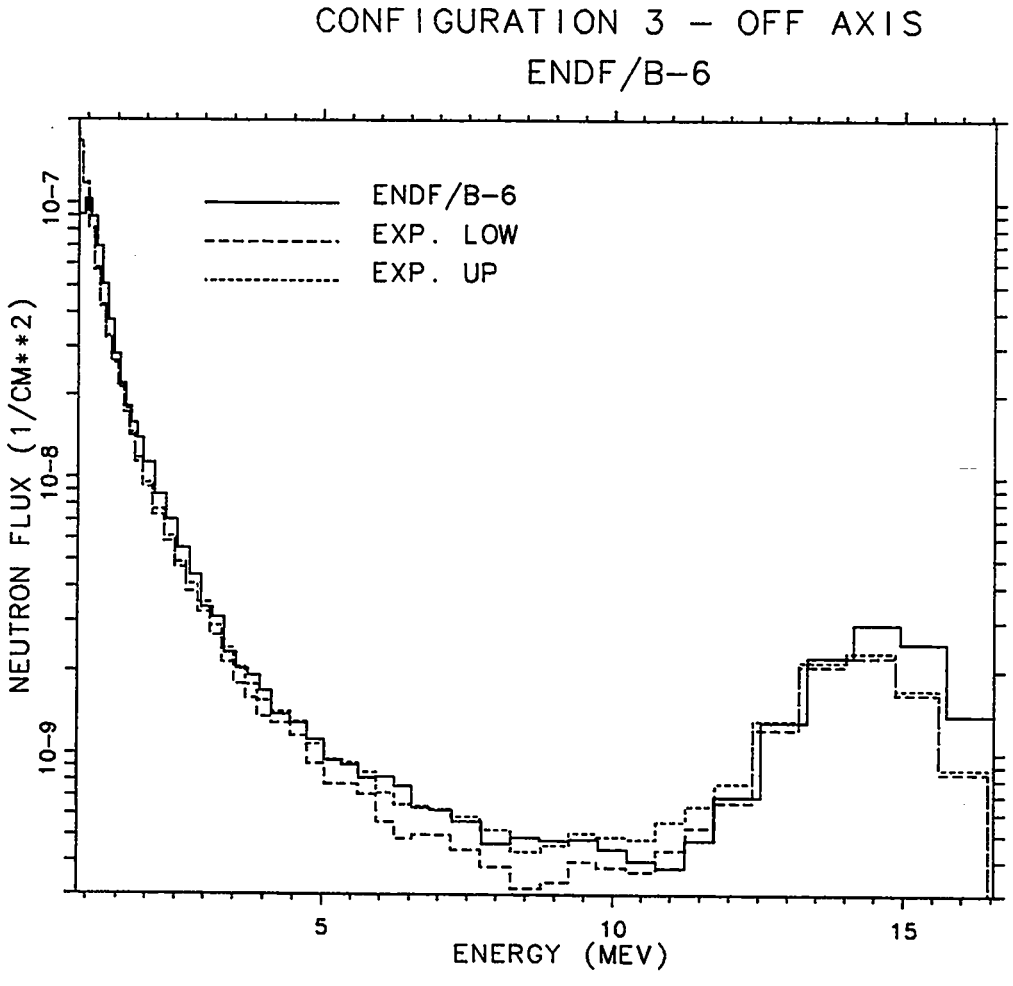

Fig. 25. Plot of ENDF/B-VI calculated and experimental upper and lower confidence levels for configuration 3 with the detector off axis.

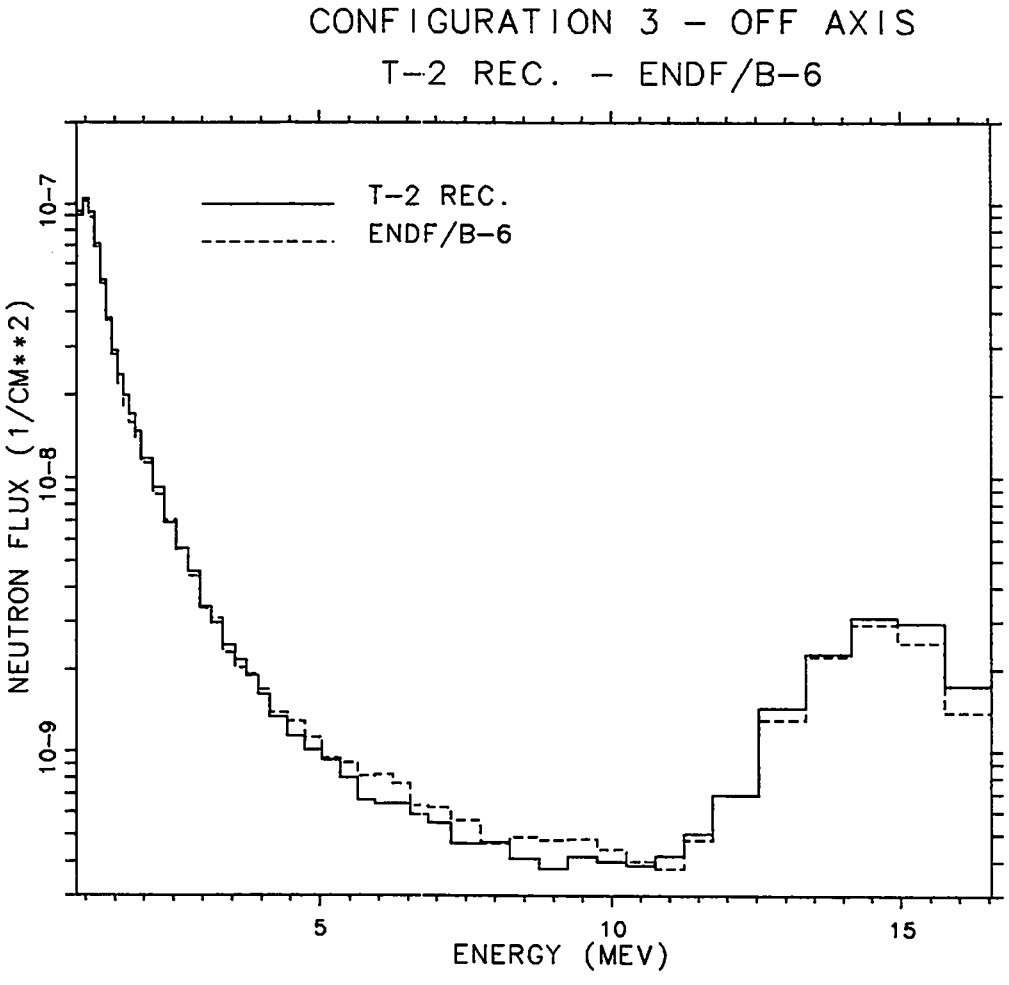

Fig. 26. Plot of MCNP Recommended and ENDF/B-VI calculated for configuration 3 with the detector off axis.

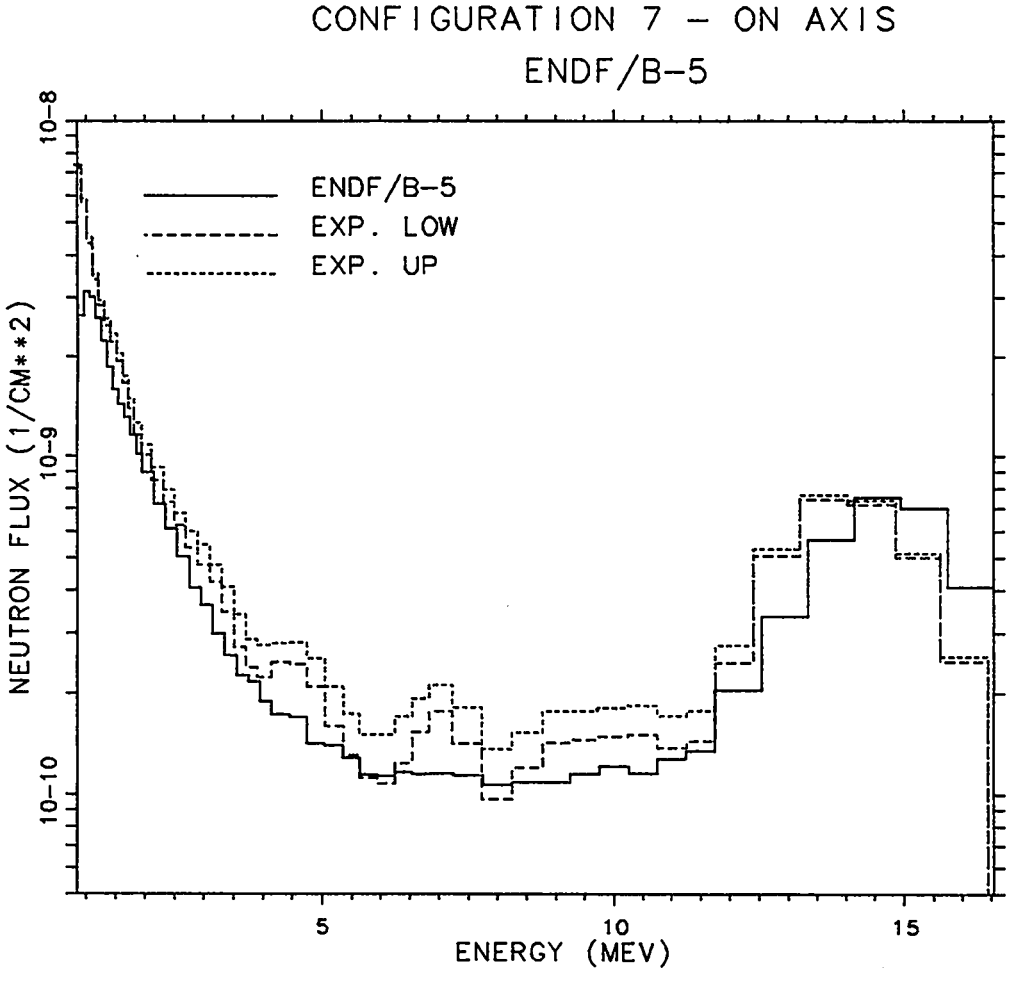

Fig. 27. Plot of ENDF/B-V calculated and experimental upper and lower confidence levels for configuration 7 with the detector on axis.

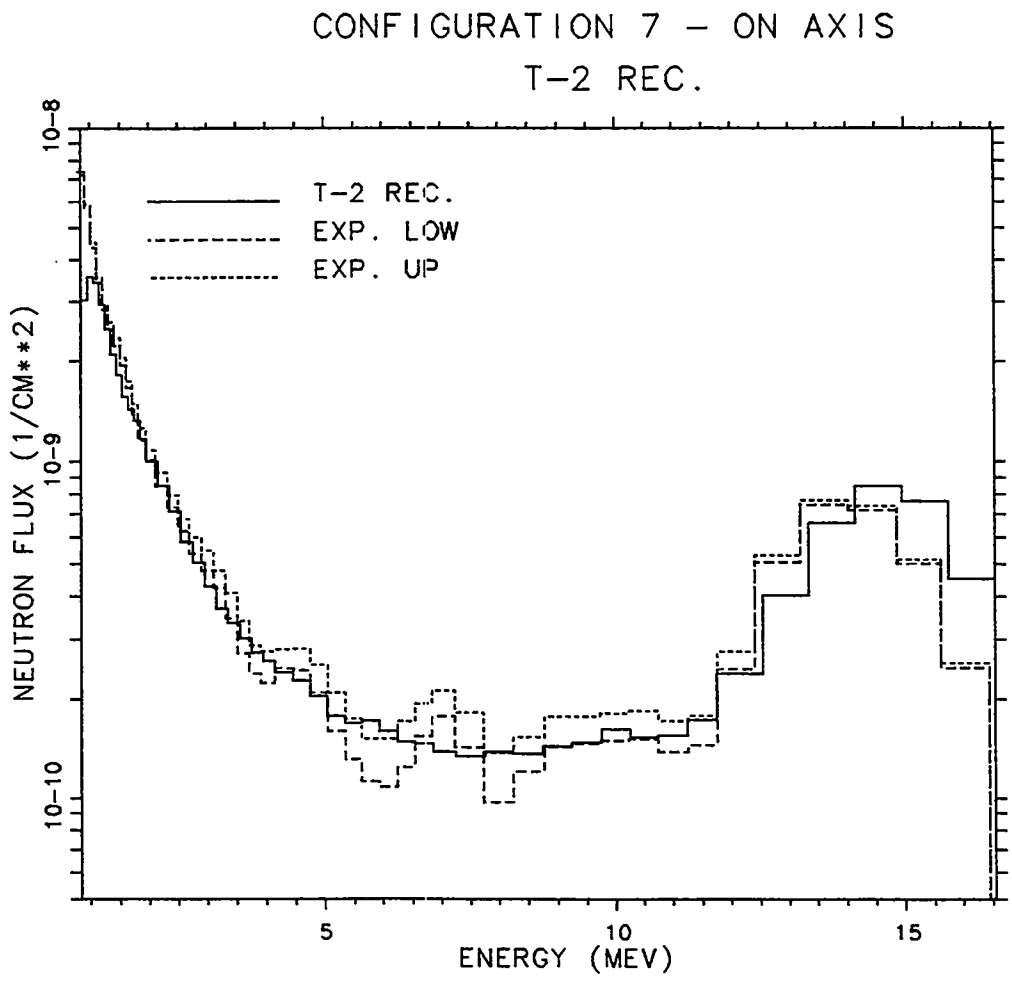

Fig. 28. Plot of MCNP Recommended calculated and experimental upper and lower confidence levels for configuration 7 with the detector on axis.

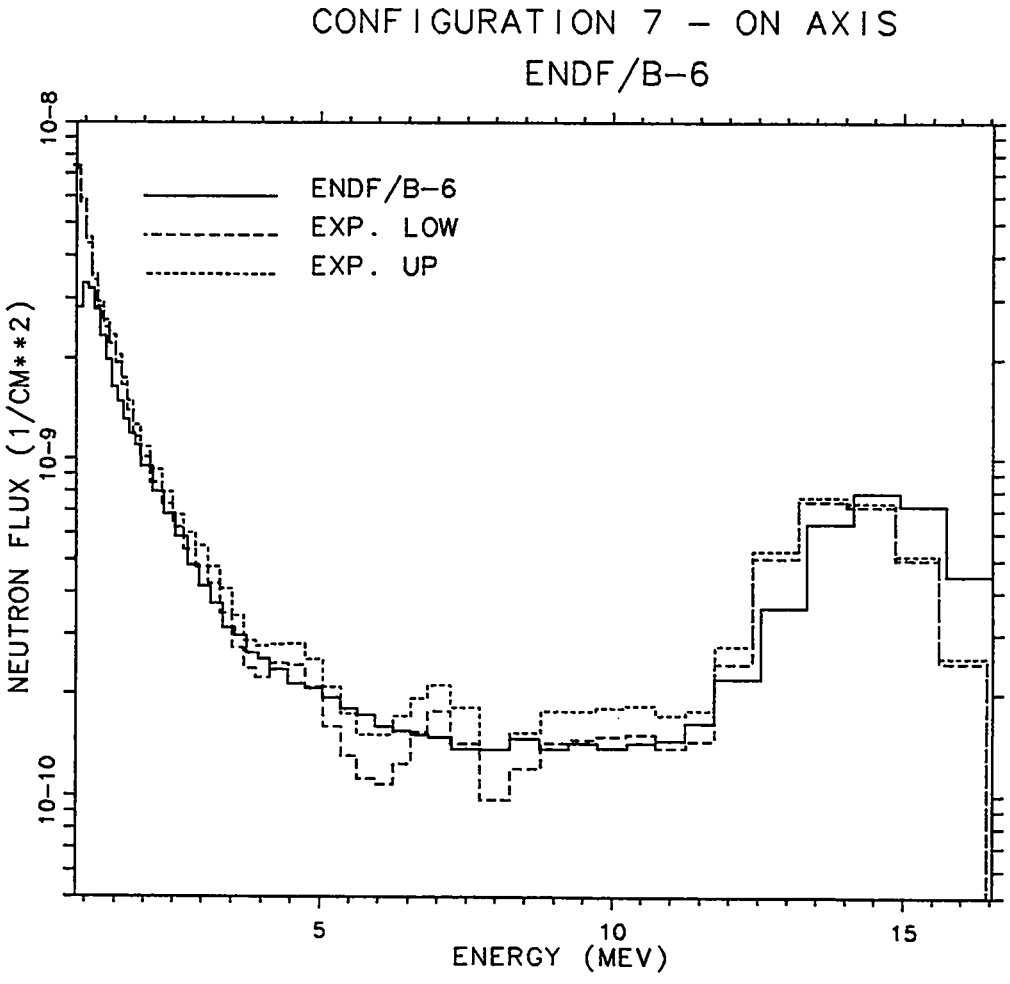

Fig. 29. Plot of ENDF/B-VI calculated and experimental upper and lower confidence levels for configuration 7 with the detector on axis.

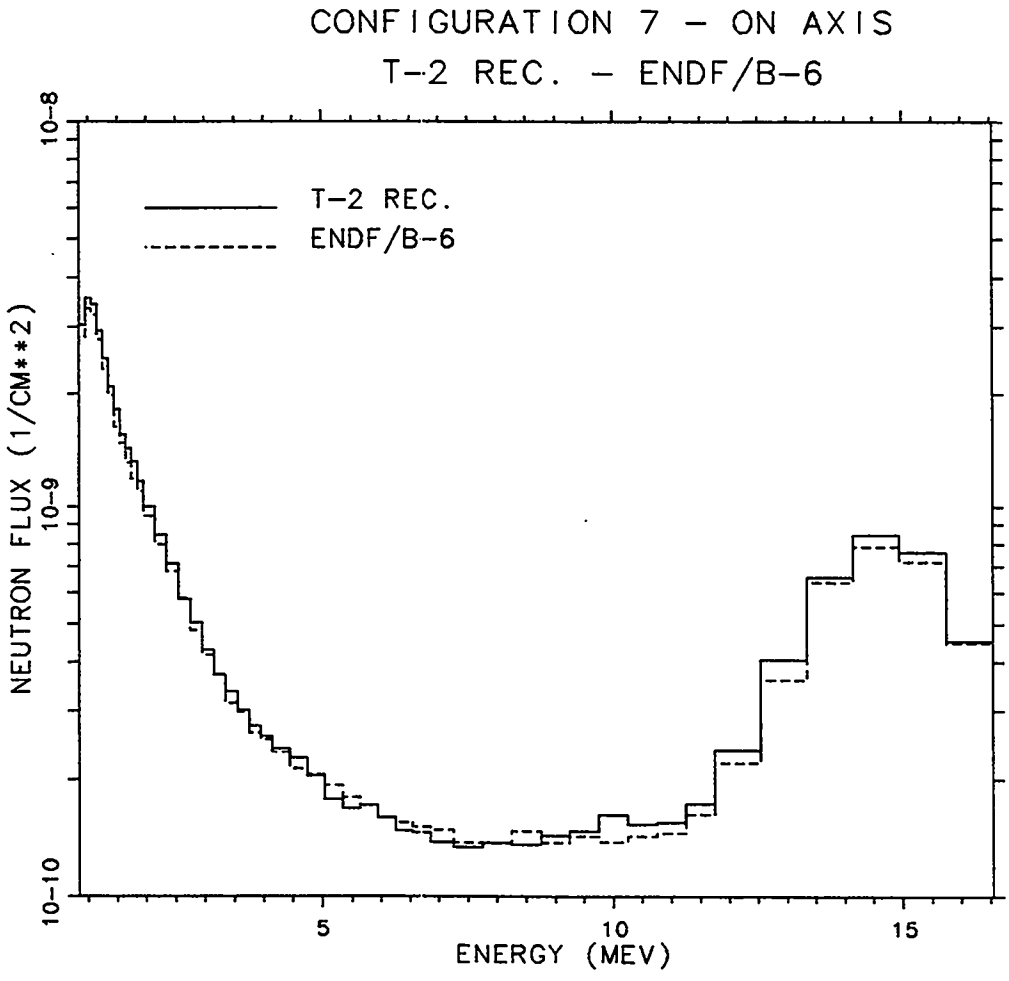

Fig. 30. Plot of MCNP Recommended and ENDF/B-VI calculated for configuration 7 with the detector on axis.

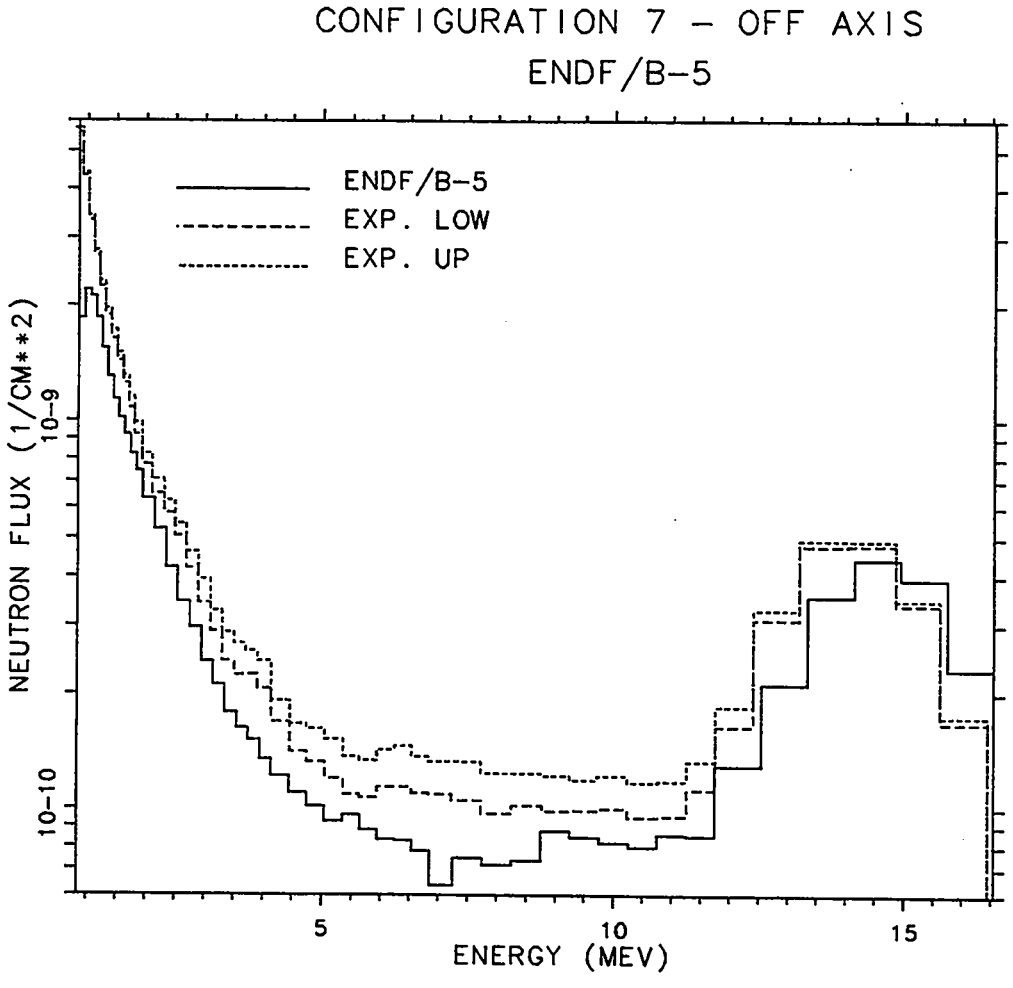

Fig. 31. Plot of ENDF/B-V calculated and experimental upper and lower confidence levels for configuration 7 with the detector off axis.

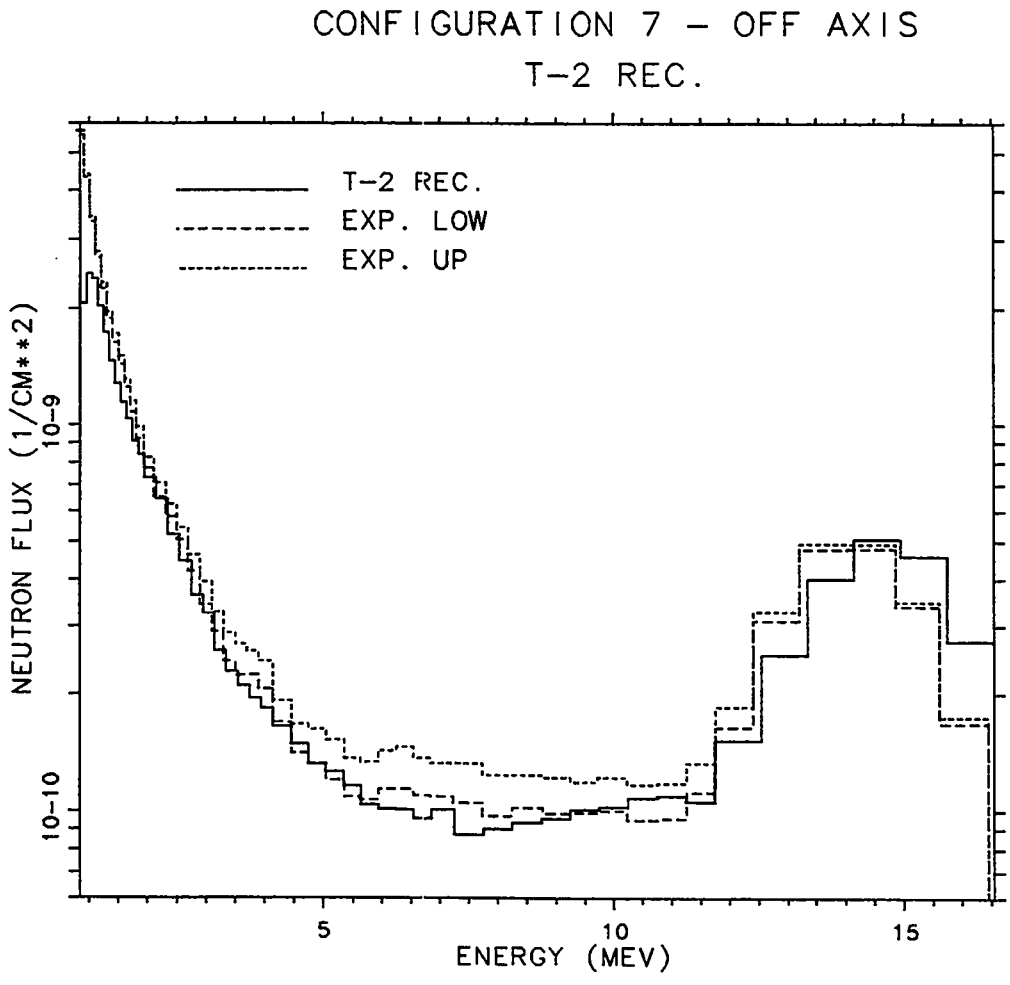

Fig. 32. Plot of MCNP Recommended calculated and experimental upper and lower confidence levels for configuration 7 with the detector off axis.

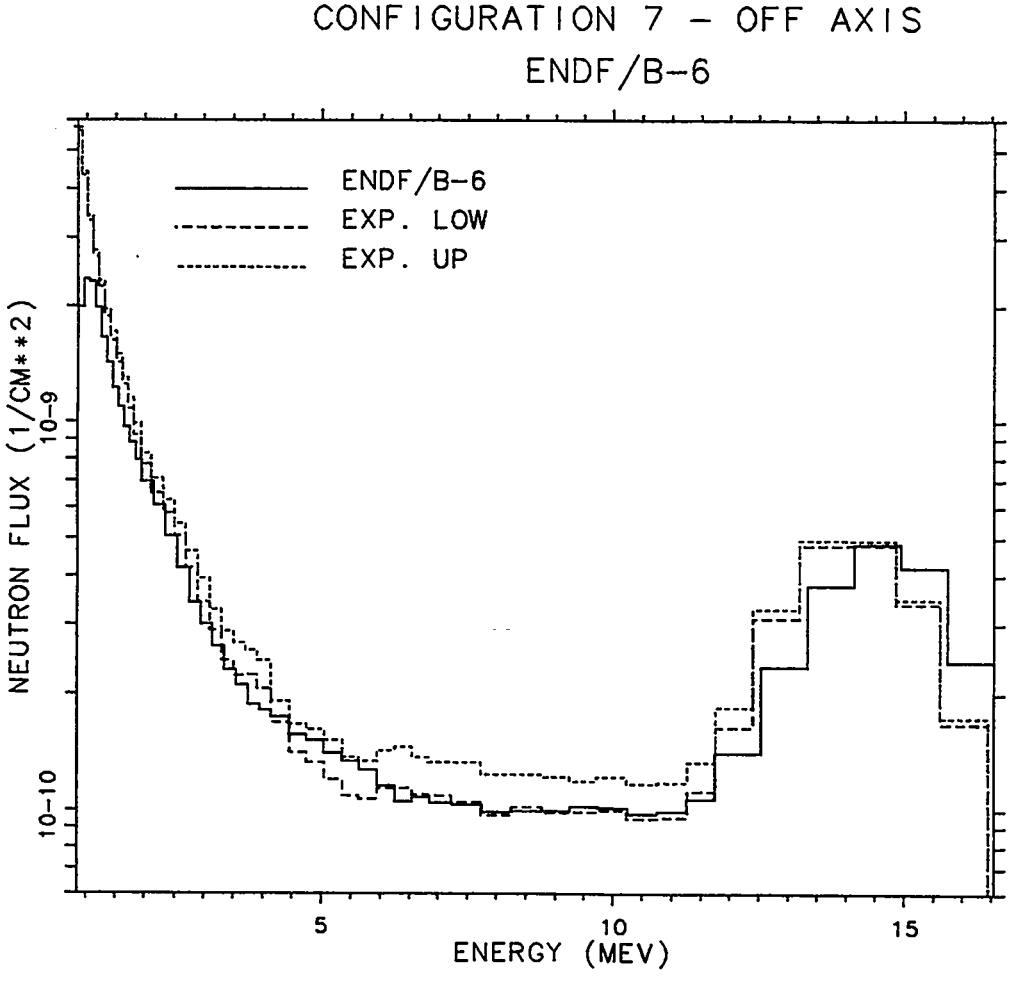

Fig. 33. Plot of ENDF/B-VI calculated and experimental upper and lower confidence levels for configuration 7 with the detector off axis.

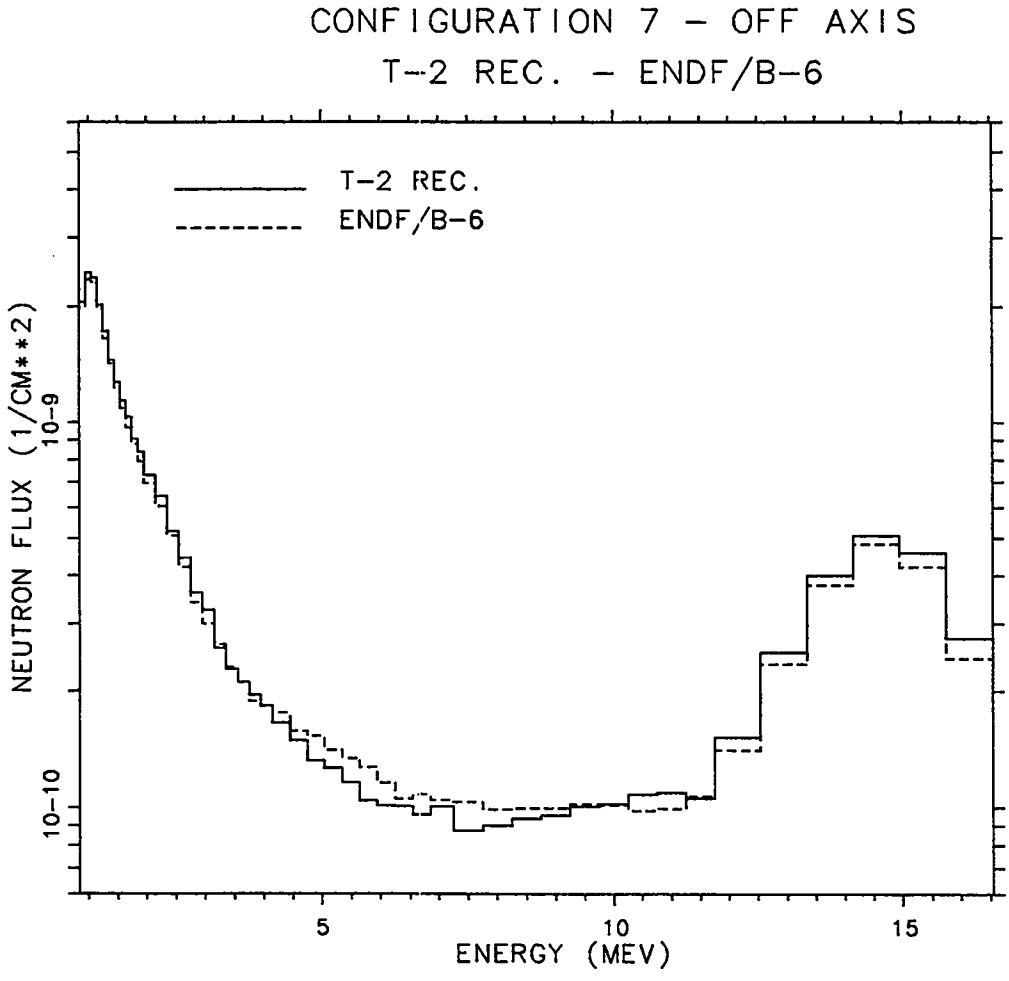

Fig. 34. Plot of MCNP Recommended and ENDF/B-VI calculated for configuration 7 with the detector off axis.

IV. 76 CM. DIAMETER IRON SPHERE BENCHMARK

A. Experimental Setup

In the early 1970's at the University of Illinois, neutron leakage measurements were made with a NE-213 spectrometry system on a 76-cm. diameter iron sphere. The sphere contained a central void of 15-cm. diameter and a re-entrant hole of 9.5-cm. diameter for the neutron generator beam tube. Two different neutron sources were used in the measurements. A neutron generator was used as a source of 14 MeV neutrons from the $T(d,n)^4He$ reaction,[11] and a ^{252}Cf source was used for another set of measurements.[10] The neutron detector was placed 2 m. from the center of the sphere at an angle of 90 degrees from the deuteron beam tube. The assumption was made that the detector was in the same position for the ^{252}Cf source spectrum. The source spectrum for the MCNP modeling was a Maxwellian fission source with a temperature of 1.425 MeV.[15]

B. Results and Discussion

In the absence of experimental data, calculations were done for the ENDF/B-IV, ENDF/B-V, the MCNP Recommended (a group T-2 evaluation), and ENDF/B-VI data sets. Both pure iron and a high carbon steel were used in separate calculations. ENDF/B-IV was not used in the high carbon steel calculations due to the absence of data for ^{31}P, ^{32}S, and ^{55}Mn. The composition of the high carbon steel is identical to the composition of the Lawrence Livermore pulsed iron sphere and can be found in Table II. Further details of the problem setup can be found in Table A.3 in the appendix.

ENDF/B-VI was compared to each of the previous data sets and the percentage difference computed. These differences are shown in Table VIII. ENDF/B-VI and the MCNP Recommended Library are generally in good agreement, while the ENDF/B-V and ENDF/B-IV libraries allow significantly lower transmission and tend to agree with each other.

Figures 35 and 36 show the complete spectrum for the iron sphere with a ^{252}Cf source, with Figures 37 through 41 showing the spectra for the different energy groups of Table VIII. Figures 42 and 43 show the complete spectrum for iron with a D-T source, with the energy groups shown in Figures 44 through 48. The high carbon steel results are given in Figures 49 through 62. In some cases, particularly Figures 41, 54, and 55, statistics are poor, and the plotted results are unreliable.

Generally, ENDF/B-VI and the MCNP Recommended Library are in fairly close agreement, and the ENDF/B-V and ENDF/B-IV libraries give somewhat lower transmissions.

TABLE VIII. **76 cm. Iron Sphere Results: ENDF/B-VI Data Set Differences**

Composition	Source	Energy Group (MeV)	% Difference $(\frac{ENDF/B-VI-ENDF/B-x}{ENDF/B-x})\times 100$		
			ENDF/B-IV	ENDF/B-V	T-2 Rec.
Pure Iron	^{252}Cf	0.5–2	+4.54	+0.342	-2.02
		2–5	+17.48	+14.11	+1.739
		5–10	+21.0	+22.8	+10.48
		10–13	+82.2	+128.2	+16.5
		> 13	+41.6	-56.8	-21.6
	T(d,n)^{4}He	0.5–2	+0.819	+1.017	-2.76
		2–5	+20.8	+19.22	-1.580
		5–10	+36.9	+39.2	+14.44
		10–13	+12.62	+11.93	-0.769
		> 13	+2.33	+3.32	-10.81
High Carbon Steel	^{252}Cf	0.5–2	*	+3.21	-0.723
		2–5	*	+11.11	+2.91
		5–10	*	+18.22	+19.48
		10–13	*	-17.72	-31.9
		> 13	*	-16.95	-1.211
	T(d,n)^{4}He	0.5–2	*	+2.53	-0.802
		2–5	*	+21.8	+1.913
		5–10	*	+43.3	+15.05
		10–13	*	+19.07	+2.86
		> 13	*	+5.22	-8.22

*Contains isotopes not available in ENDF/B-IV

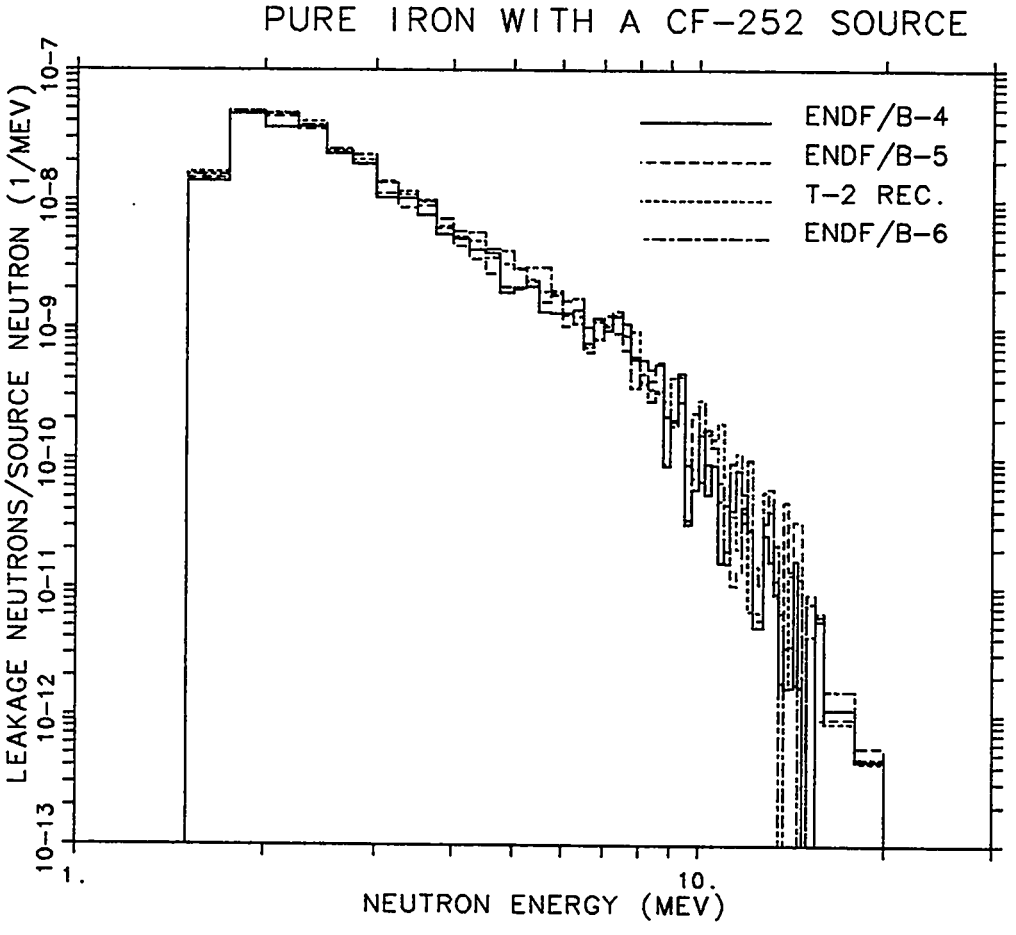

Fig. 35. Plot of ENDF/B-IV, ENDF/B-V, MCNP Recommended, and ENDF/B-VI calculated for pure iron with a ^{252}Cf source.

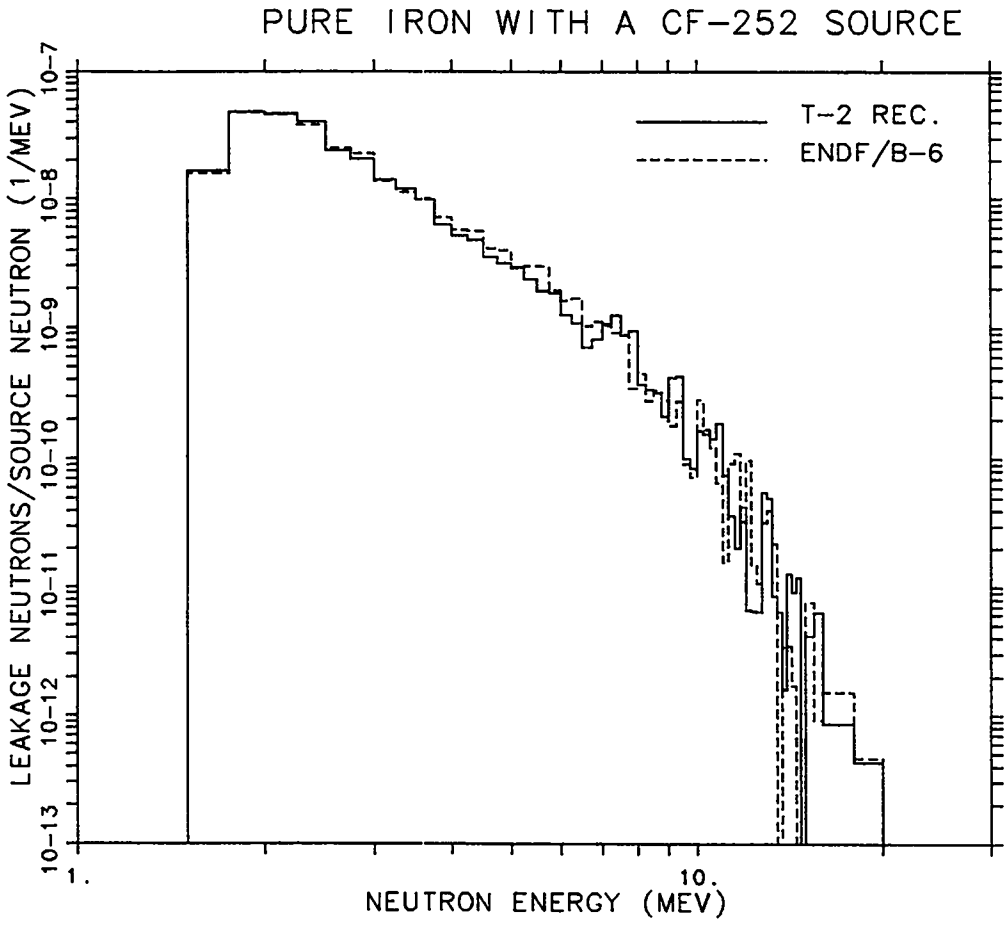

Fig. 36. Plot of MCNP Recommended and ENDF/B-VI calculated for pure iron with a ^{252}Cf source.

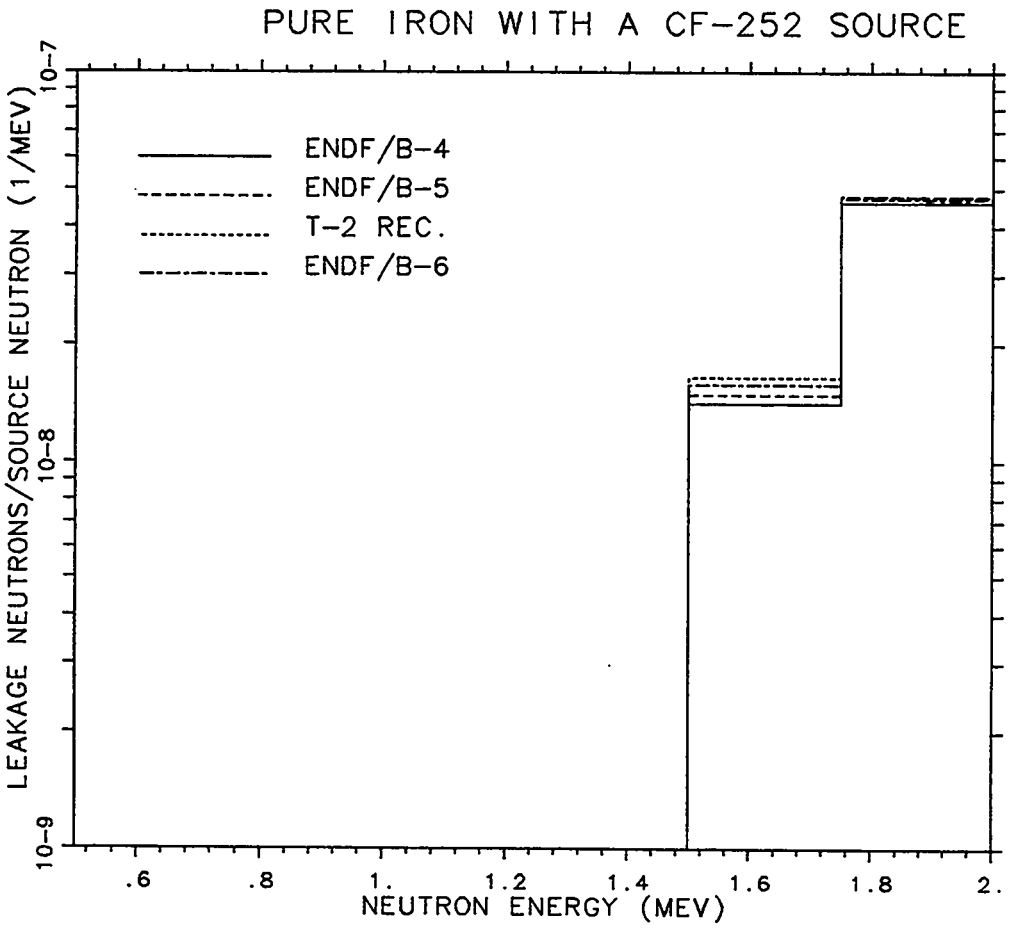

Fig. 37. Plot of pure iron with a ^{252}Cf source for the energy group 1.5–2 MeV.

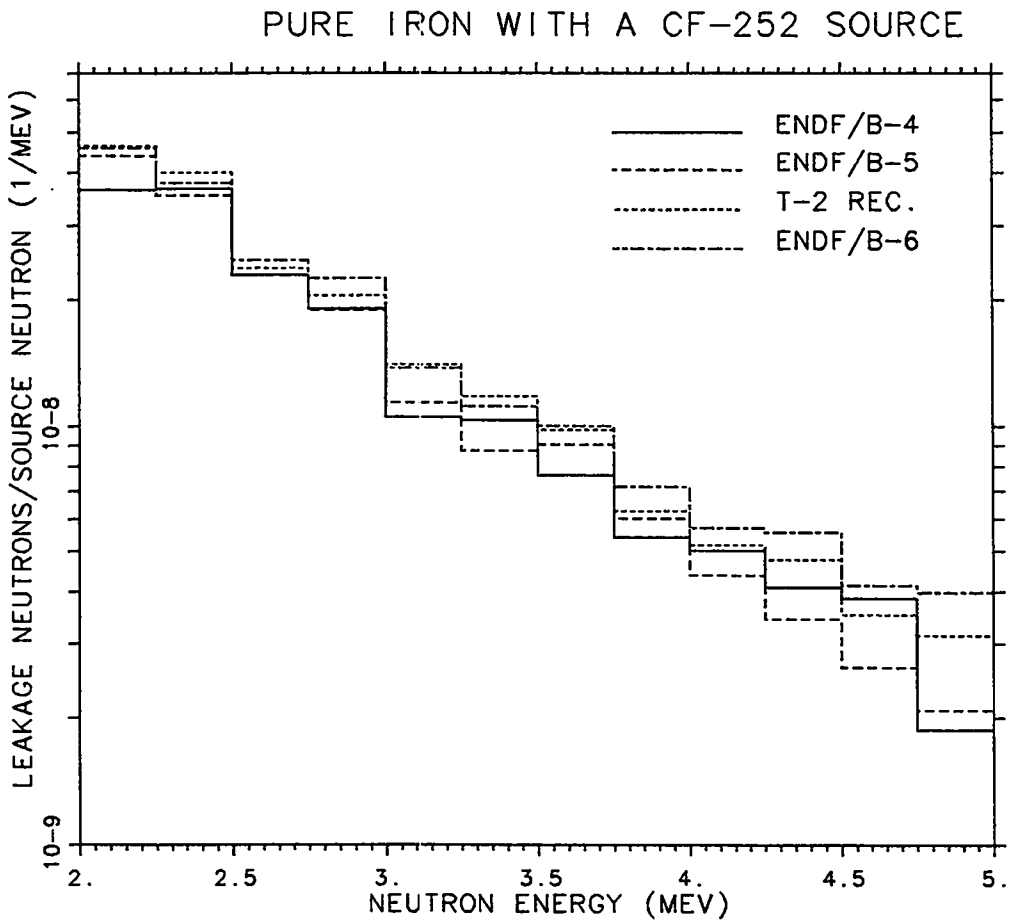

Fig. 38. Plot of pure iron with a ^{252}Cf source for the energy group 2–5 MeV.

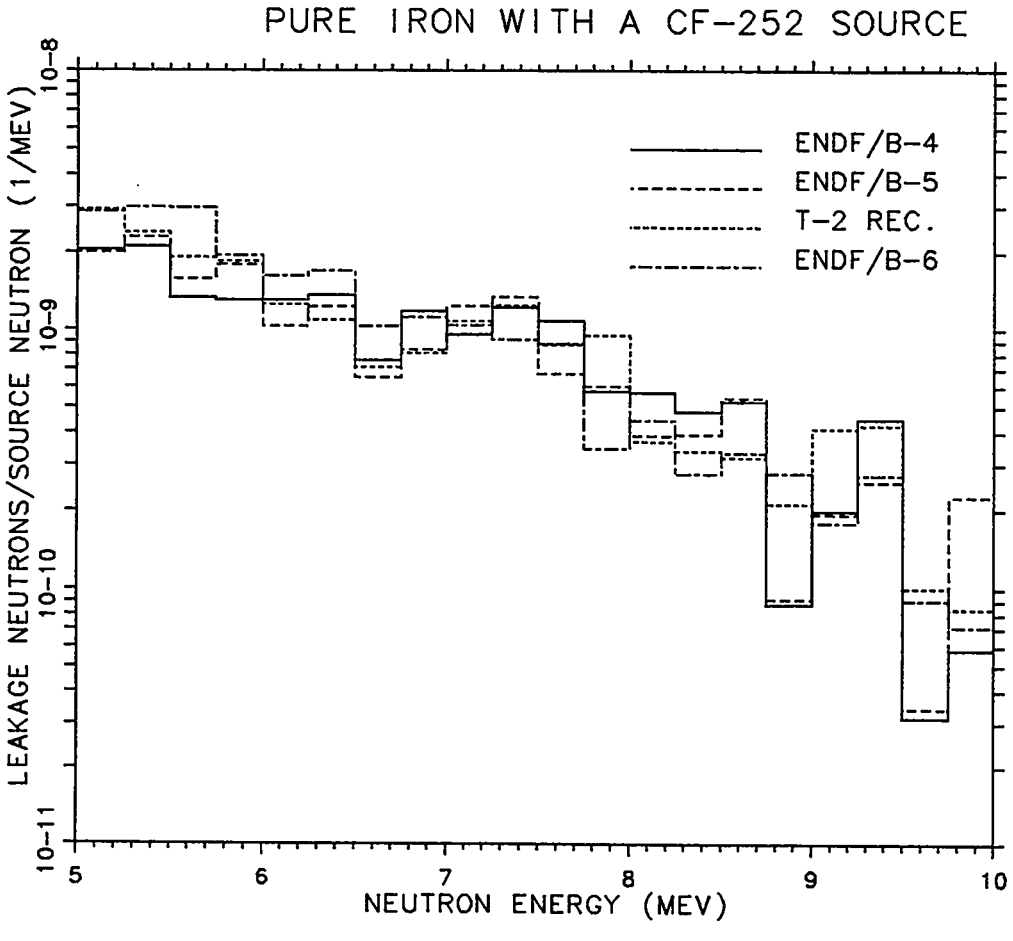

Fig. 39. Plot of pure iron with a ^{252}Cf source for the energy group 5–10 MeV.

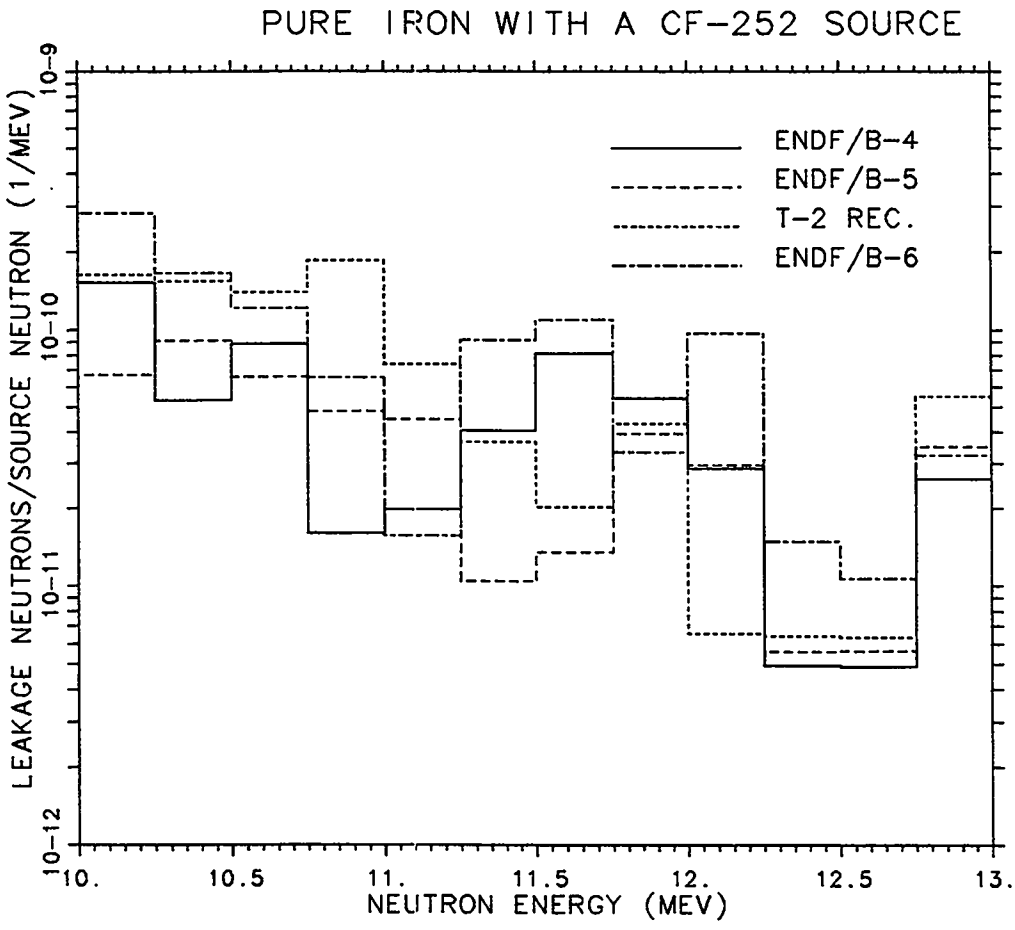

Fig. 40. Plot of pure iron with a ^{252}Cf source for the energy group 10–13 MeV.

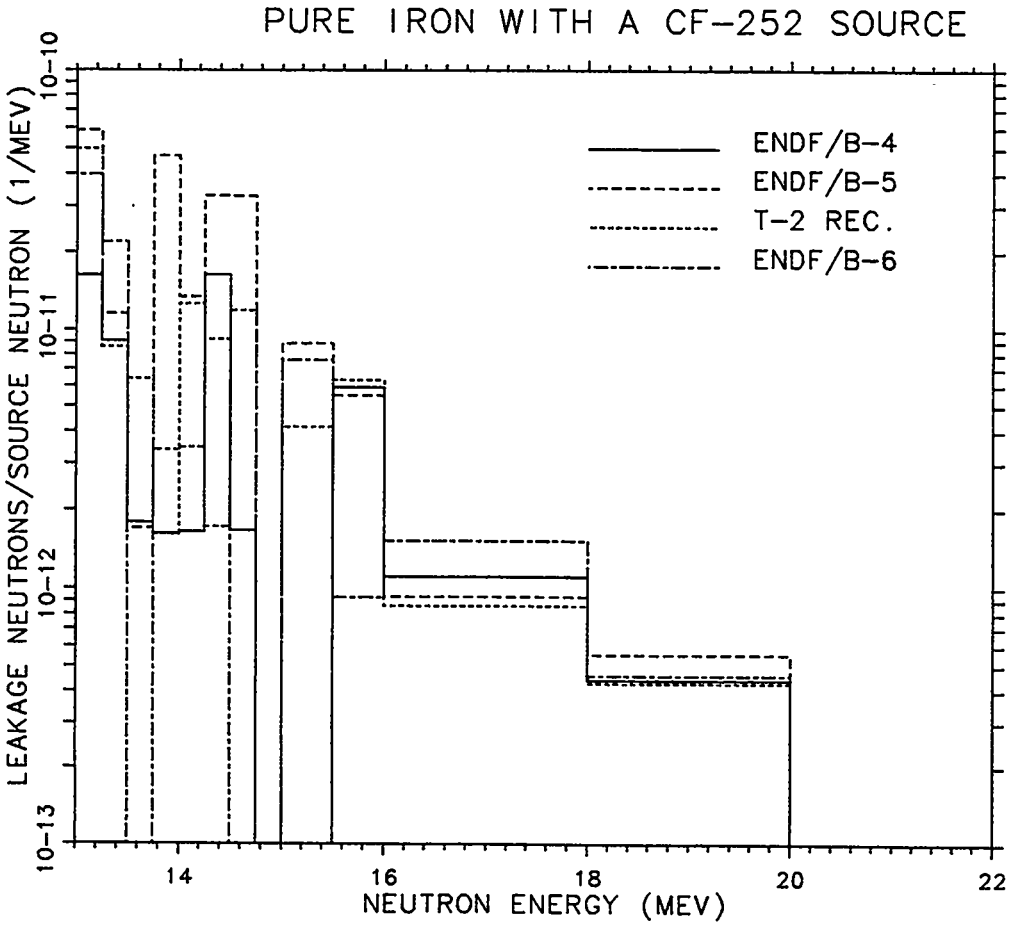

Fig. 41. Plot of pure iron with a ^{252}Cf source for the energy group > 13 MeV. The results are affected by a lack of good statistics.

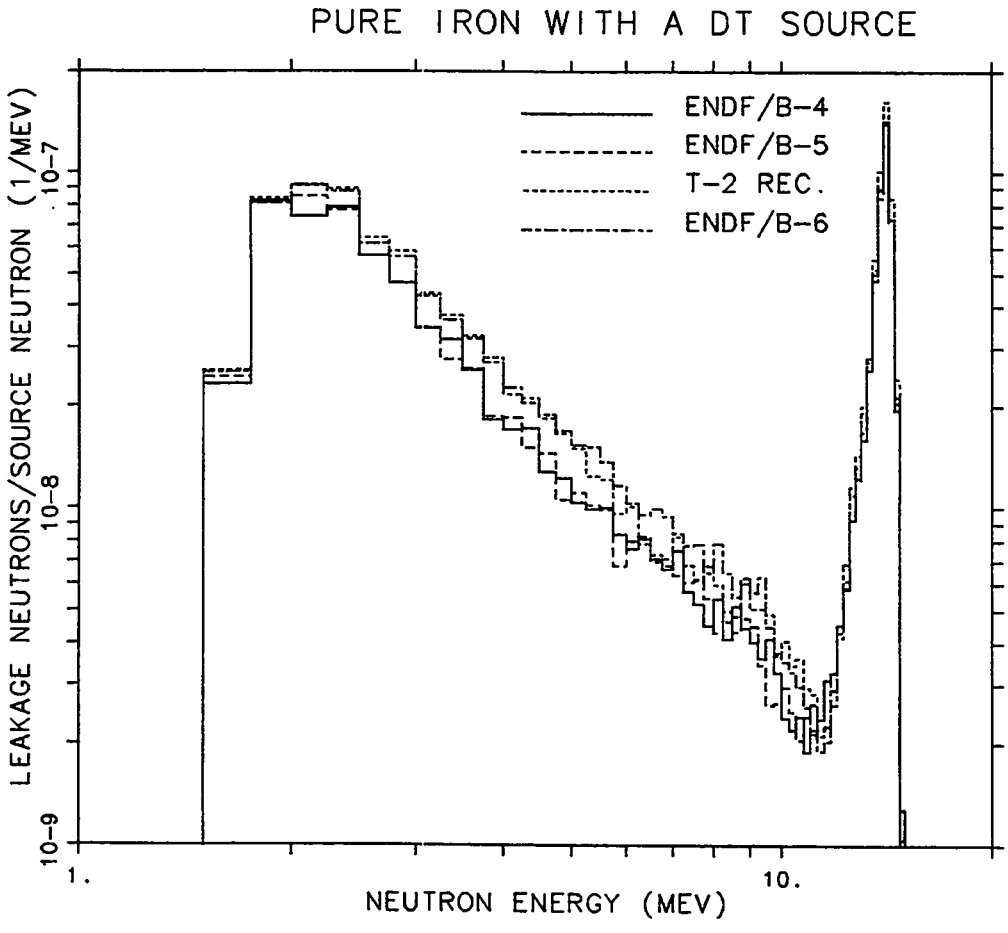

Fig. 42. Plot of ENDF/B-IV, ENDF/B-V, MCNP Recommended, and ENDF/B-VI calculated for pure iron with a $T(d,n)^4He$ source.

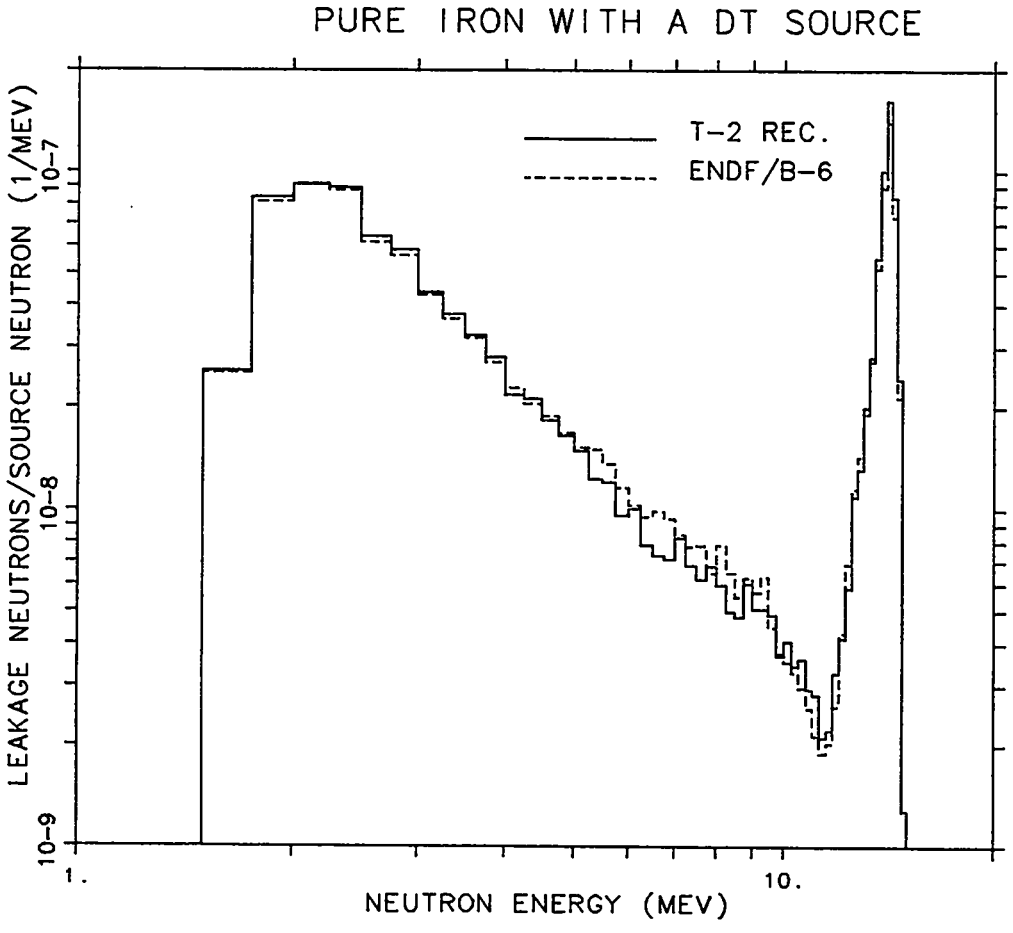

Fig. 43. Plot of MCNP Recommended and ENDF/B-VI calculated for pure iron with a $T(d,n)^4He$ source.

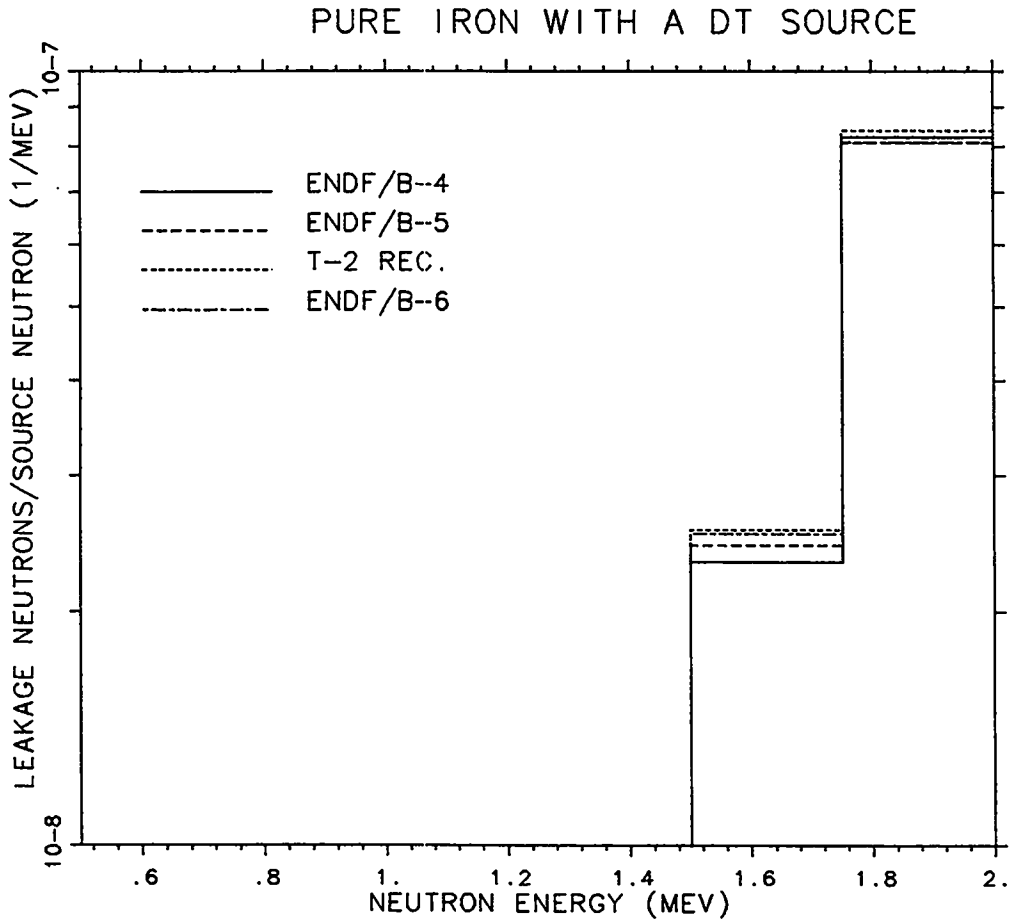

Fig. 44. Plot of pure iron with a T(d,n)^{4}He source for the energy group 0.5–2 MeV.

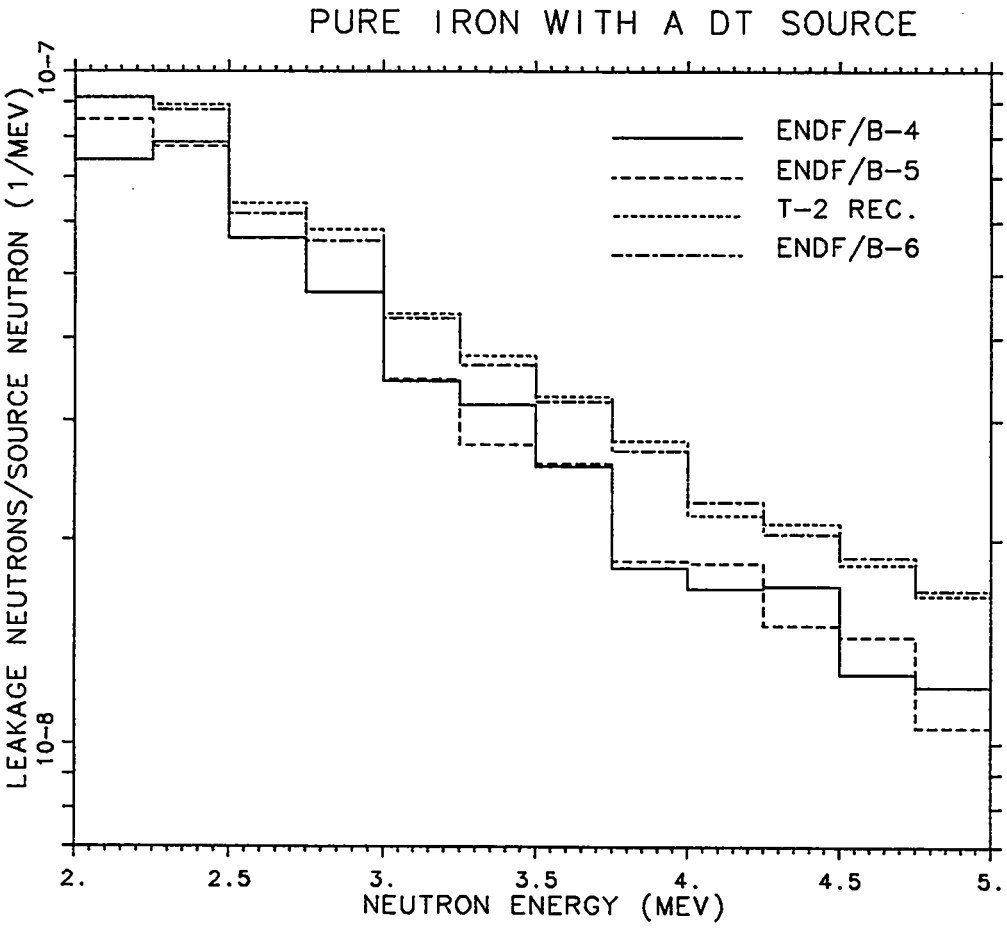

Fig. 45. Plot of pure iron with a T(d,n)^{4}He source for the energy group 2–5 MeV.

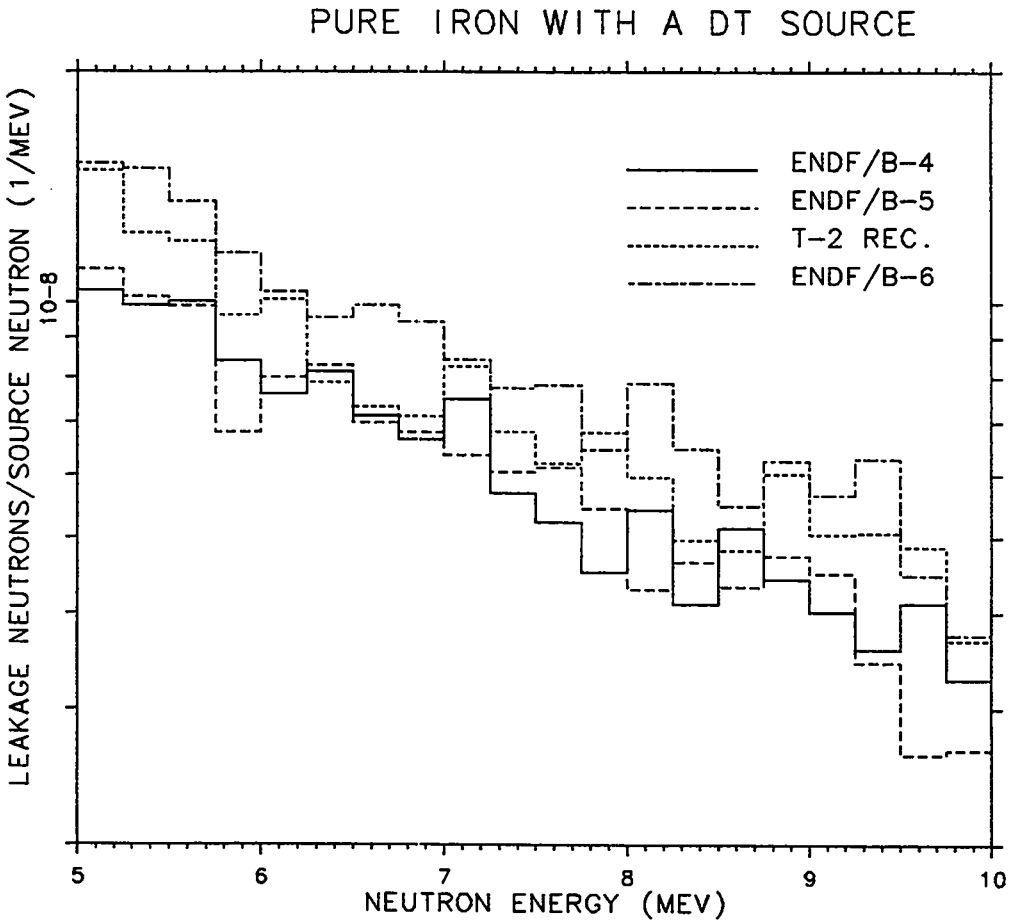

Fig. 46. Plot of pure iron with a T(d,n)^{4}He source for the energy group 5–10 MeV.

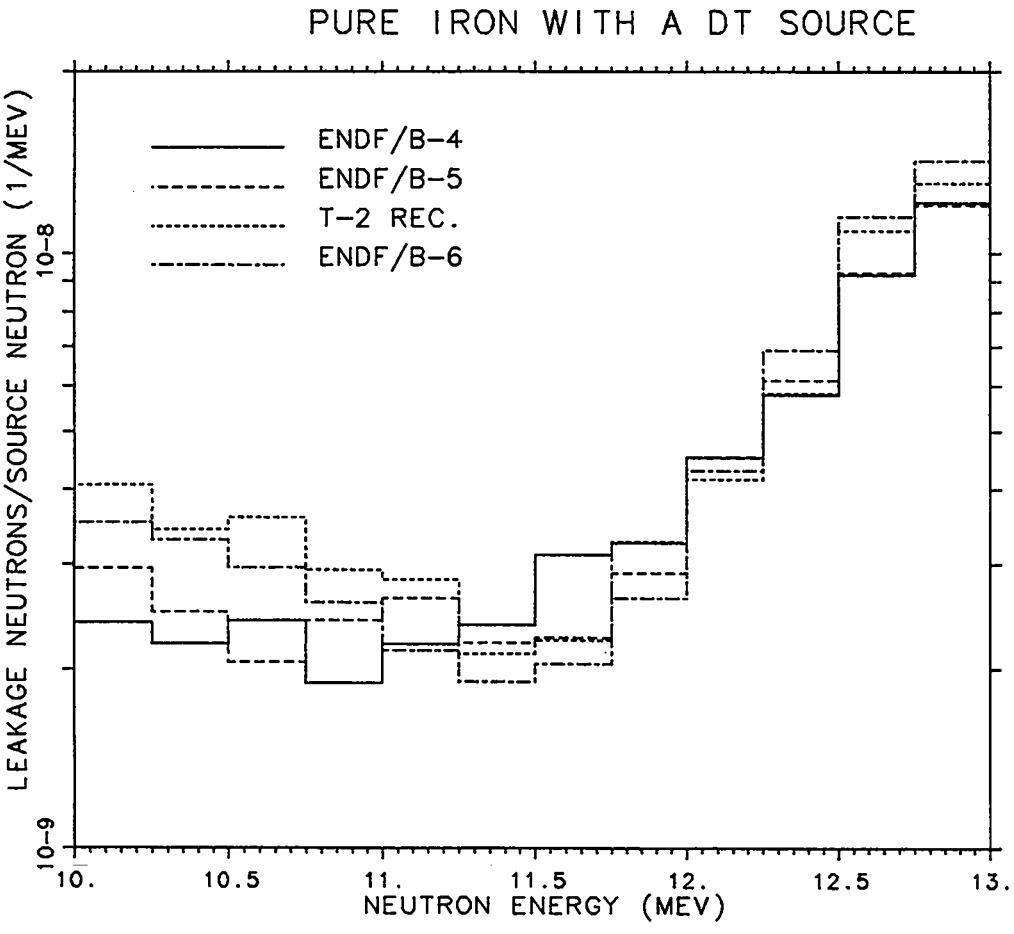

Fig. 47. Plot of pure iron with a T(d,n)^{4}He source for the energy group 10–13 MeV.

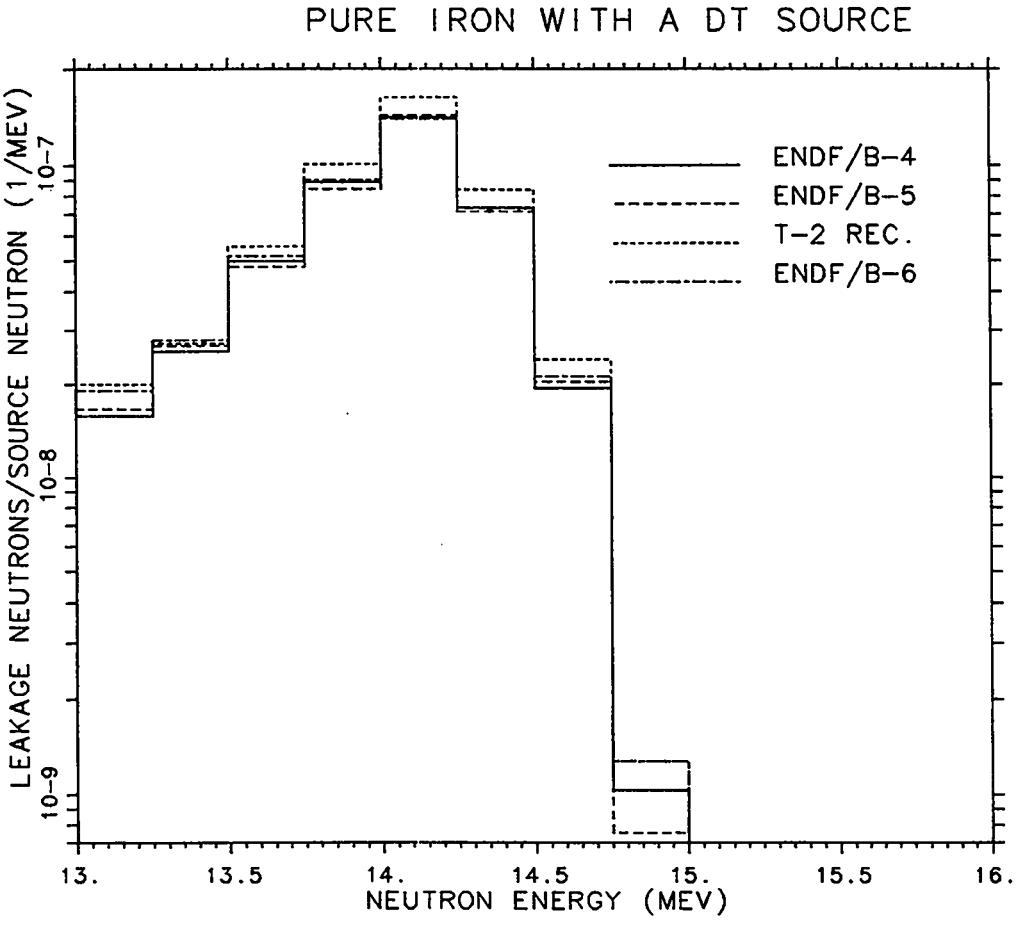

Fig. 48. Plot of pure iron with a $T(d,n)^4He$ source for the energy group > 13 MeV.

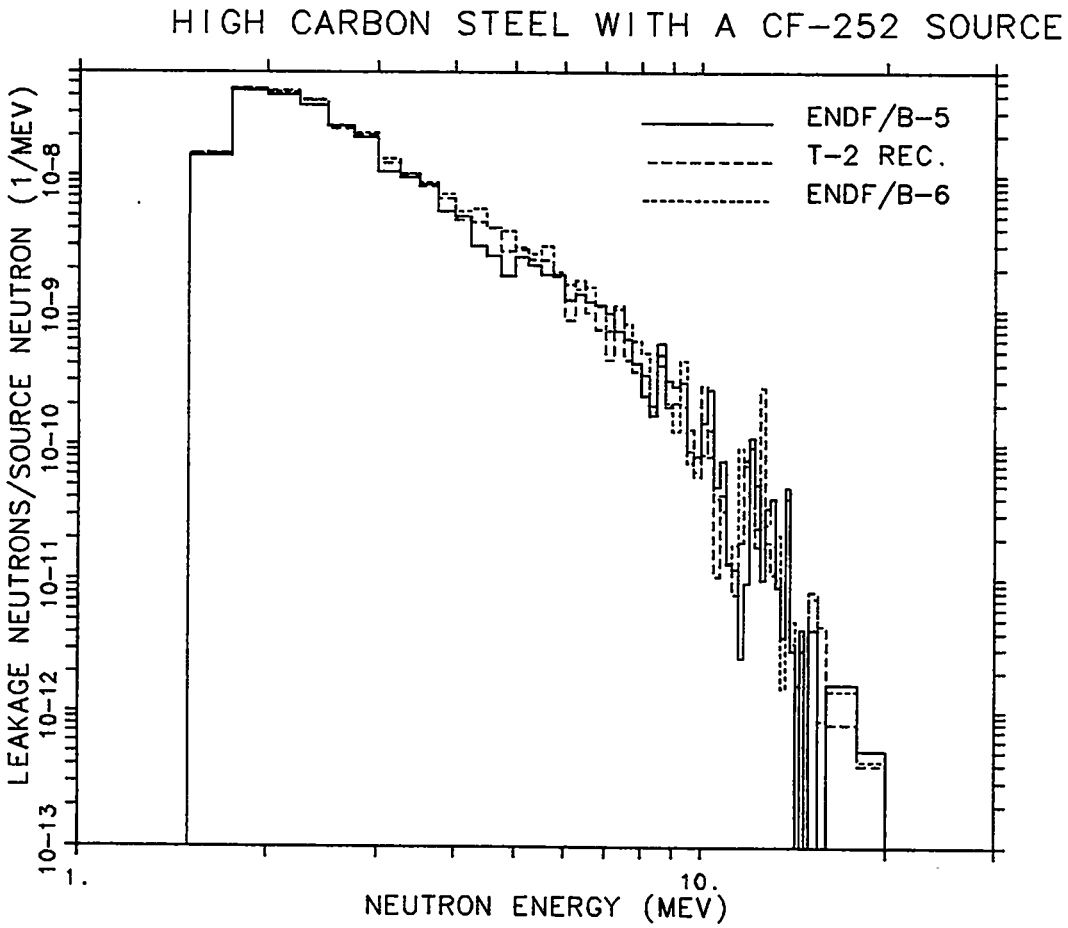

Fig. 49. Plot of ENDF/B-V, MCNP Recommended, and ENDF/B-VI calculated for high carbon steel with a ^{252}Cf source.

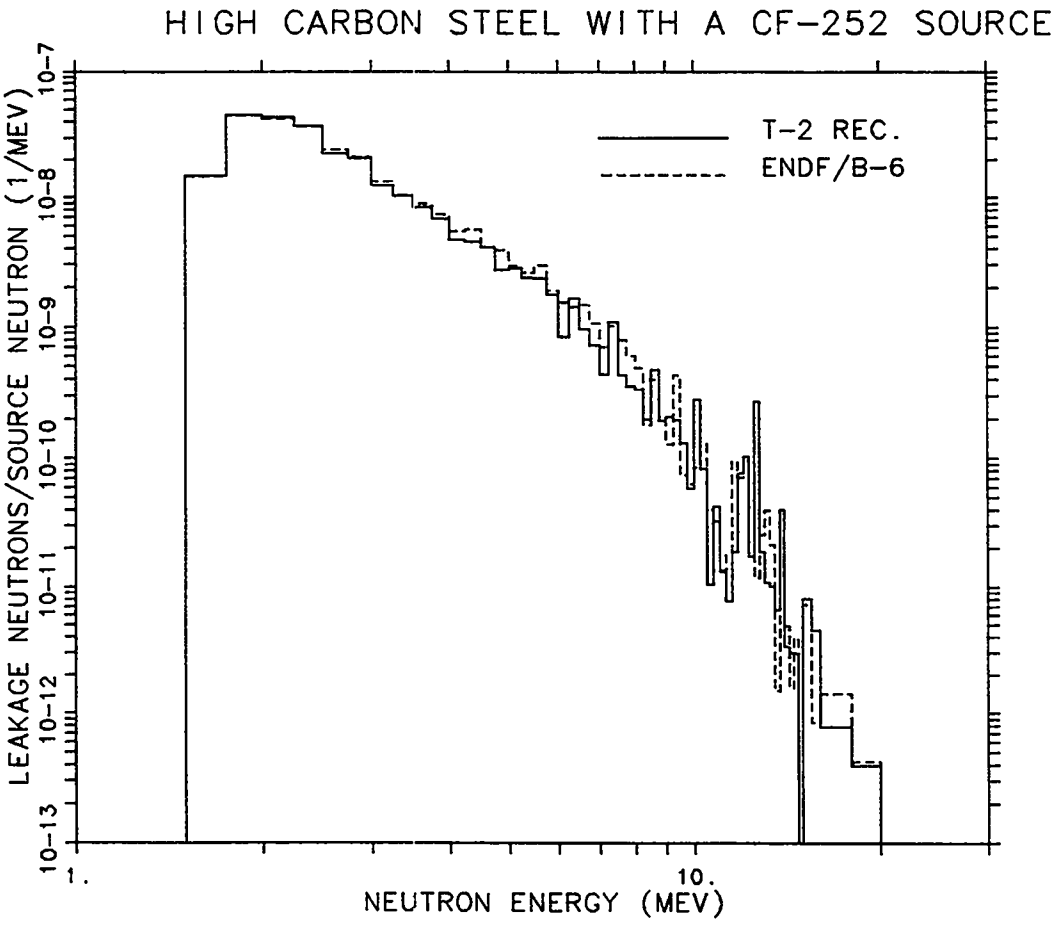

Fig. 50. Plot of MCNP Recommended and ENDF/B-VI calculated for high carbon steel with a ^{252}Cf source.

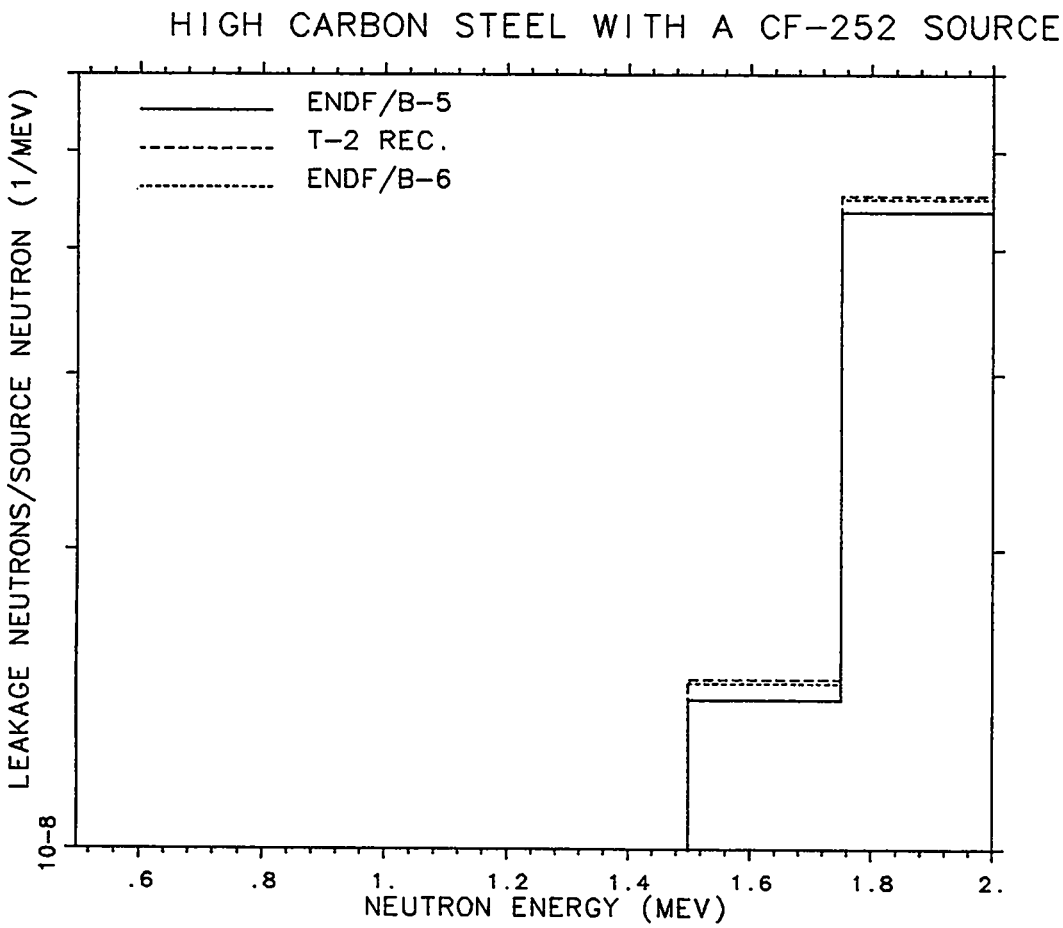

Fig. 51. Plot of high carbon steel with a ^{252}Cf source for the energy group 0.5–2 MeV.

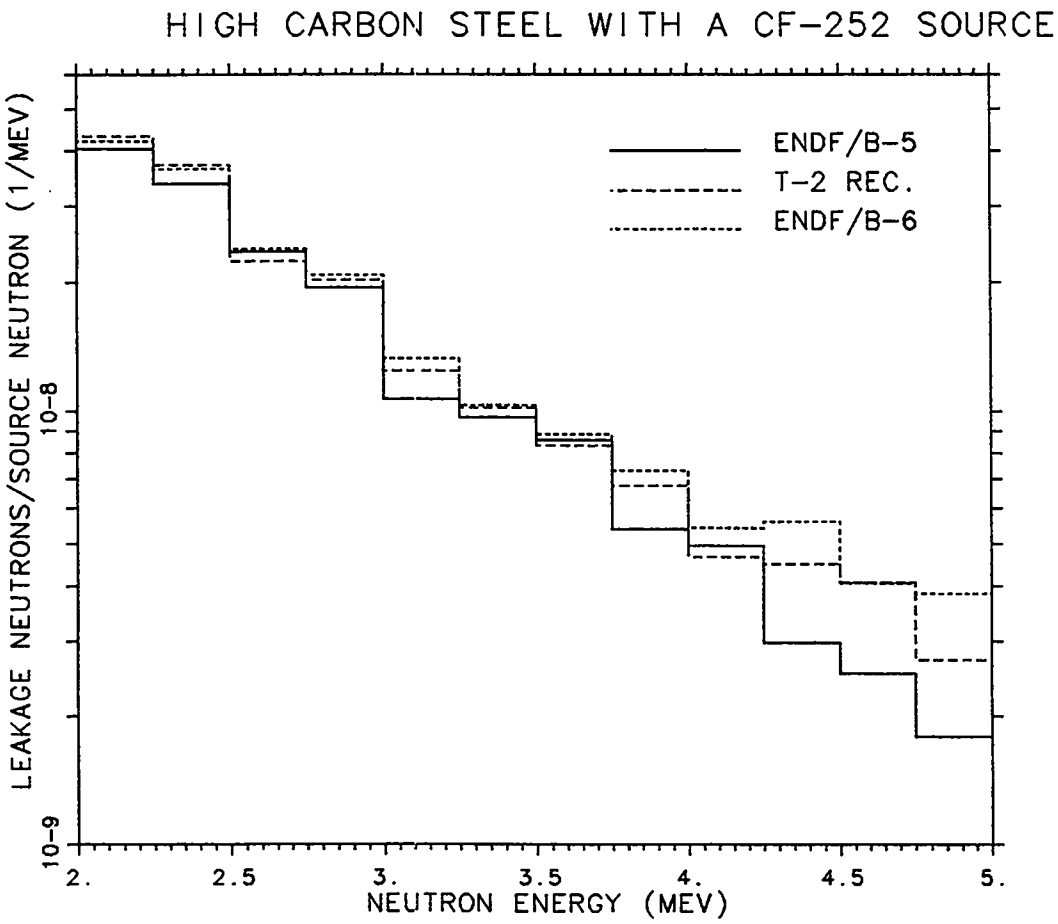

Fig. 52. Plot of high carbon steel with a ^{252}Cf source for the energy group 2–5 MeV.

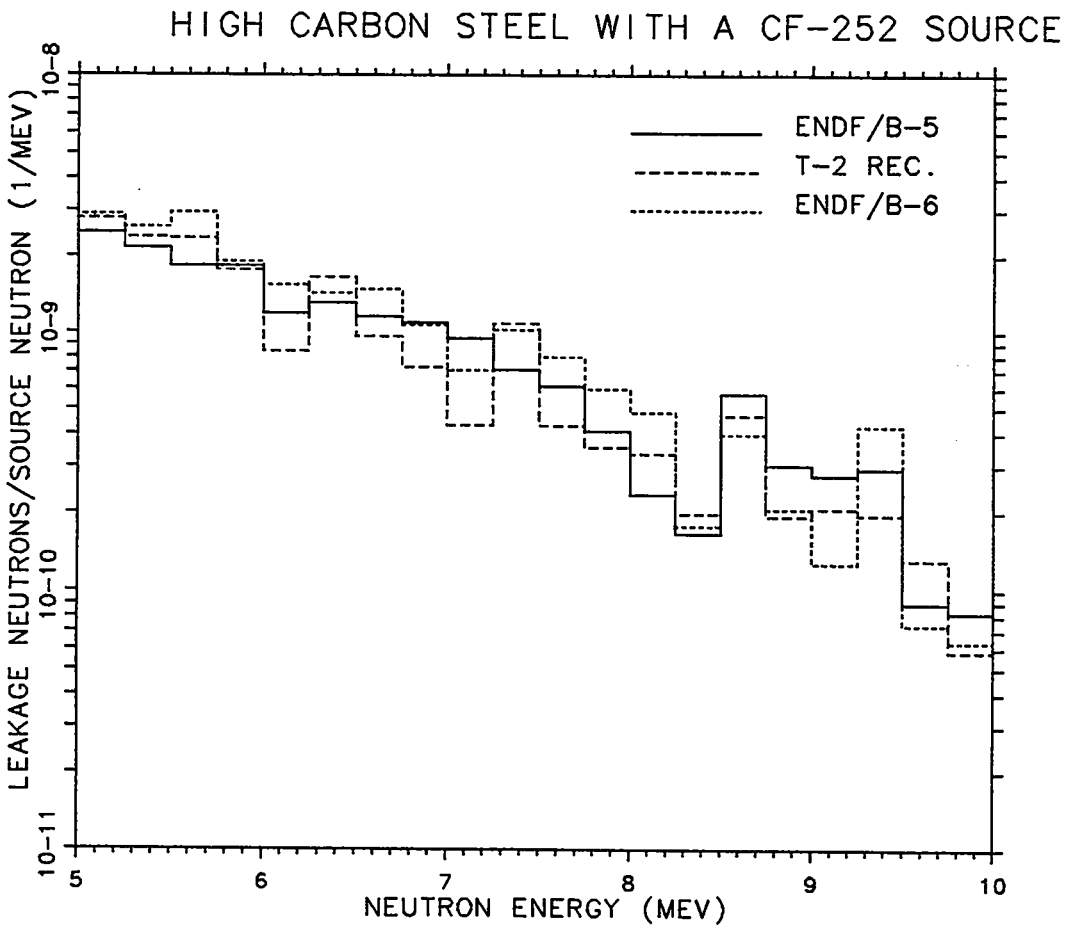

Fig. 53. Plot of high carbon steel with a ^{252}Cf source for the energy group 5–10 MeV.

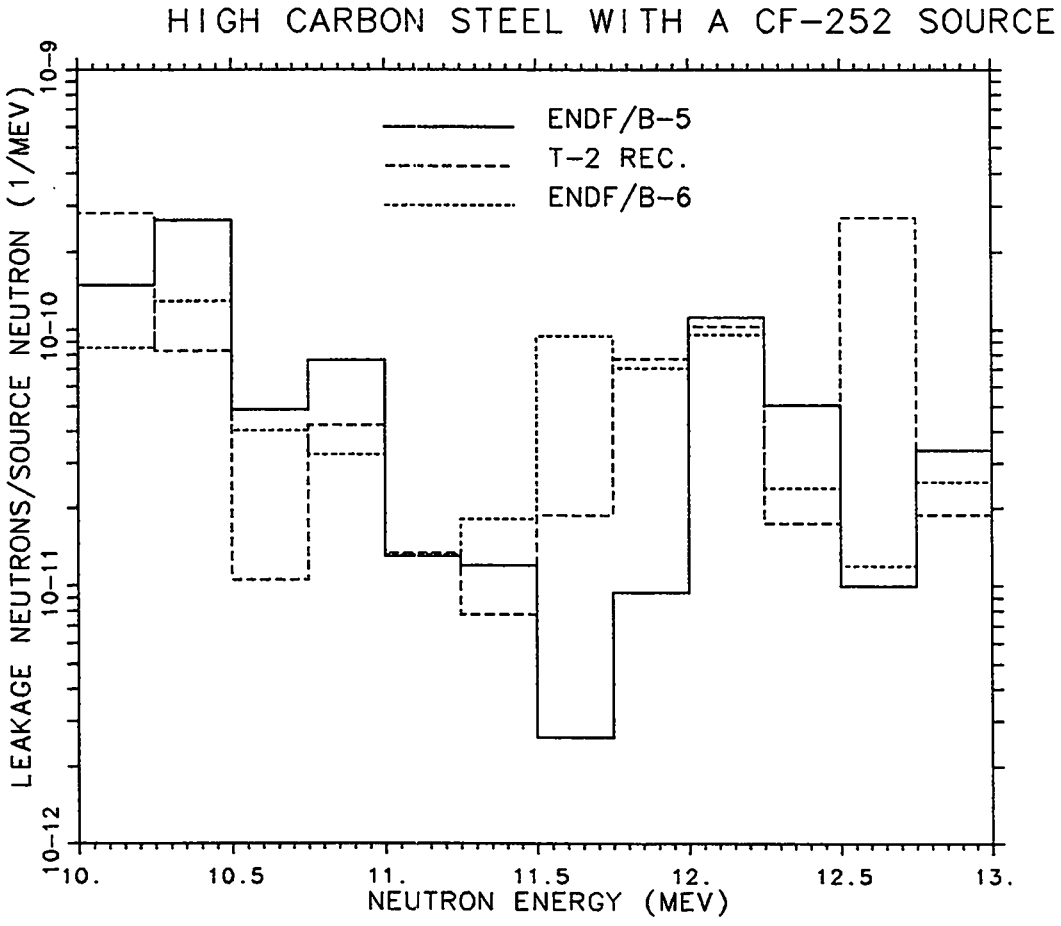

Fig. 54. Plot of high carbon steel with a ^{252}Cf source for the energy group 10–13 MeV.

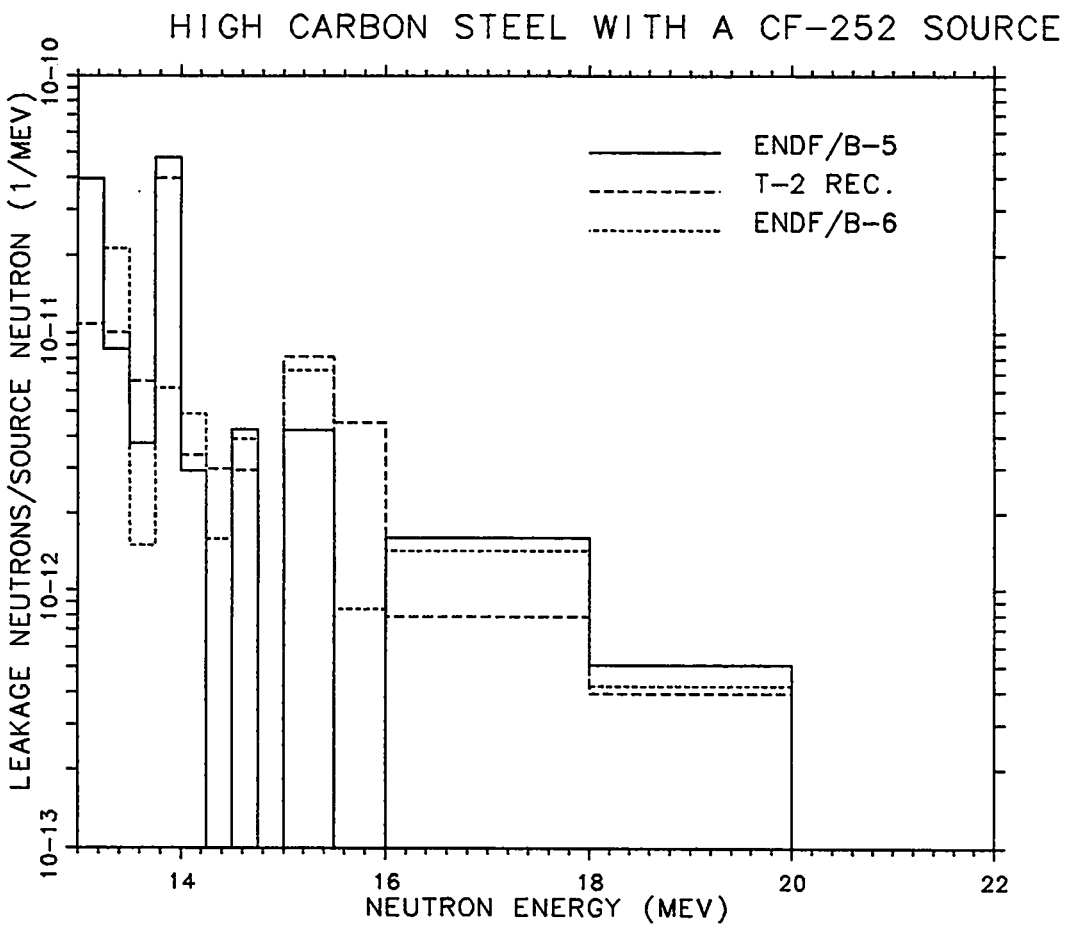

Fig. 55. Plot of high carbon steel with a ^{252}Cf source for the energy group > 13 MeV.

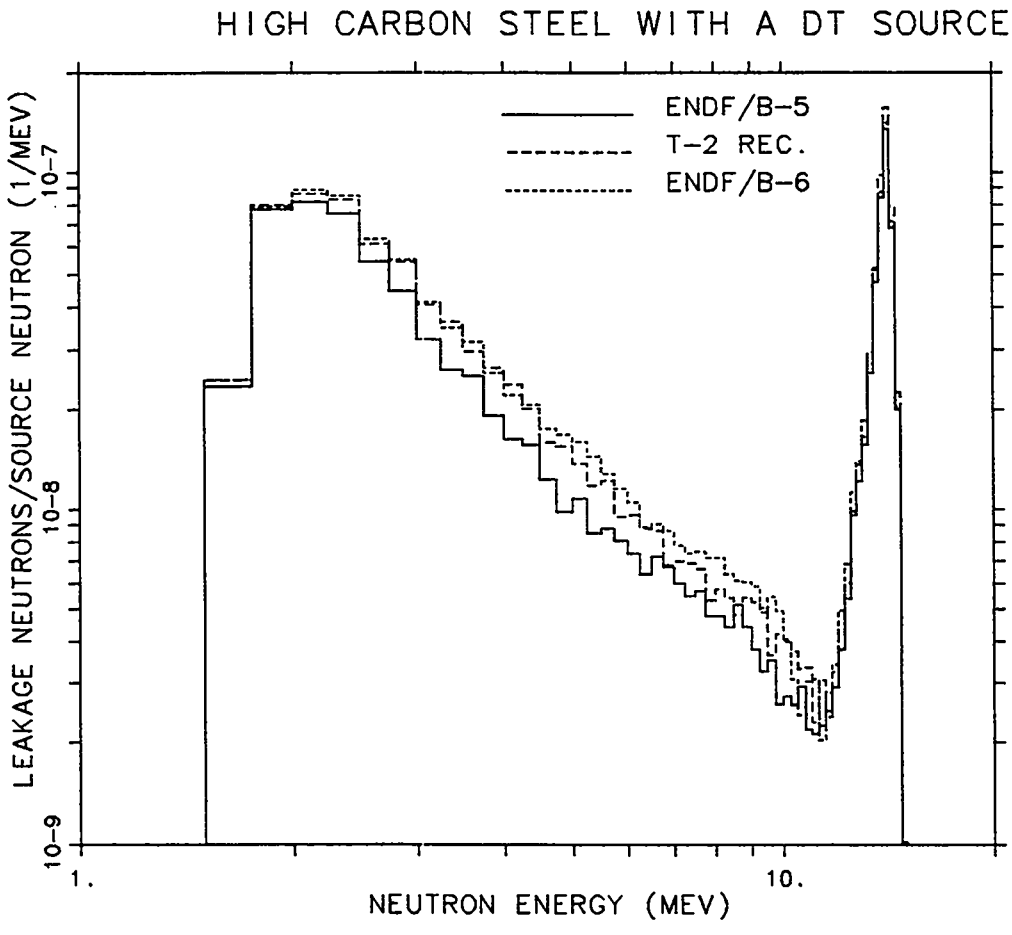

Fig. 56. Plot of ENDF/B-V, MCNP Recommended, and ENDF/B-VI calculated for high carbon steel with a $T(d,n)^4He$ source.

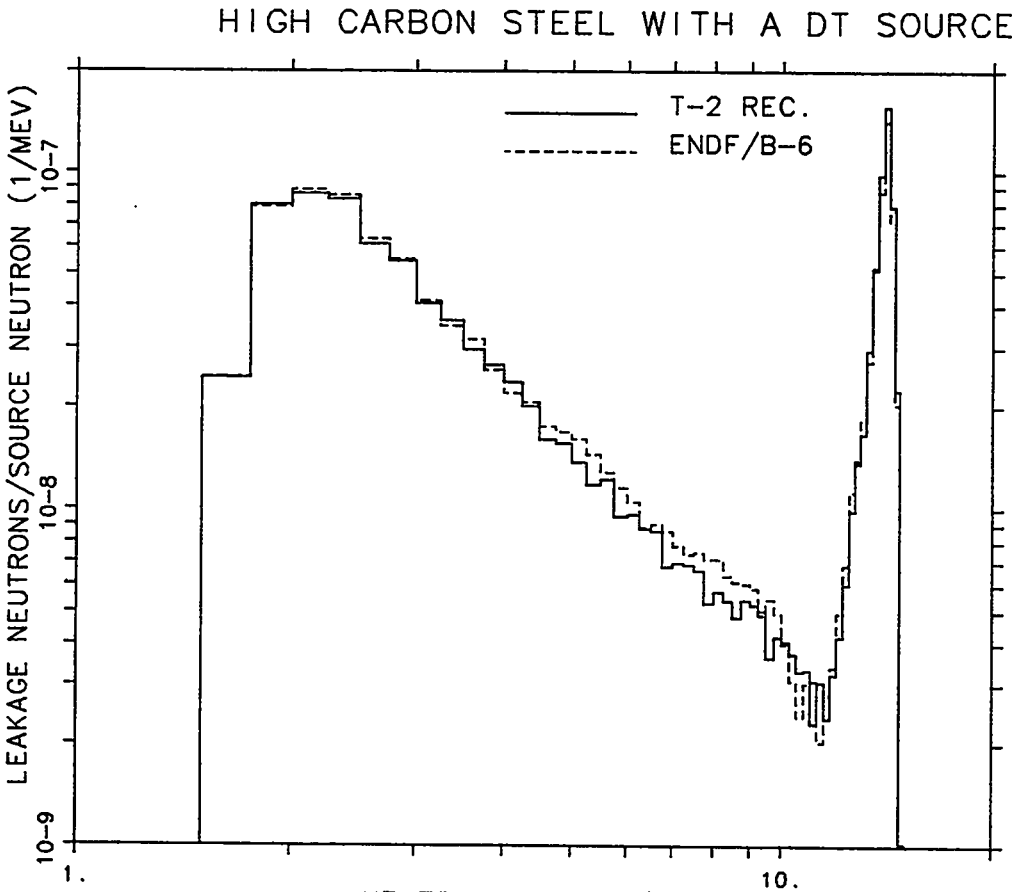

Fig. 57. Plot of MCNP Recommended and ENDF/B-VI calculated for high carbon steel with a $T(d,n)^4He$ source.

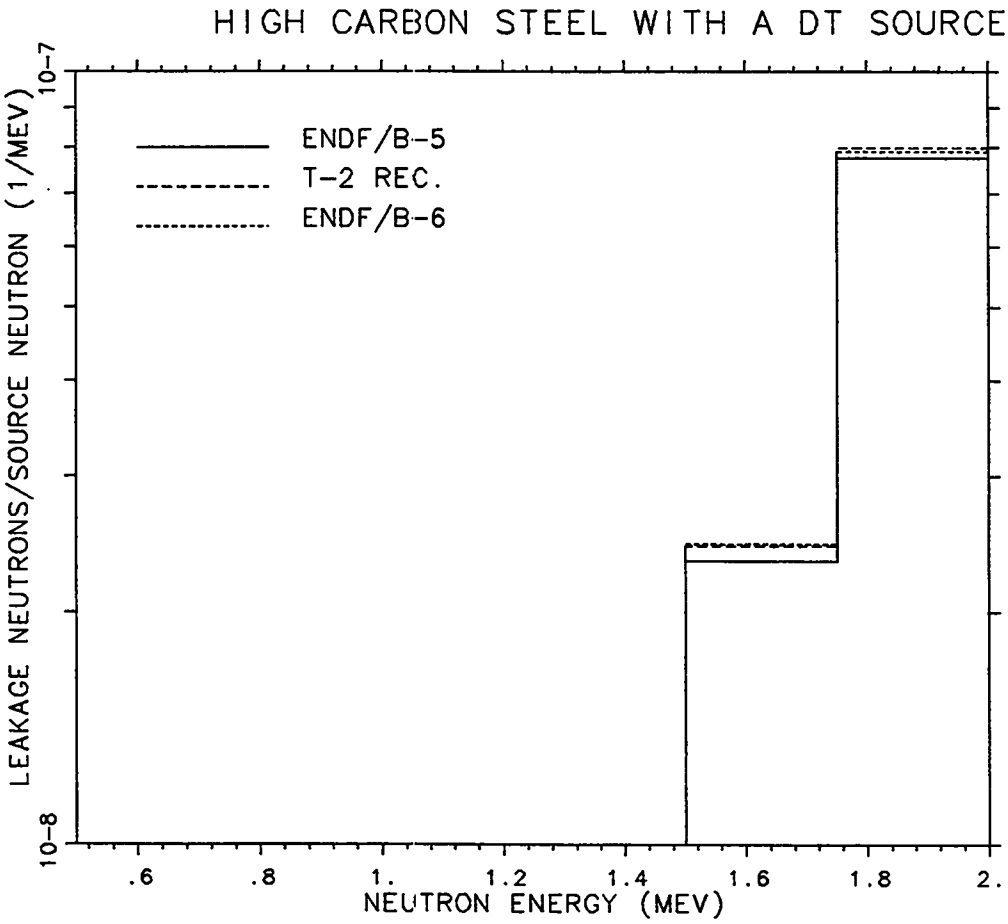

Fig. 58. Plot of high carbon steel with a $T(d,n)^4He$ source for the energy group 0.5–2 MeV.

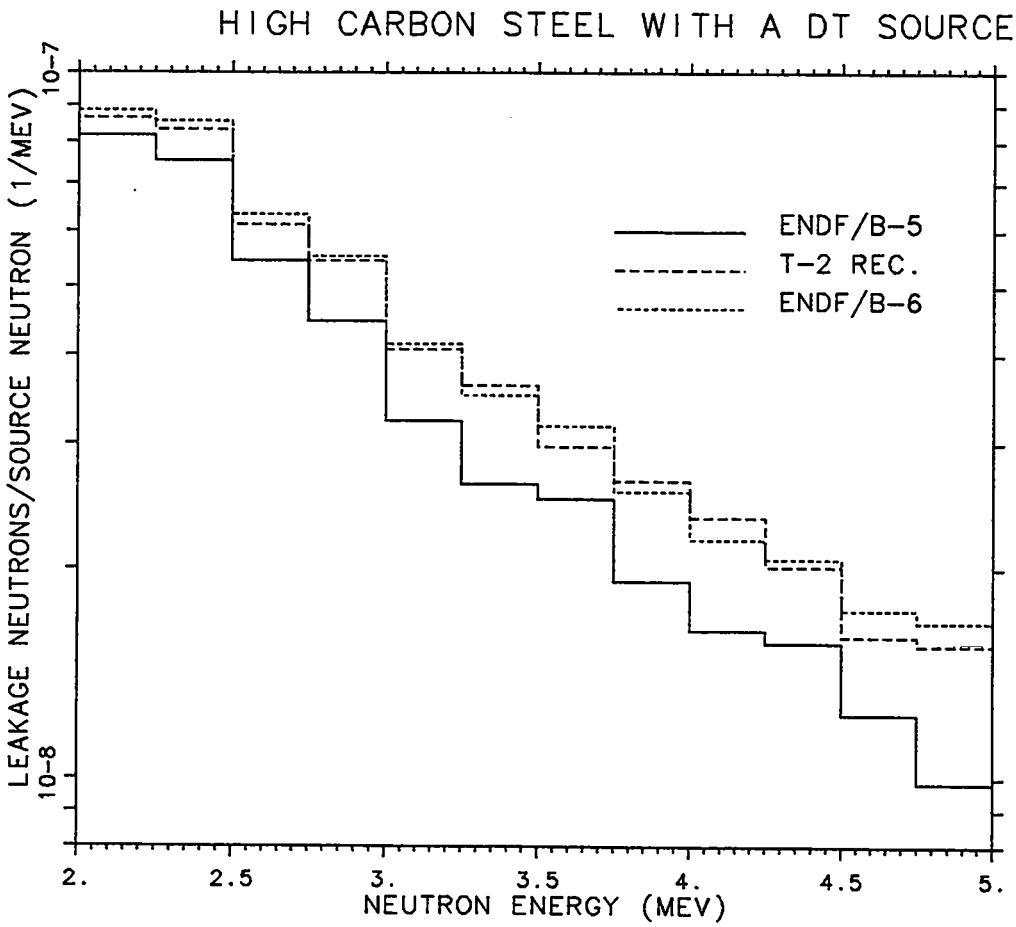

Fig. 59. Plot of high carbon steel with a T(d,n)^{4}He source for the energy group 2–5 MeV.

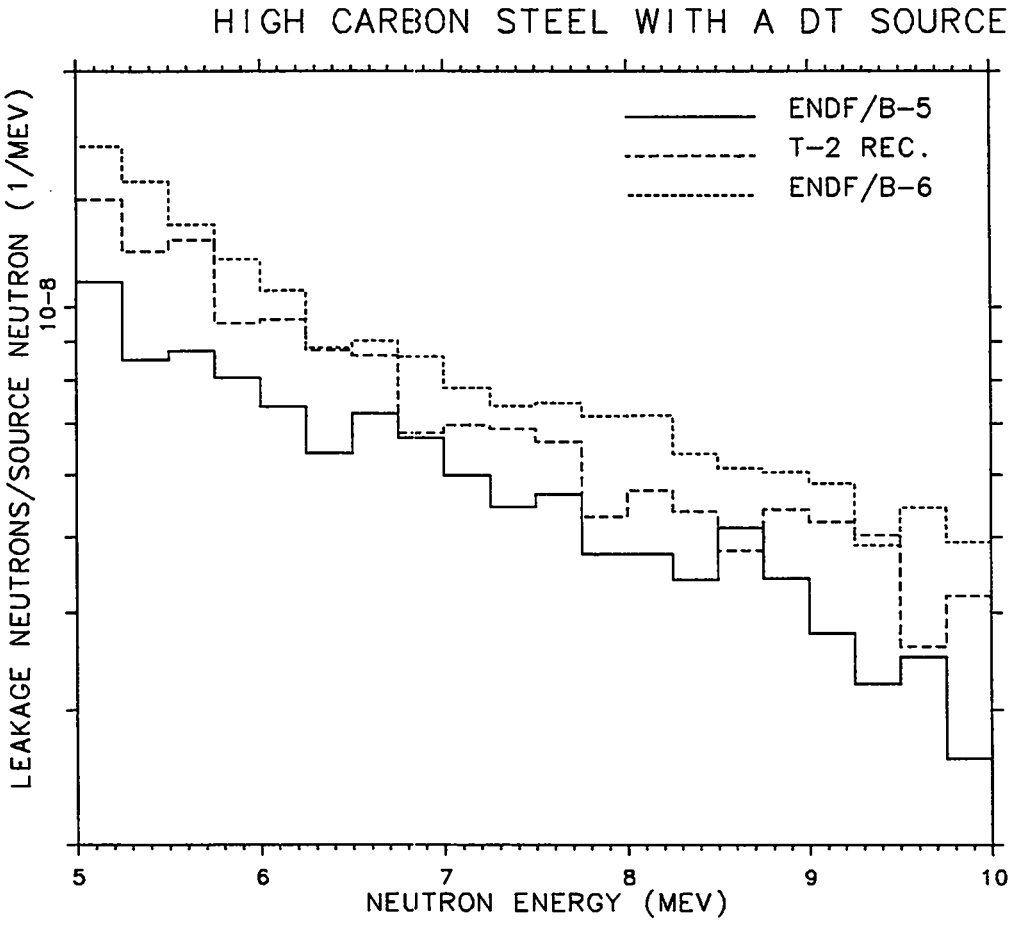

Fig. 60. Plot of high carbon steel with a $T(d,n)^4He$ source for the energy group 5–10 MeV.

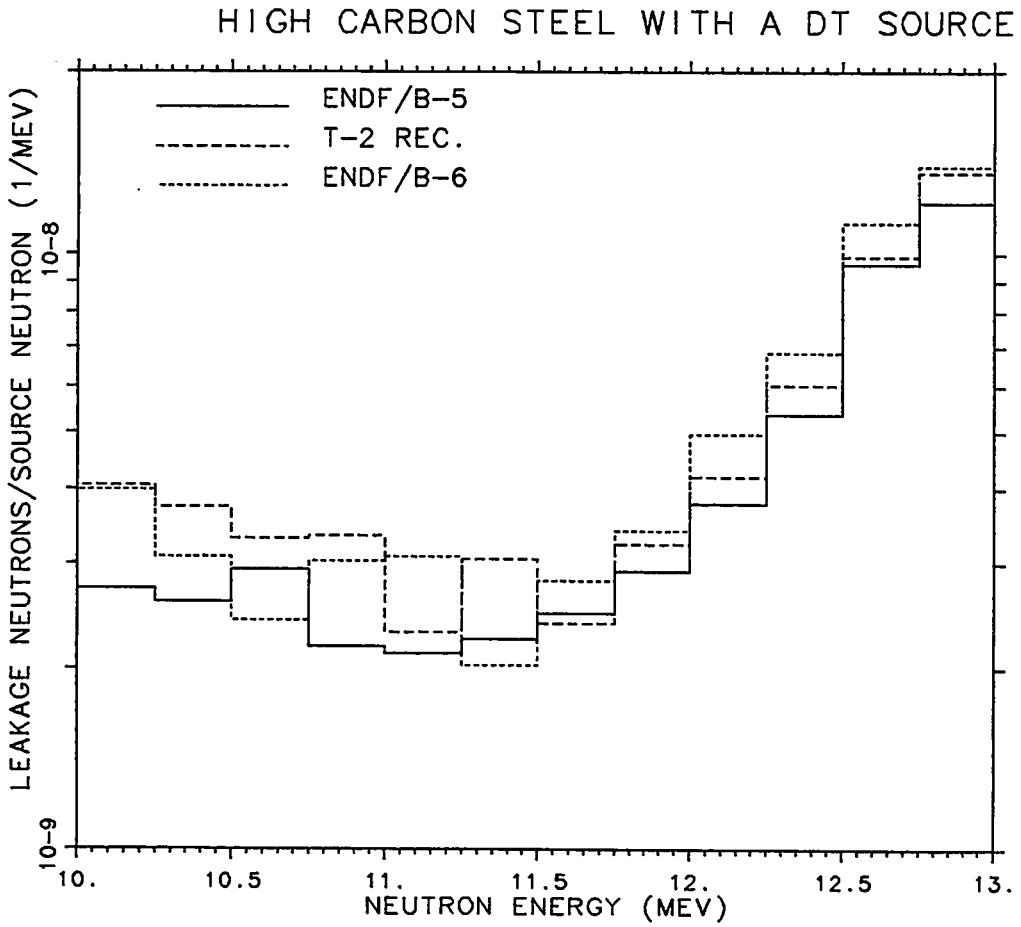

Fig. 61. Plot of high carbon steel with a $T(d,n)^4He$ source for the energy group 10–13 MeV.

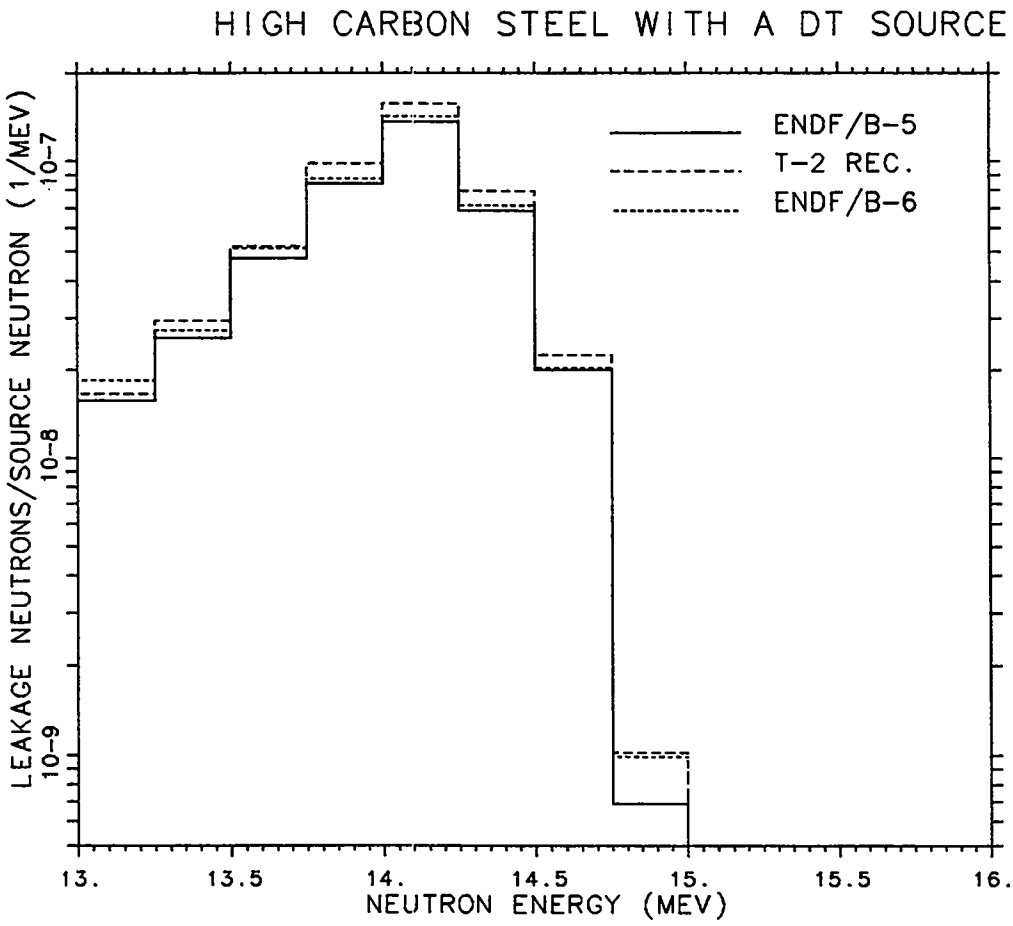

Fig. 62. Plot of high carbon steel with a $T(d,n)^4He$ source for the energy group > 13 MeV.

V. BENCHMARK FOR NEUTRON TRANSPORT THROUGH IRON

A. Experimental Setup

In the early 70's, measurements were undertaken at the Oak Ridge National Laboratory's Tower Shielding Facility to determine the neutron fluence and neutron spectra behind slabs of iron up to 3 feet thick. Using a collimated beam of reactor neutrons as a source, measurements of neutrons above thermal energy through various thicknesses of iron slabs were made with the use of spherical BF_3 detectors surrounded by various thicknesses of polyethylene and an outside shell of cadmium. These Bonner Ball detectors provided measurements of weighted integral flux. Figure 63 shows a schematic of the experimental setup.[16]

Four different thicknesses of iron slab were exposed to the neutron beam, and measurements were made at three different points behind the slab with three different size Bonner Ball detectors, giving nine measurements for each iron slab thickness. The density of the iron slabs averaged 7.79 grams/cm^3. The average composition of the iron slab is shown in Table IX, where it is to be noted that the iron slabs were actually carbon steel. Table X shows the position of the Bonner Ball detectors with respect to the MCNP source, which is located at the origin of the coordinate system.

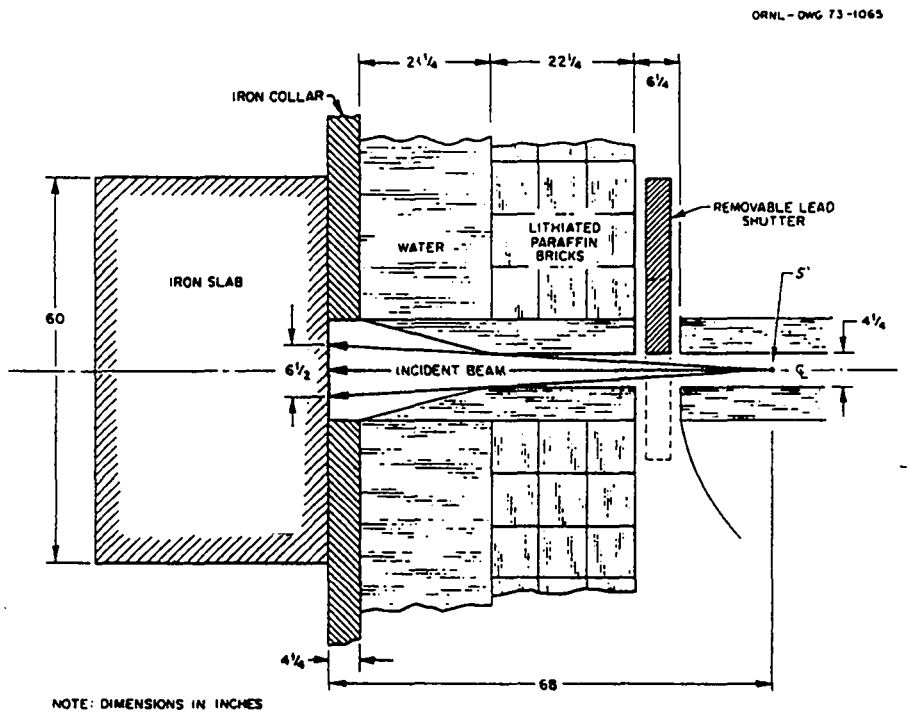

Fig. 63. Oak Ridge Iron Transport Benchmark Layout.

TABLE IX. **Composition of the Iron Slabs in atom/cm Barns.**

Element	Composition
Carbon	9.815×10^{-4}
Manganese	5.55×10^{-4}
Iron	8.372×10^{-2}

TABLE X. **Experimental Configuration for the Iron Transmission Measurements.**

Detector Locations		
Iron Slab Thickness (cm)	Observation Angle[a] With Respect to Centerline (degrees)	Coordinate Position
3.937	0	(-562.74, 0, 0)
	15	(-547.50, 99.06. 0)
	45	(-448.44, 271.78, 0)
30.810	0	(-561.67, 0, 0)
	15	(-548.97, 92.71. 0)
	45	(-457.53, 254.00, 0)
62.001	0	(-559.84, 0, 0)
	15	(-549.68, 83.82, 0)
	45	(-464.59, 229.87, 0)
92.862	0	(-548.68, 0, 0)
	15	(-538.52, 76.20, 0)
	45	(-463.59, 207.01, 0)

[a]The observation angle is defined as the angle between the centerline and a line connecting the detector and the midpoint of the emergent face of the slab. The vertex of this angle is the pivot point for the angular traverses.

B. Results and Discussion

The MCNP calculations were done for each iron slab thickness using the four data sets of interest:

- ENDF/B-IV
- ENDF/B-V
- T-2 Recommended MCNP Library
- ENDF/B-VI

An attempt to duplicate previous results[17] produced results that grew progressively worse as the slabs got thicker. It is unfortunate that the problem setup for the earlier analysis of this experiment is not available and the present model inadequately models the experiment. The disagreement with experimental results indicates that there is a fundamental problem in the manner in which the problem is set up. The comparisons to experimental results are given in Tables XI through XIV and, if anything, ENDF/B-VI appears to give the worst results. Fortunately, the results can be compared between data sets, which is the focus of this work. Each Bonner Ball detector calculation was normalized to the ENDF/B-V results for the detector type and position. These normalized results are shown with the resultant spectra in Figures 64 through 99. In these comparisons, ENDF/B-VI proves to be about the same as the other data libraries.

TABLE XI. **Comparison to Experiment for the 3.94 cm Iron Slab.**

Data Set	Observation Angle (deg)	% Deviation from Experiment		
		3.09 inch	5.88 inch	9.86 inch
ENDF/B-IV	0	2.0	-3.3	0.1
	15	10.3	0.9	-0.3
	45	10.9	8.0	7.5
ENDF/B-V	0	1.7	-4.4	-0.7
	15	10.1	1.1	0.3
	45	9.7	7.6	8.0
T-2 Rec.	0	2.4	-3.2	0.1
	15	9.5	0.8	1.1
	45	8.9	6.6	8.0
ENDF/B-VI	0	2.4	-2.5	0.6
	15	10.7	0.8	1.6
	45	10.4	6.3	7.9

TABLE XII. **Comparison to Experiment for the 30.81 cm Iron Slab.**

Data Set	Observation Angle (deg)	% Deviation from Experiment		
		3.09 inch	5.88 inch	9.86 inch
ENDF/B-IV	0	-4.7	-16.7	-18.5
	15	11.3	6.4	4.3
	45	12.1	10.4	7.5
ENDF/B-V	0	-6.1	-23.5	-28.9
	15	11.0	4.6	0.1
	45	11.4	8.0	2.3
T-2 Rec.	0	-4.6	-17.2	-19.3
	15	9.8	5.6	3.6
	45	10.5	9.3	6.4
ENDF/B-VI	0	1.5	-3.1	-3.1
	15	10.2	5.7	5.3
	45	10.6	9.9	9.2

TABLE XIII. **Comparison to Experiment for the 62.00 cm Iron Slab.**

Data Set	Observation Angle (deg)	% Deviation from Experiment		
		3.09 inch	5.88 inch	9.86 inch
ENDF/B-IV	0	6.7	-9.3	-18.3
	15	17.8	9.9	-0.1
	45	40.0	27.6	10.6
ENDF/B-V	0	13.6	-6.2	-21.7
	15	20.3	9.4	-5.4
	45	42.9	27.3	5.7
T-2 Rec.	0	10.0	-6.1	-16.4
	15	18.0	9.2	-2.3
	45	38.1	26.1	7.9
ENDF/B-VI	0	16.6	15.4	15.8
	15	12.1	9.6	4.3
	45	32.0	26.9	16.1

TABLE XIV. **Comparison to Experiment for the 92.86 cm Iron Slab.**

Data Set	Observation Angle (deg)	% Deviation from Experiment		
		3.09 inch	5.88 inch	9.86 inch
ENDF/B-IV	0	18.5	5.2	-7.7
	15	34.2	26.4	8.4
	45	77.4	70.6	47.3
ENDF/B-V	0	31.0	17.9	0.1
	15	40.3	30.7	8.4
	45	81.7	73.5	45.7
T-2 Rec.	0	23.8	11.8	-2.4
	15	35.4	27.3	7.5
	45	77.2	69.4	43.8
ENDF/B-VI	0	28.0	36.9	40.6
	15	29.3	31.0	20.9
	45	81.6	86.1	69.8

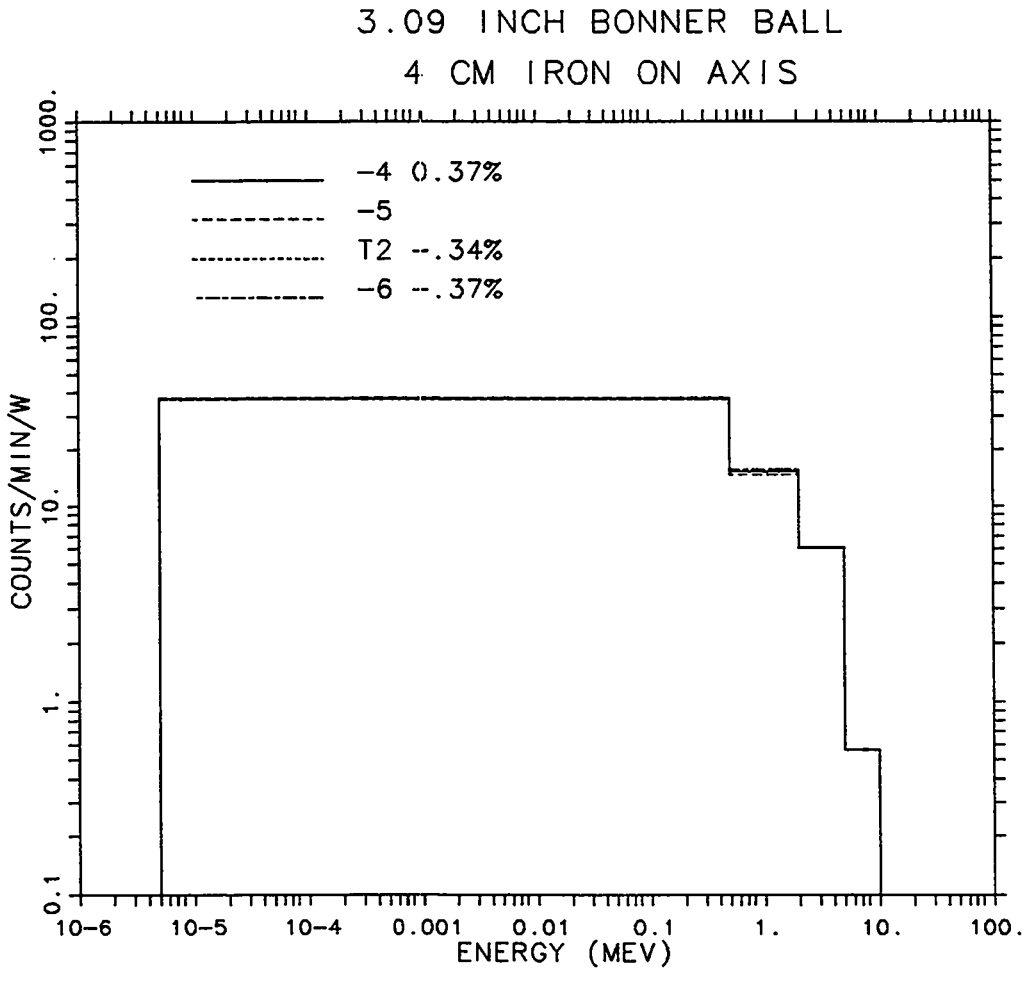

Fig. 64. Data set comparisons for the 4 cm iron slab, with the 3.09 in Bonner Ball on axis. (Normalized to ENDF/B-V)

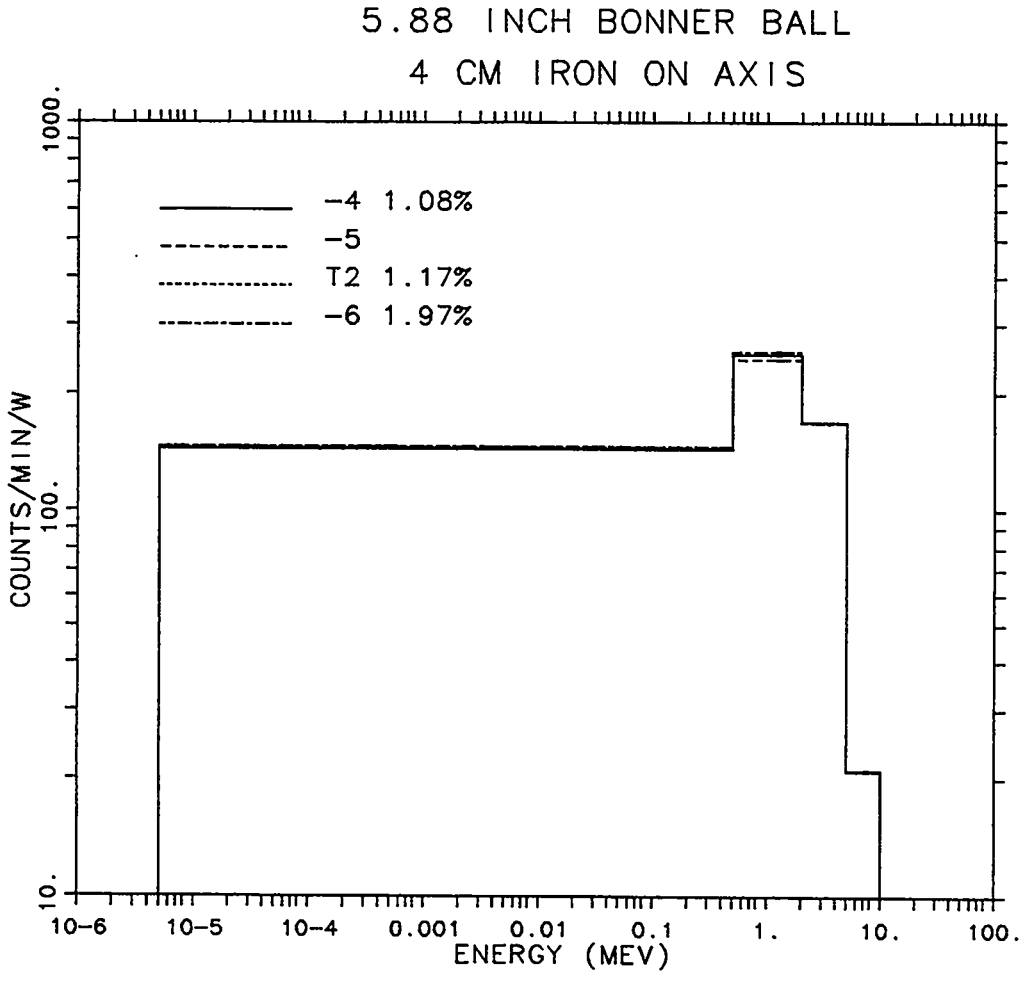

Fig. 65. Data set comparisons for the 4 cm iron slab, with the 5.88 in Bonner Ball on axis. (Normalized to ENDF/B-V)

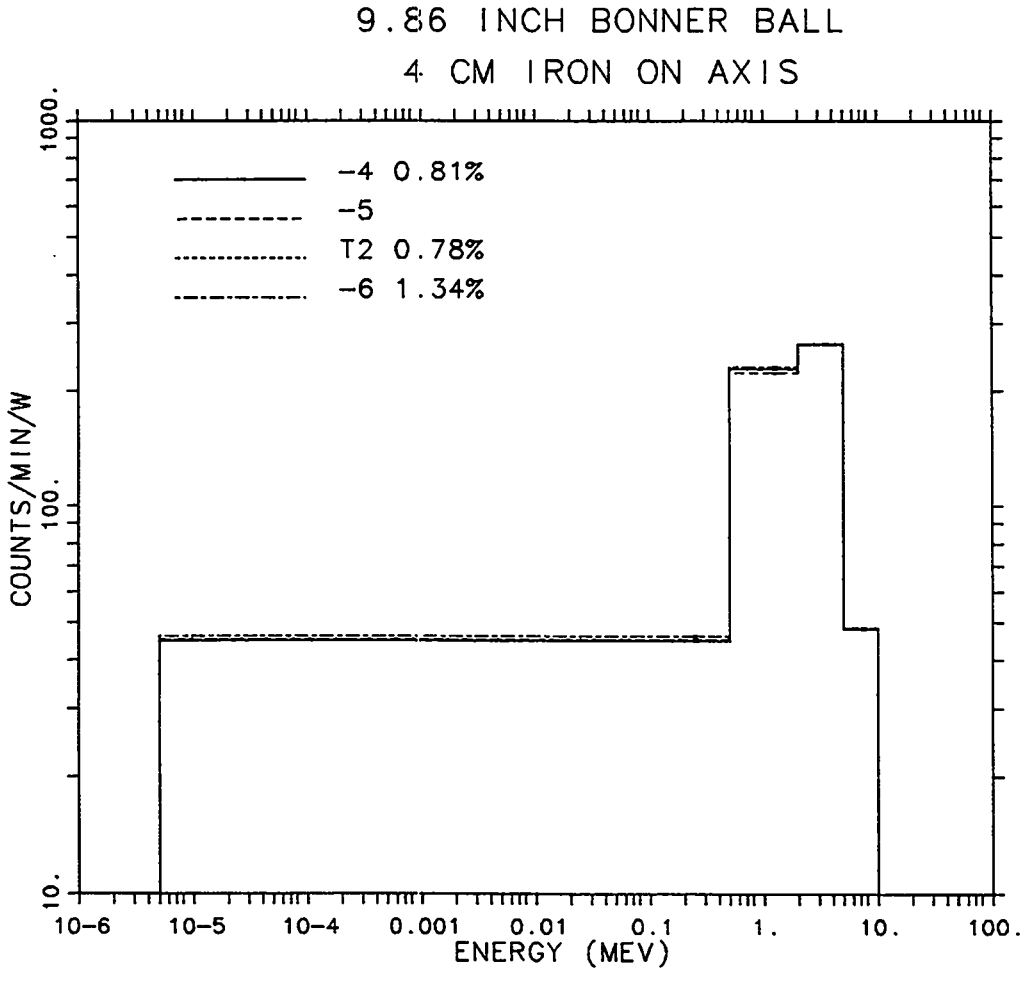

Fig. 66. Data set comparisons for the 4 cm iron slab, with the 9.86 in Bonner Ball on axis. (Normalized to ENDF/B-V)

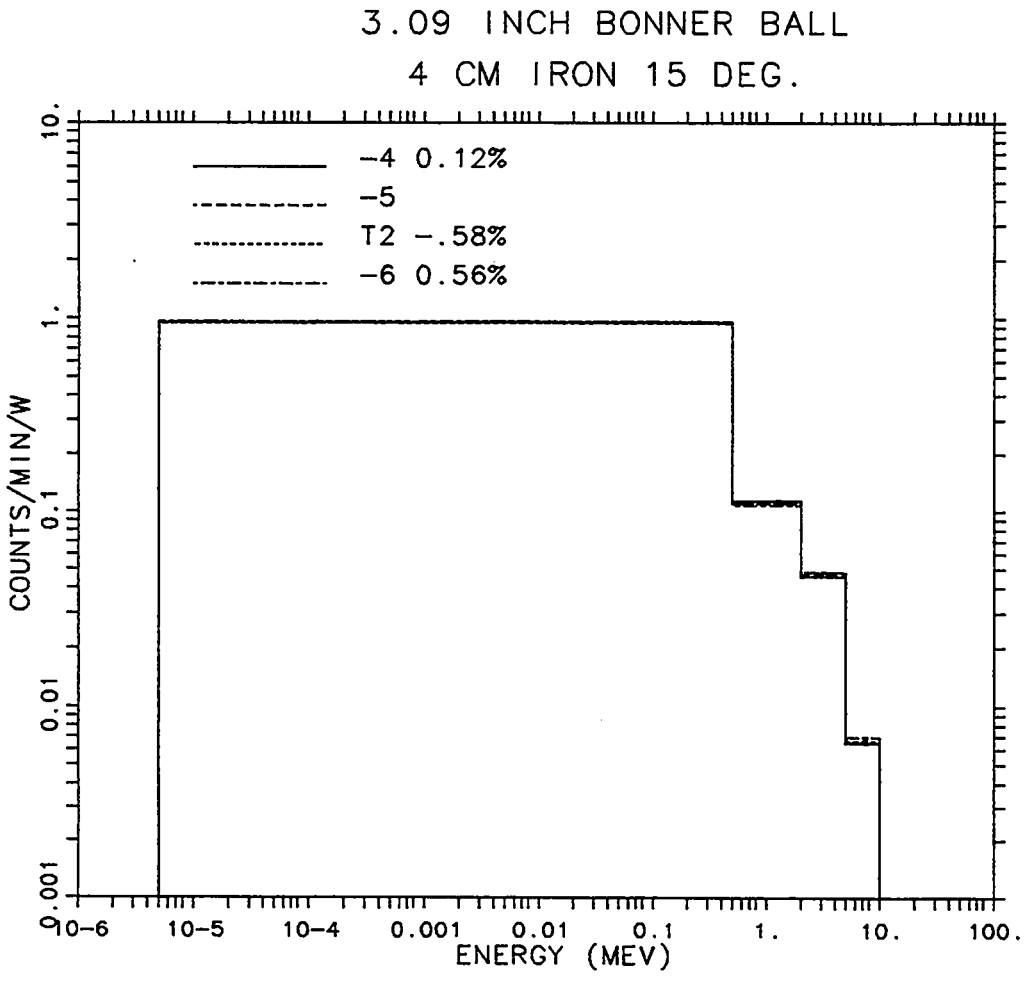

Fig. 67. Data set comparisons for the 4 cm iron slab, with the 3.09 in Bonner Ball at the 15 degree observation angle. (Normalized to ENDF/B-V)

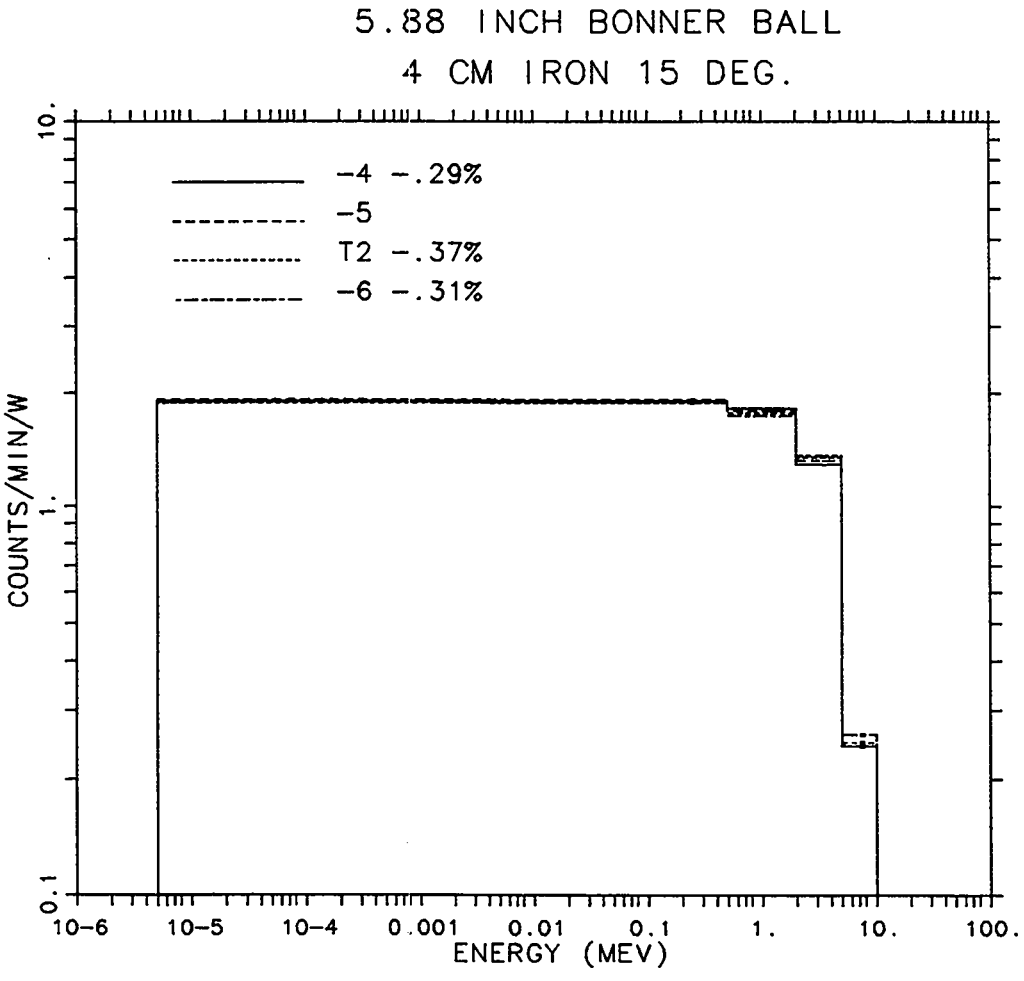

Fig. 68. Data set comparisons for the 4 cm iron slab, with the 5.88 in Bonner Ball at the 15 degree observation angle. (Normalized to ENDF/B-V)

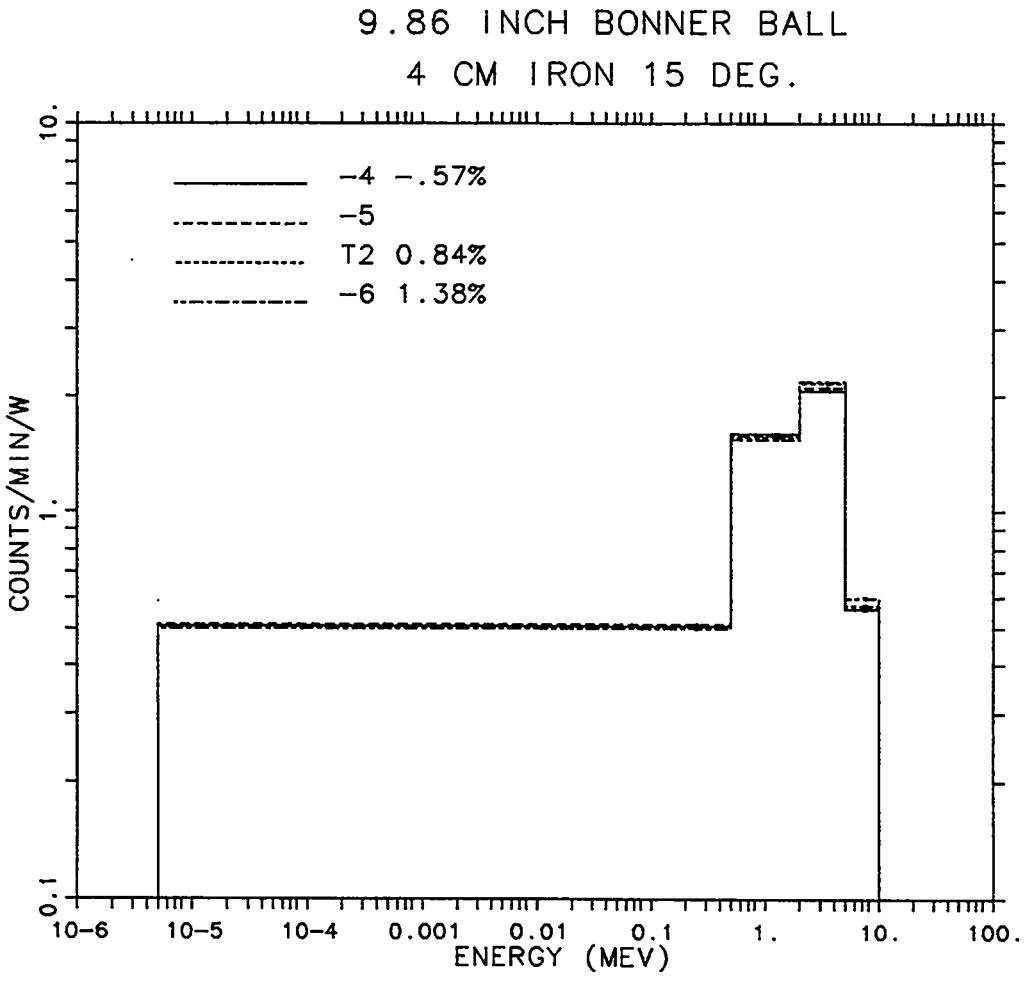

Fig. 69. Data set comparisons for the 4 cm iron slab, with the 9.86 in Bonner Ball at the 15 degree observation angle. (Normalized to ENDF/B-V)

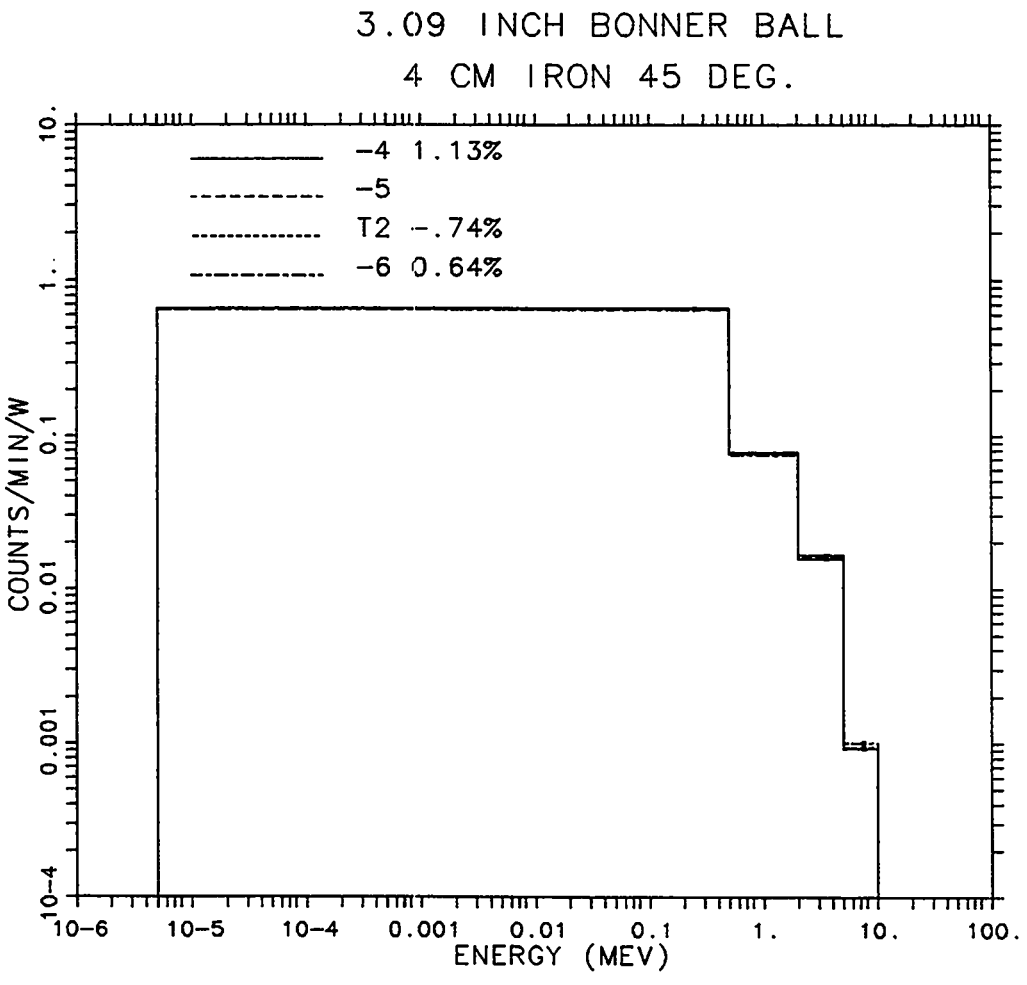

Fig. 70. Data set comparisons for the 4 cm iron slab, with the 3.09 in Bonner Ball at the 45 degree observation angle. (Normalized to ENDF/B-V)

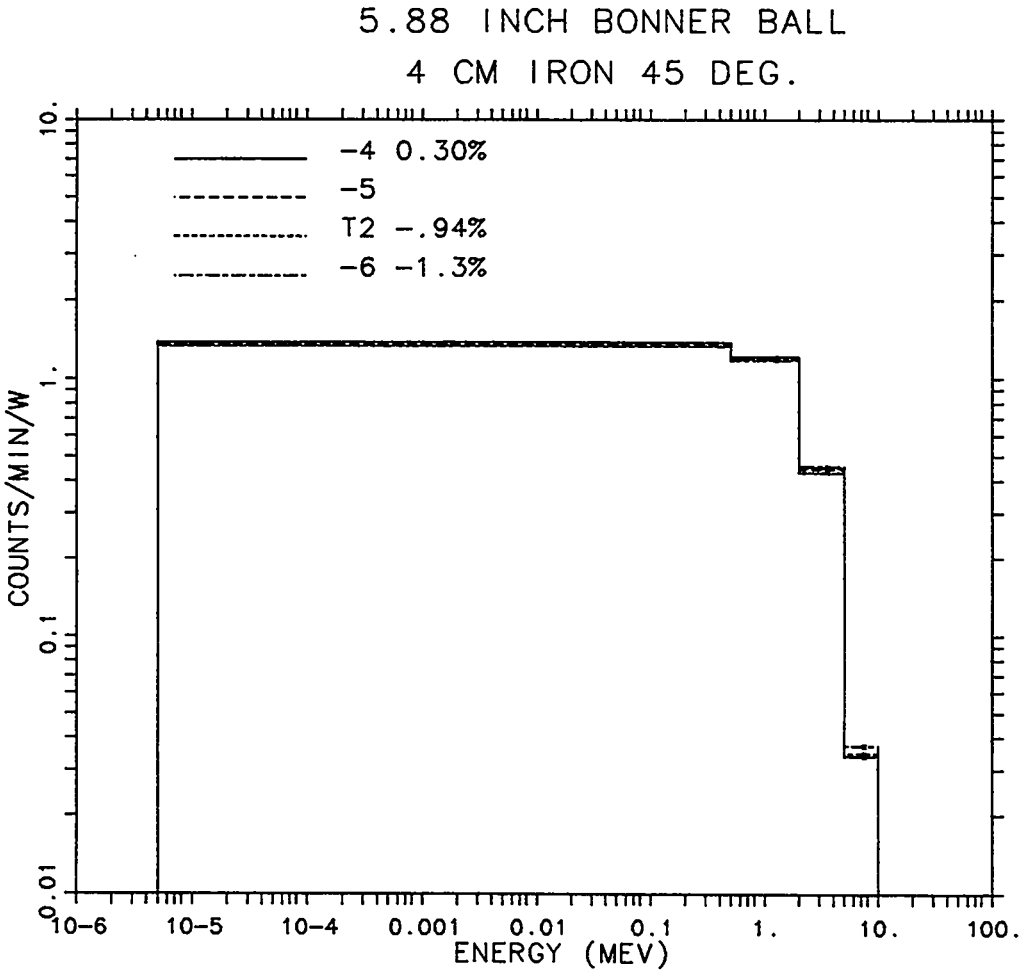

Fig. 71. Data set comparisons for the 4 cm iron slab, with the 5.88 in Bonner Ball at the 45 degree observation angle. (Normalized to ENDF/B-V)

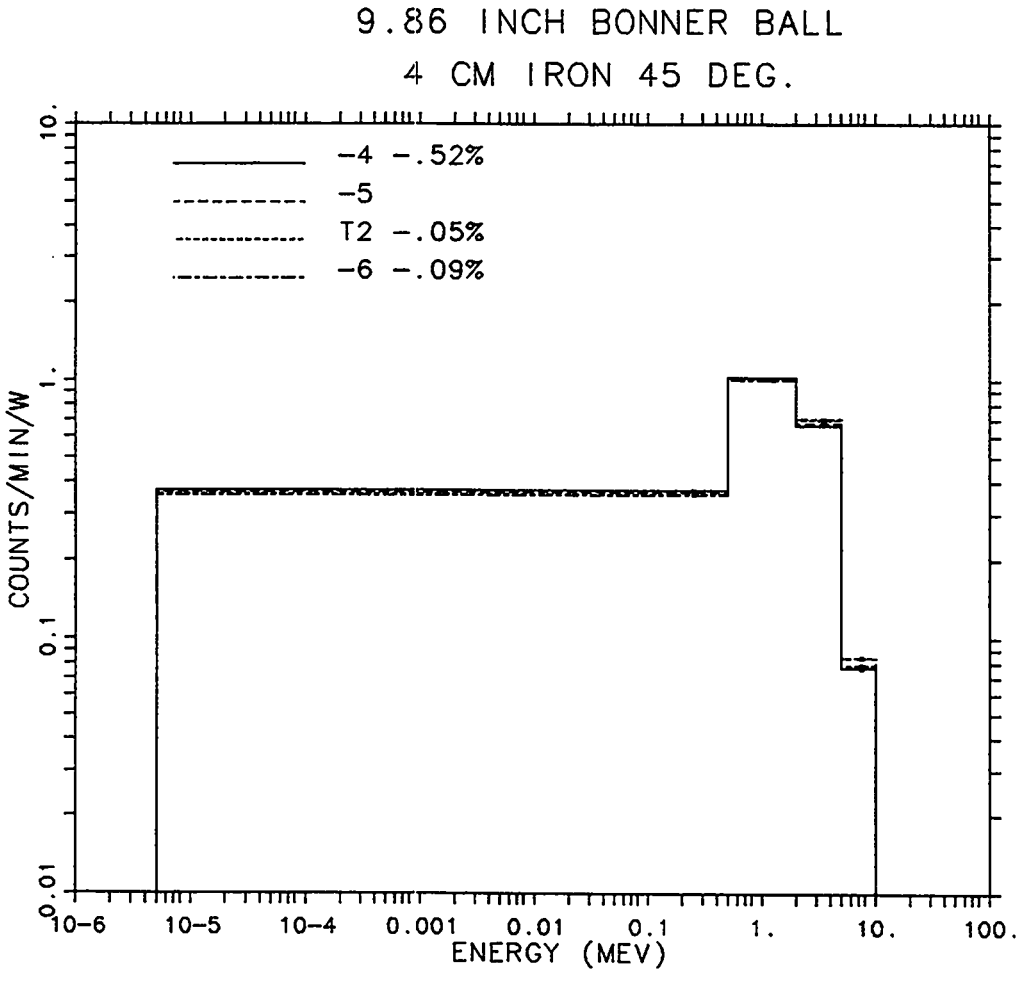

Fig. 72. Data set comparisons for the 4 cm iron slab, with the 9.86 in Bonner Ball at the 45 degree observation angle. (Normalized to ENDF/B-V)

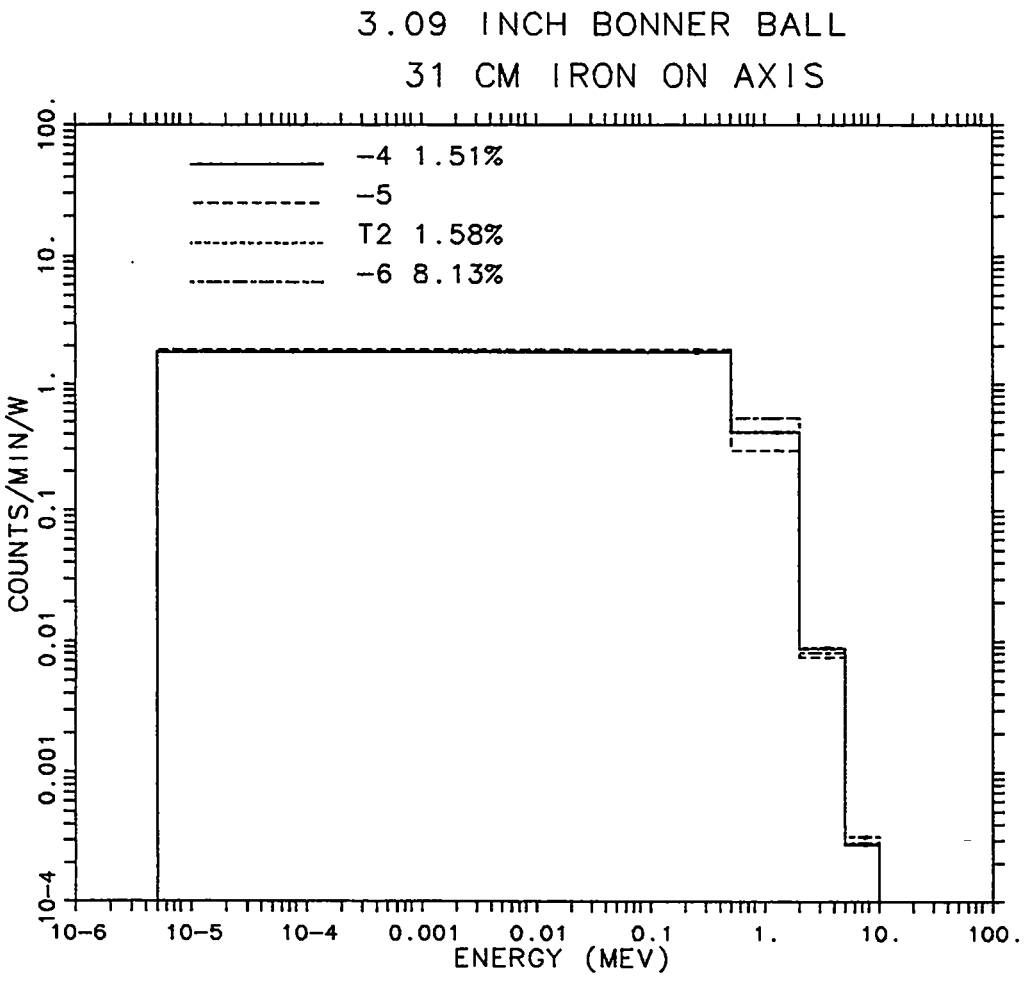

Fig. 73. Data set comparisons for the 31 cm iron slab, with the 3.09 in Bonner Ball on axis. (Normalized to ENDF/B-V)

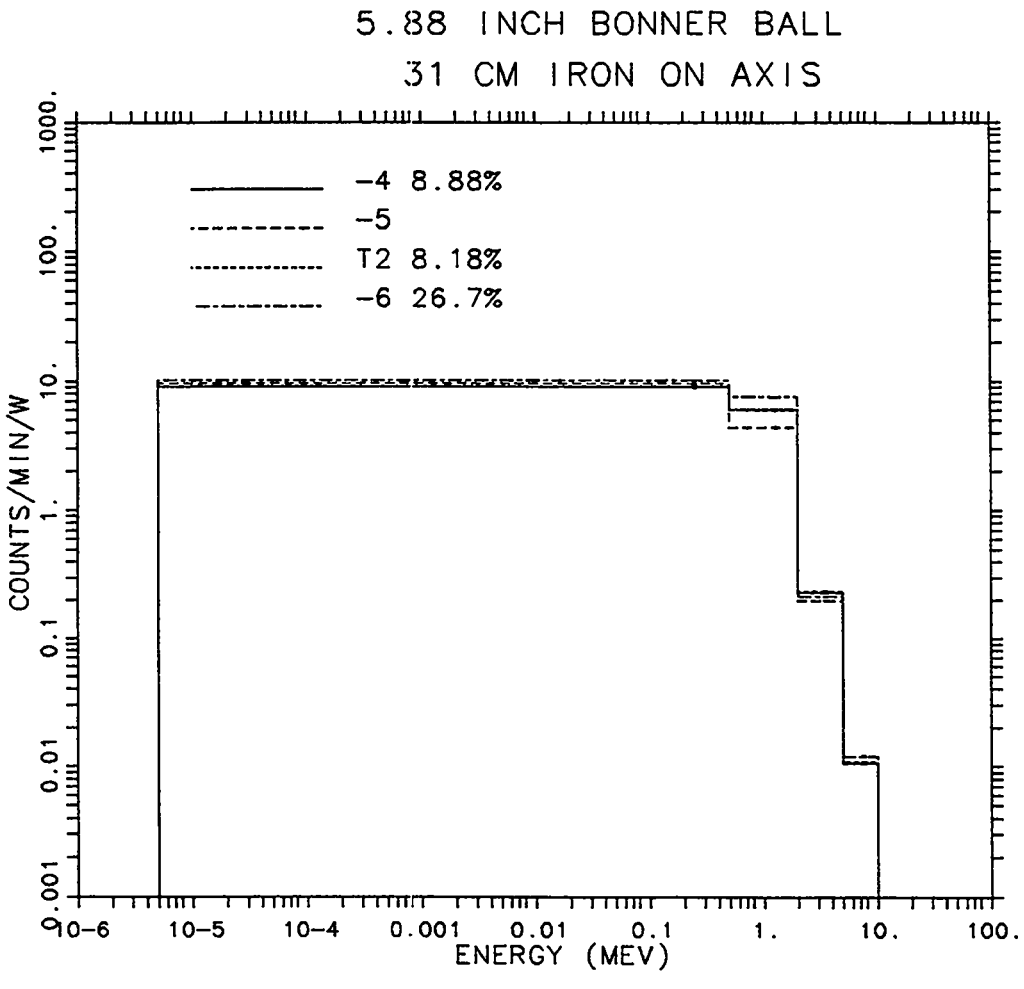

Fig. 74. Data set comparisons for the 31 cm iron slab, with the 5.88 in Bonner Ball on axis. (Normalized to ENDF/B-V)

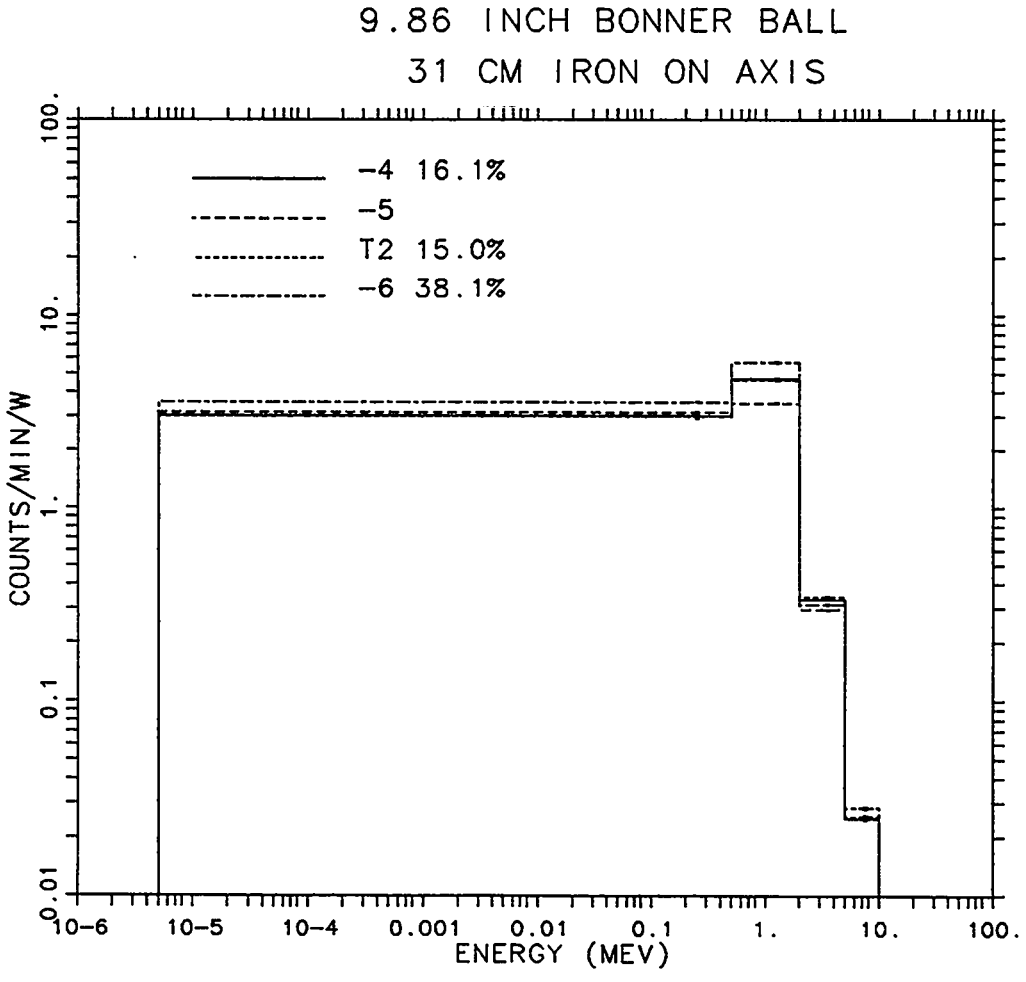

Fig. 75. Data set comparisons for the 31 cm iron slab, with the 9.86 in Bonner Ball on axis. (Normalized to ENDF/B-V)

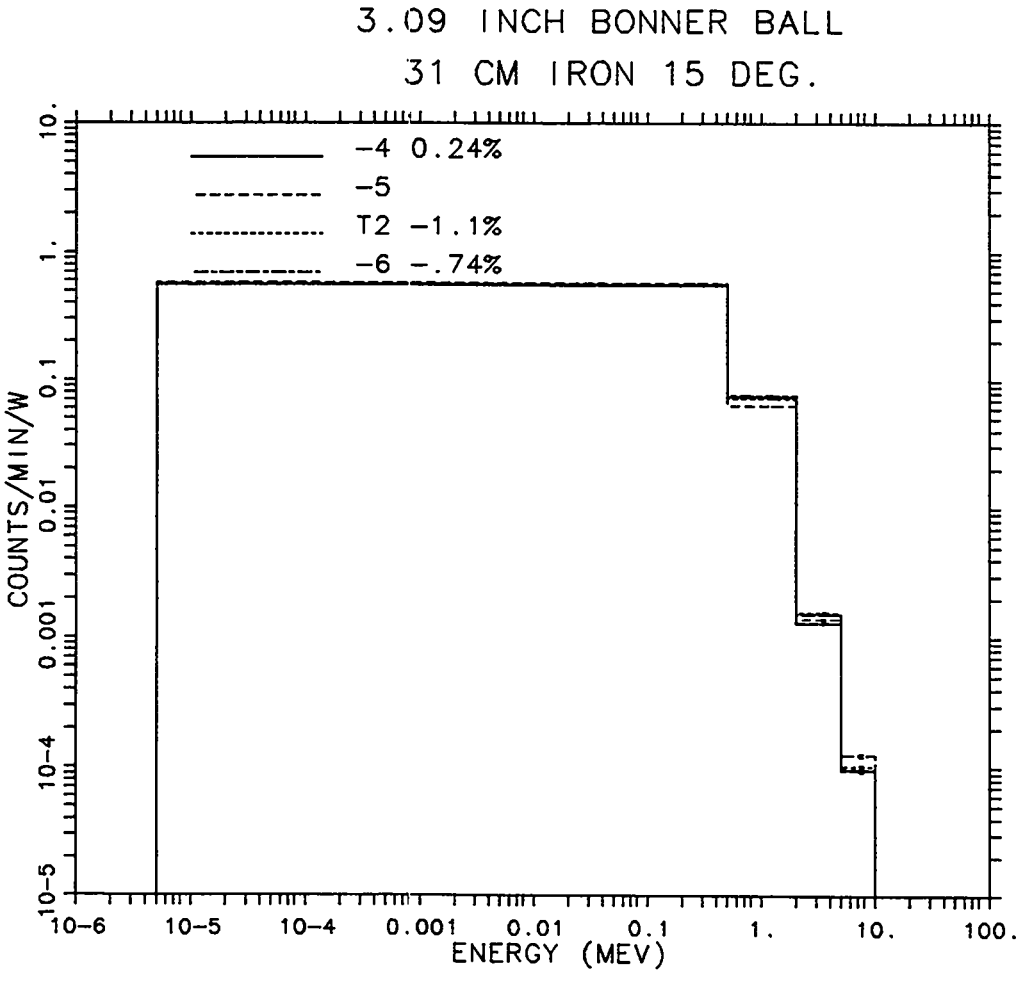

Fig. 76. Data set comparisons for the 31 cm iron slab, with the 3.09 in Bonner Ball at the 15 degree observation angle. (Normalized to ENDF/B-V)

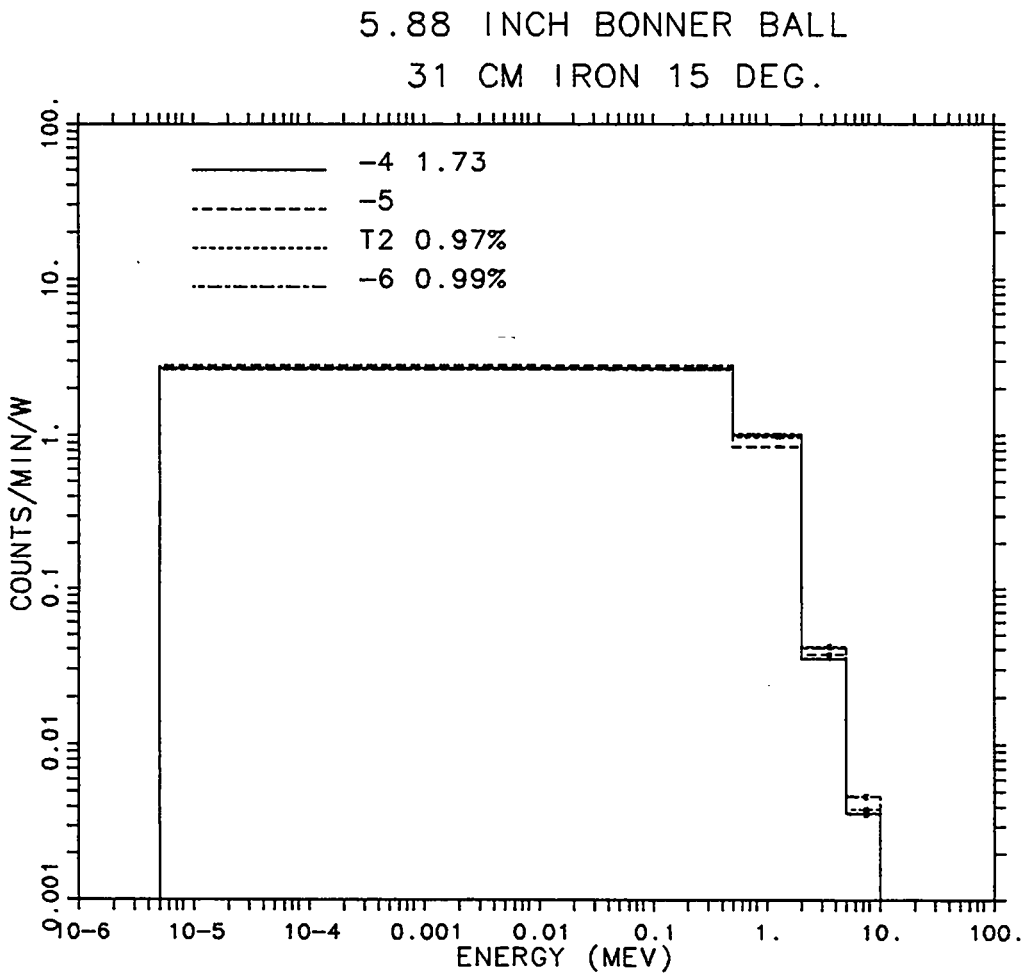

Fig. 77. Data set comparisons for the 31 cm iron slab, with the 5.88 in Bonner Ball at the 15 degree observation angle. (Normalized to ENDF/B-V)

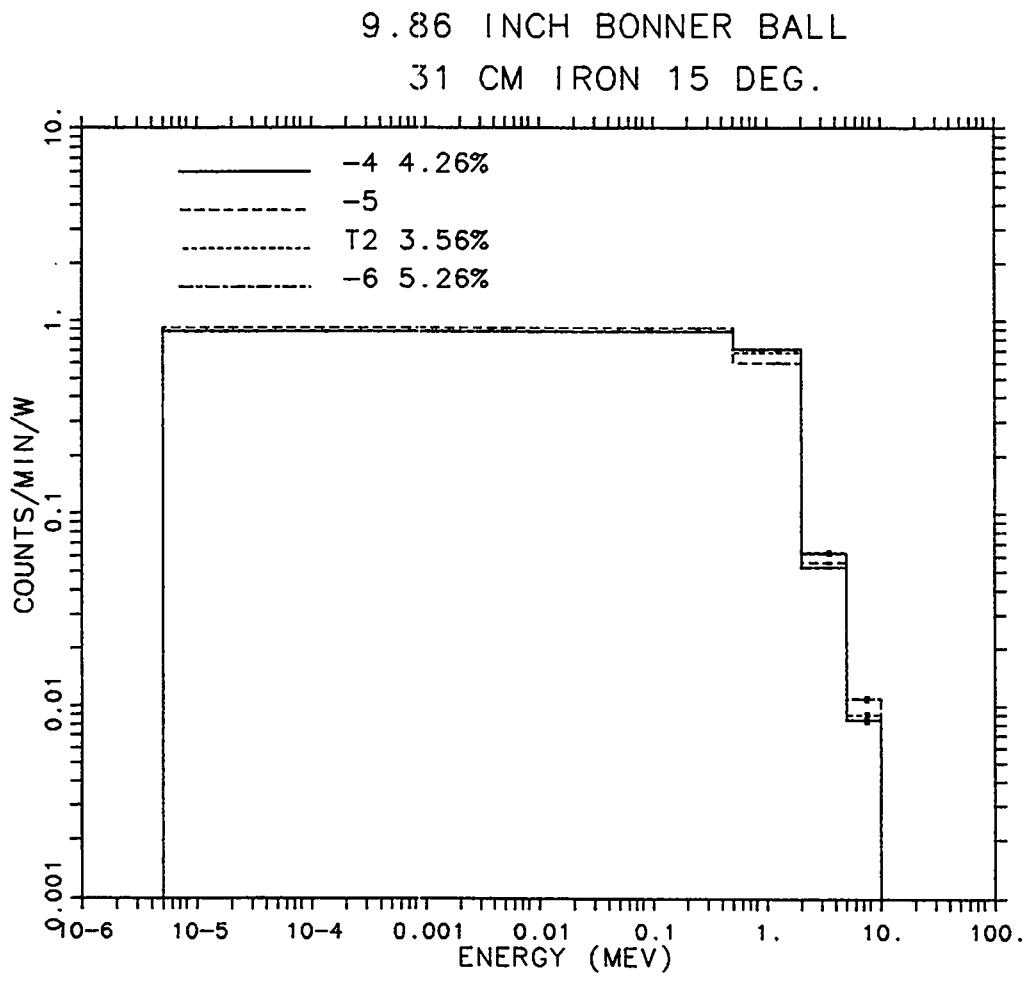

Fig. 78. Data set comparisons for the 31 cm iron slab, with the 9.86 in Bonner Ball at the 15 degree observation angle. (Normalized to ENDF/B-V)

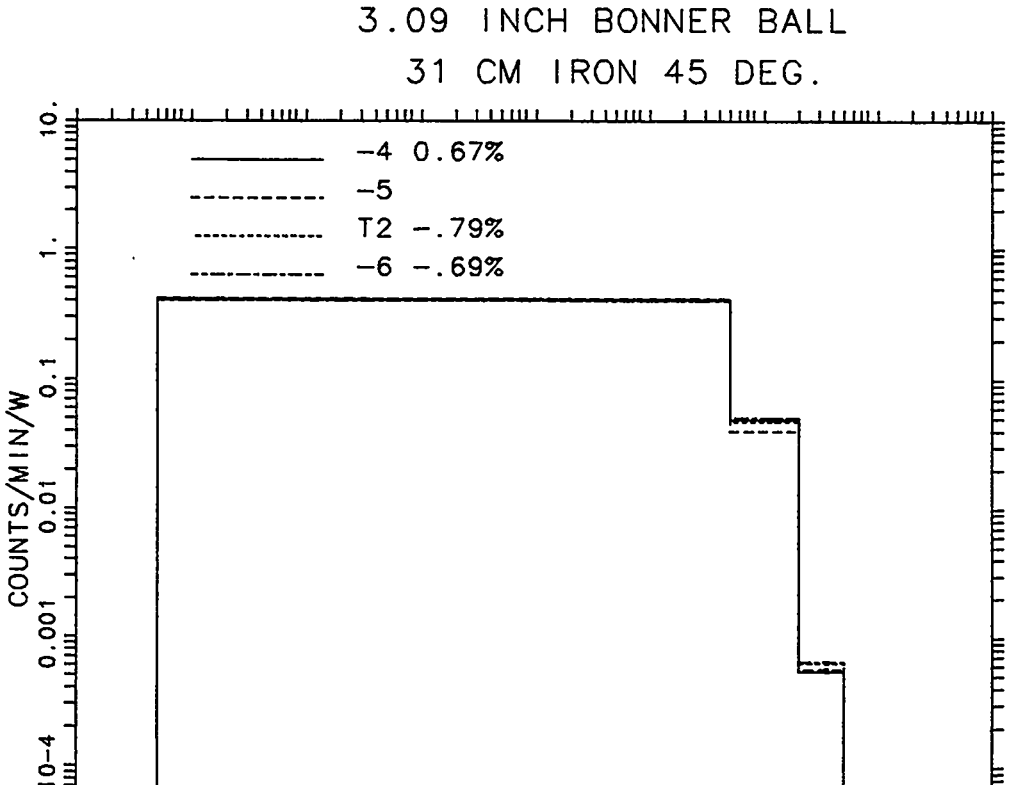

Fig. 79. Data set comparisons for the 31 cm iron slab, with the 3.09 in Bonner Ball at the 45 degree observation angle. (Normalized to ENDF/B-V)

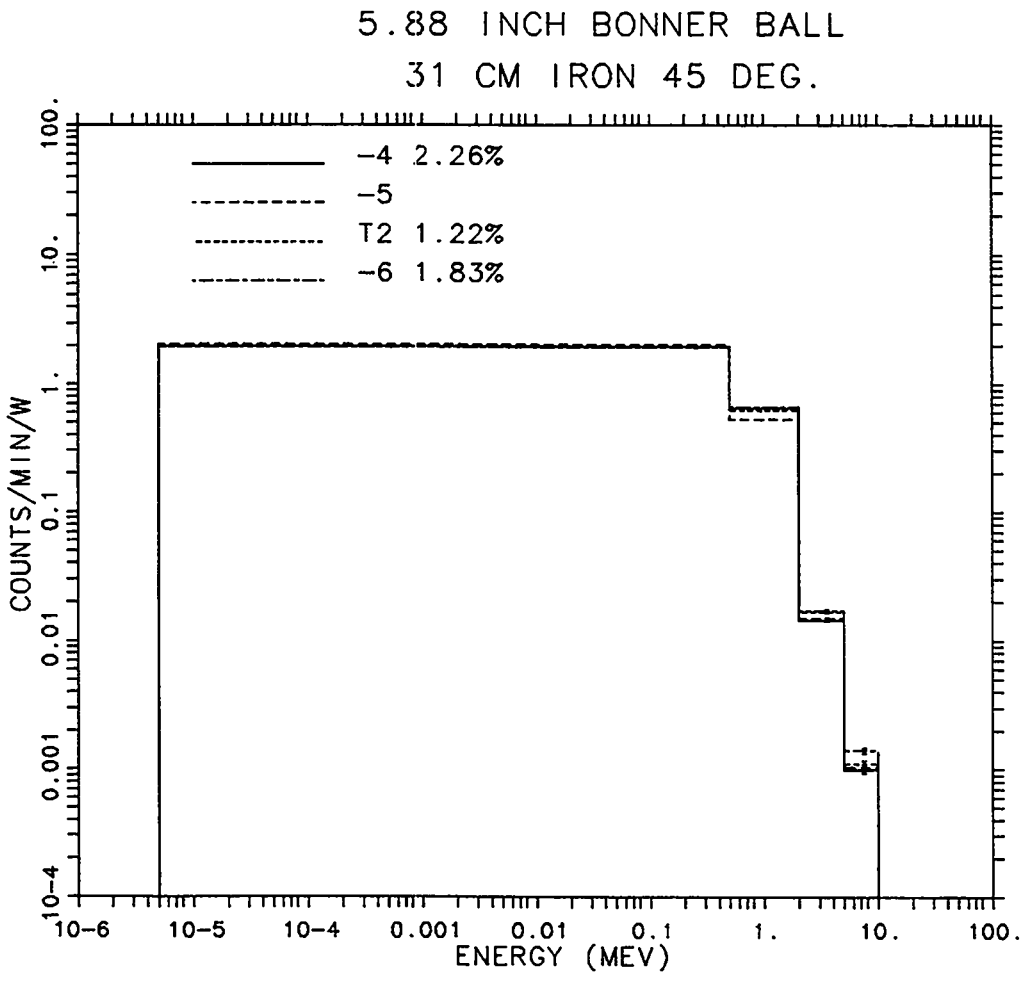

Fig. 80. Data set comparisons for the 31 cm iron slab, with the 5.88 in Bonner Ball at the 45 degree observation angle. (Normalized to ENDF/B-V)

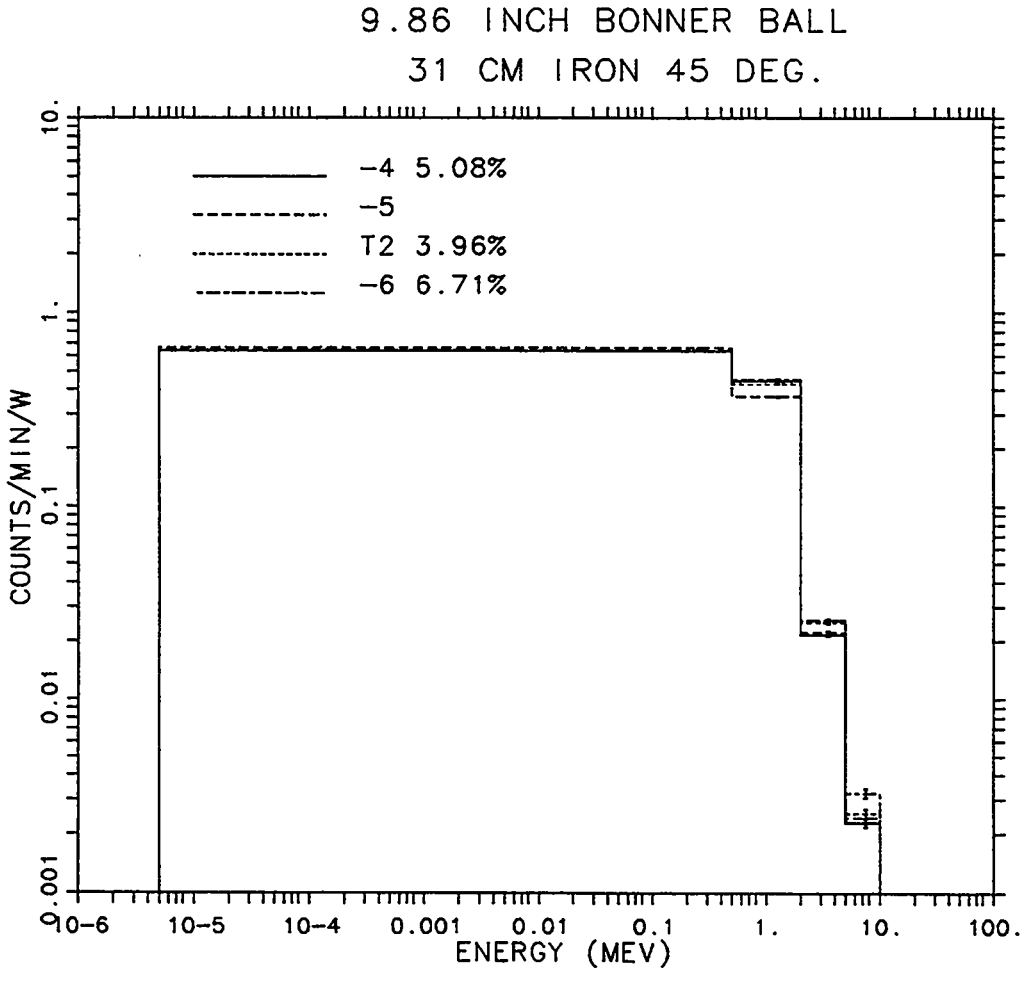

Fig. 81. Data set comparisons for the 31 cm iron slab, with the 9.86 in Bonner Ball at the 45 degree observation angle. (Normalized to ENDF/B-V)

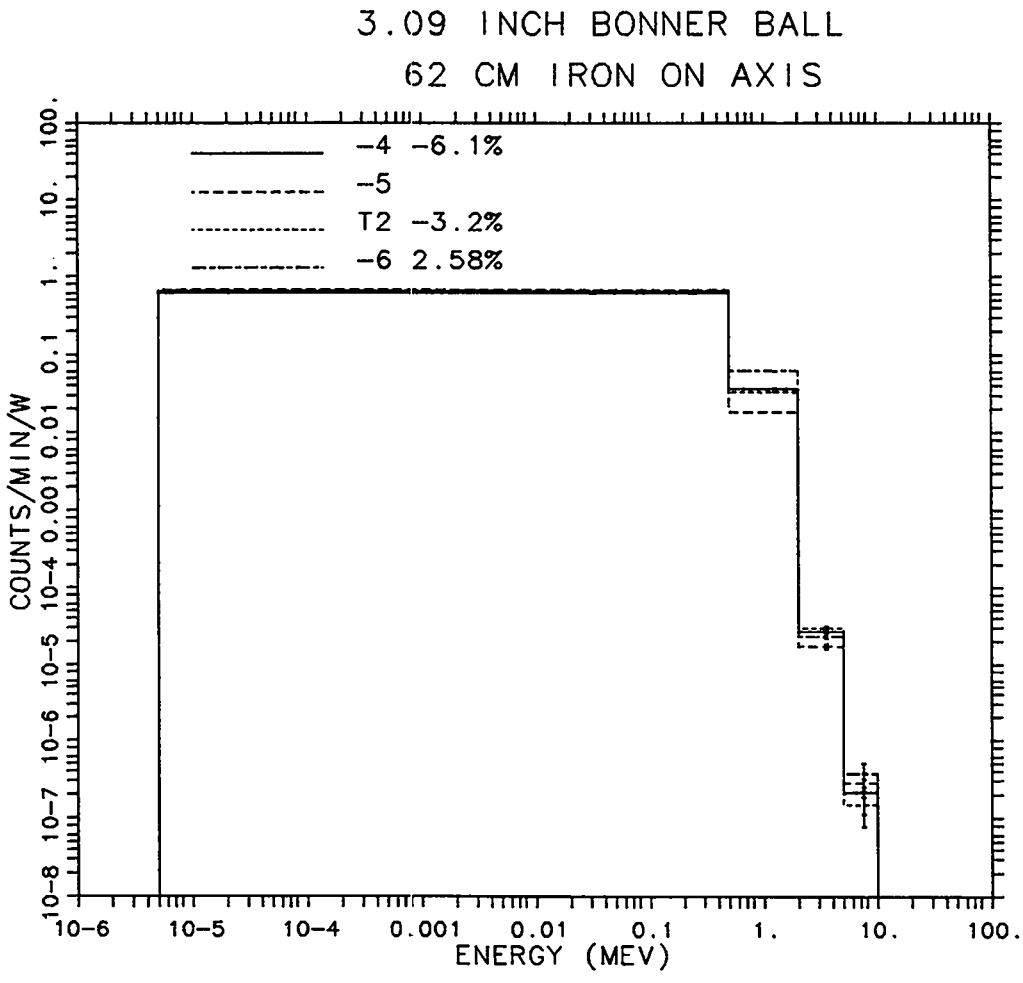

Fig. 82. Data set comparisons for the 62 cm iron slab, with the 3.09 in Bonner Ball on axis. (Normalized to ENDF/B-V)

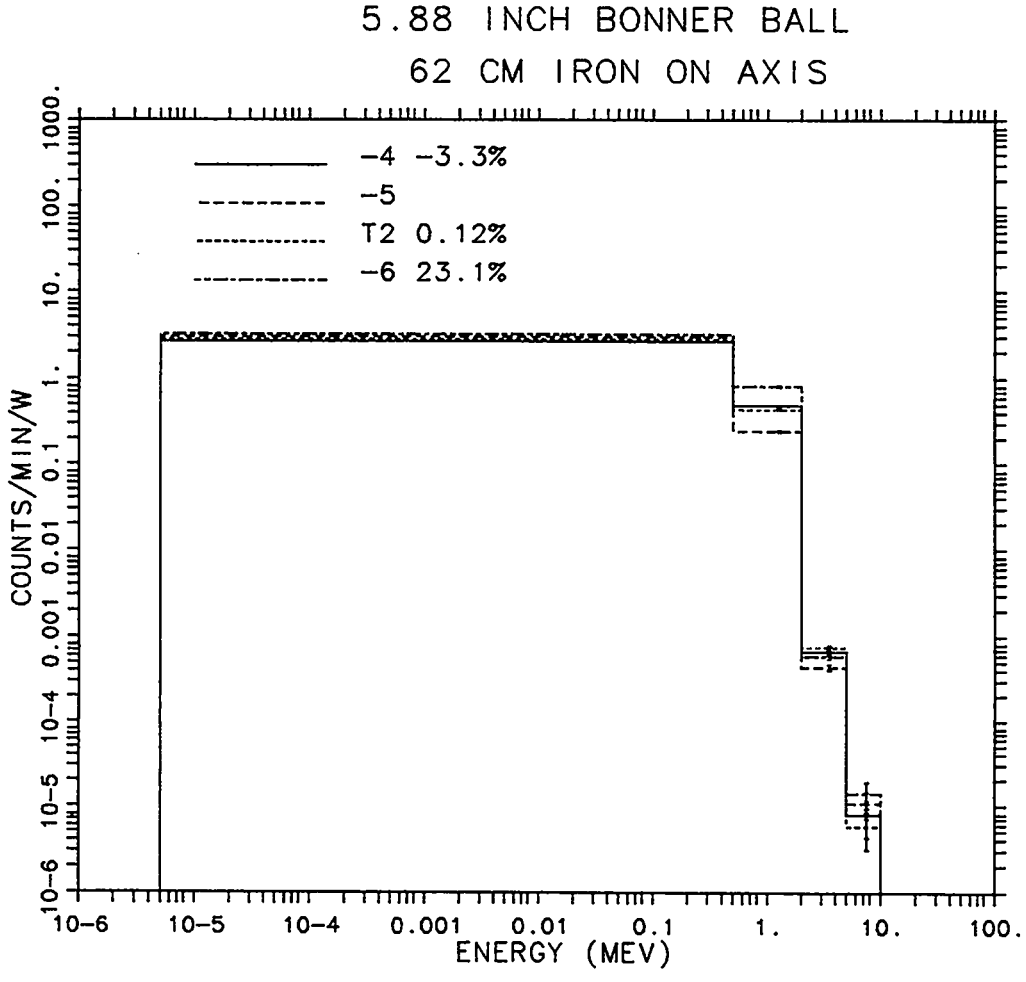

Fig. 83. Data set comparisons for the 62 cm iron slab, with the 5.88 in Bonner Ball on axis. (Normalized to ENDF/B-V)

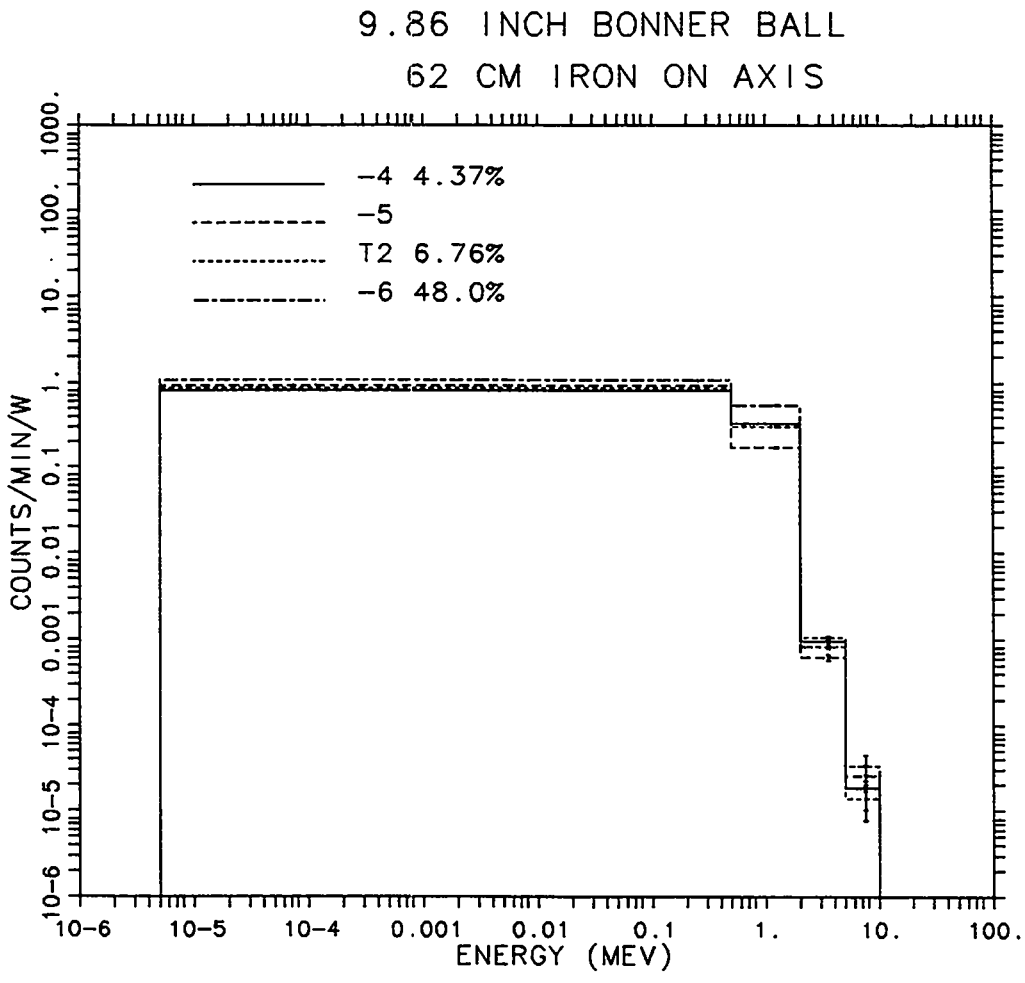

Fig. 84. Data set comparisons for the 62 cm iron slab, with the 9.86 in Bonner Ball on axis. (Normalized to ENDF/B-V)

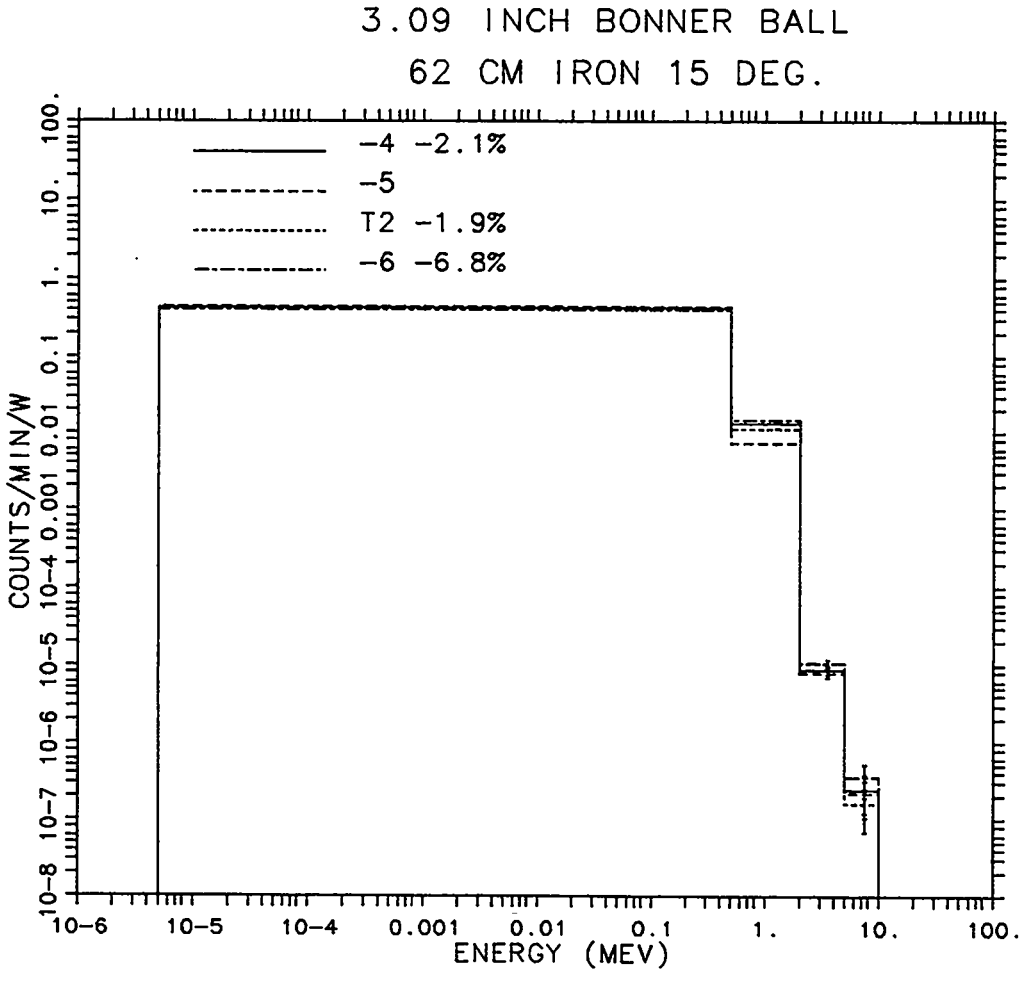

Fig. 85. Data set comparisons for the 62 cm iron slab, with the 3.09 in Bonner Ball at the 15 degree observation angle. (Normalized to ENDF/B-V)

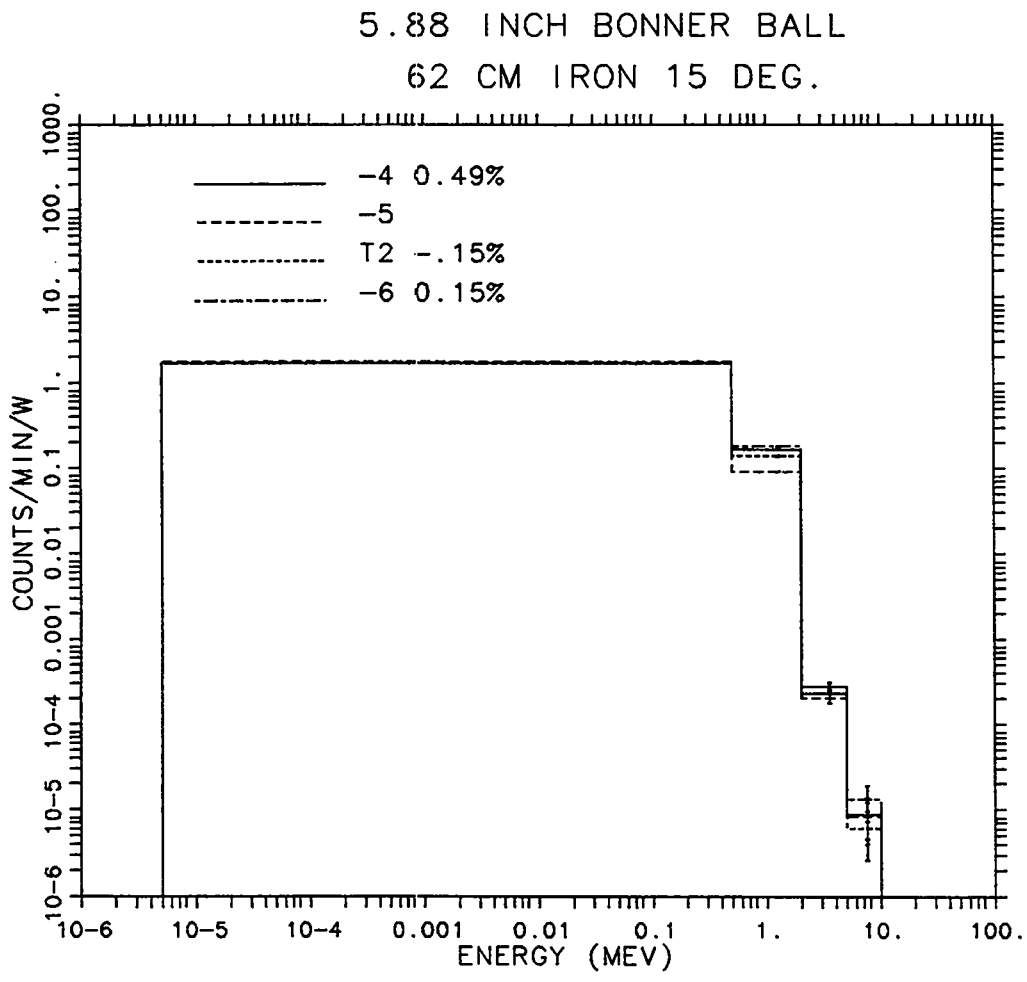

Fig. 86. Data set comparisons for the 62 cm iron slab, with the 5.88 in Bonner Ball at the 15 degree observation angle. (Normalized to ENDF/B-V)

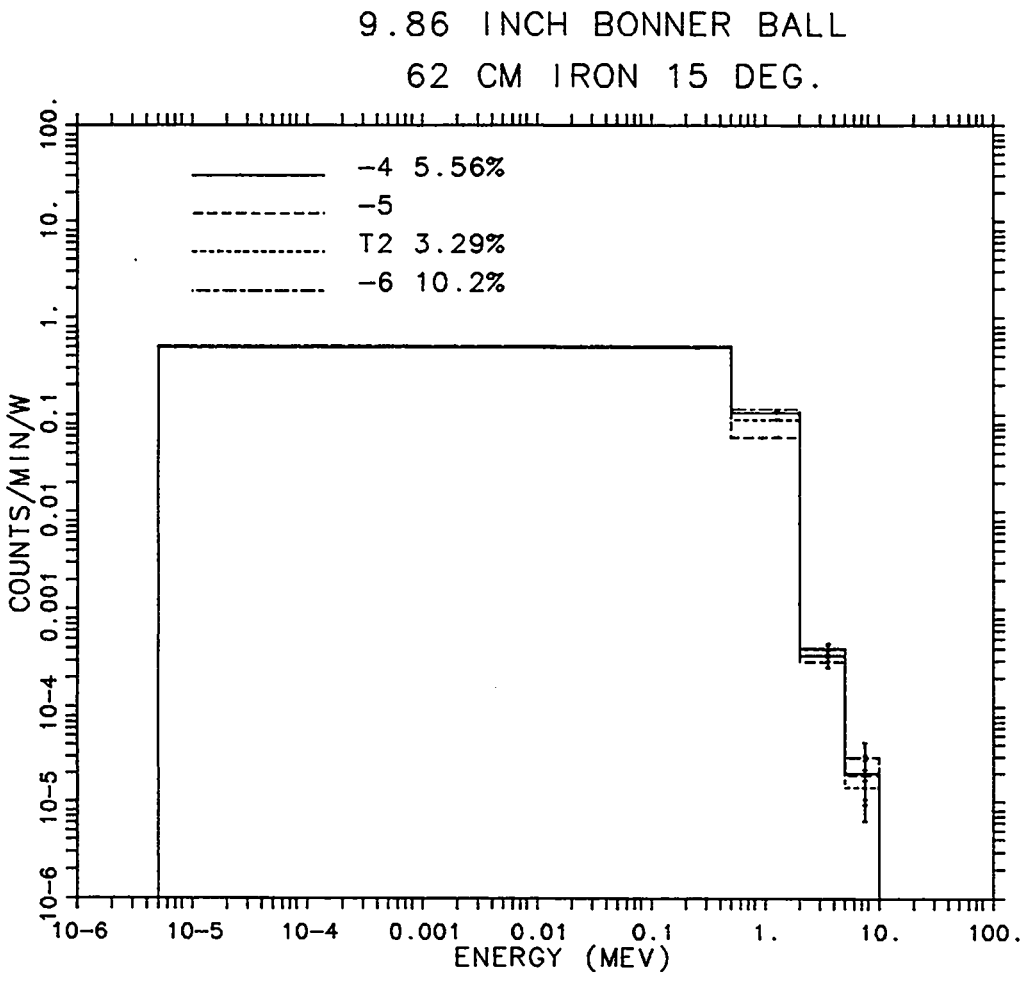

Fig. 87. Data set comparisons for the 62 cm iron slab, with the 9.86 in Bonner Ball at the 15 degree observation angle. (Normalized to ENDF/B-V)

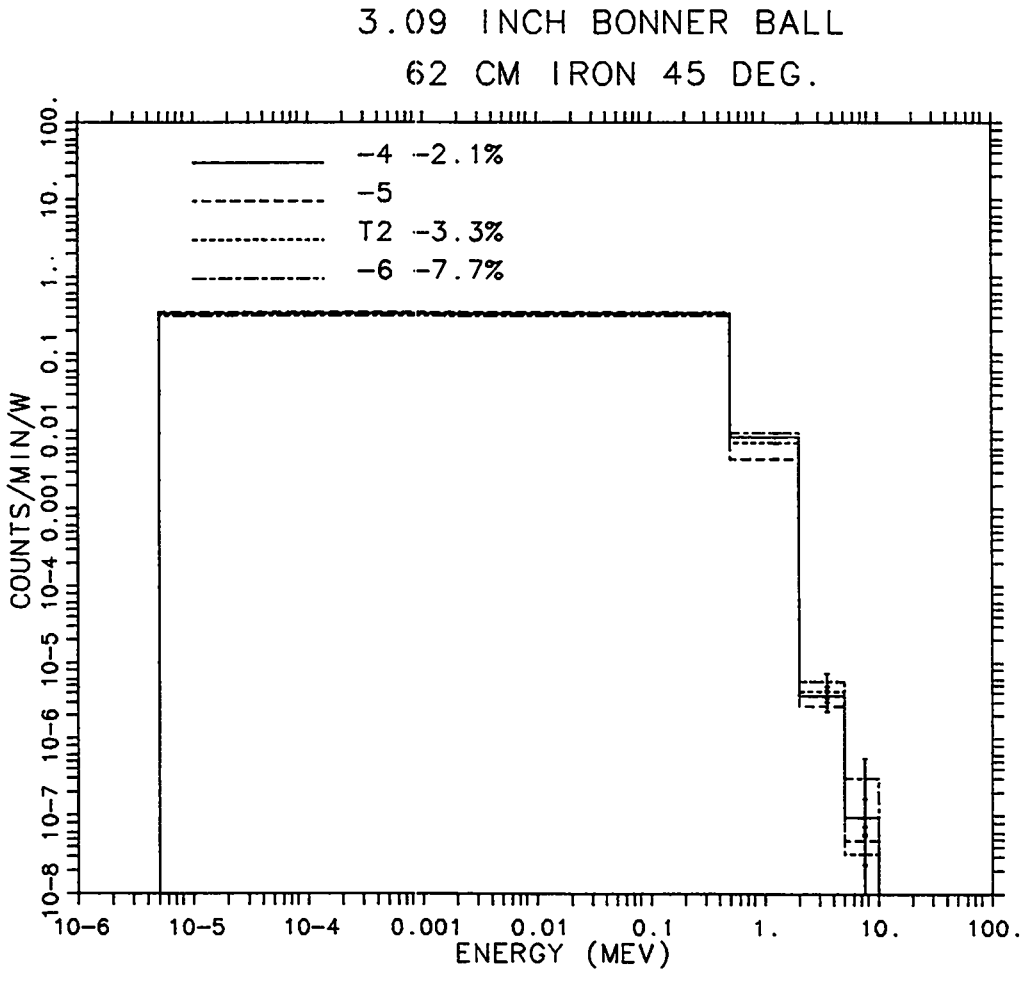

Fig. 88. Data set comparisons for the 62 cm iron slab, with the 3.09 in Bonner Ball at the 45 degree observation angle. (Normalized to ENDF/B-V)

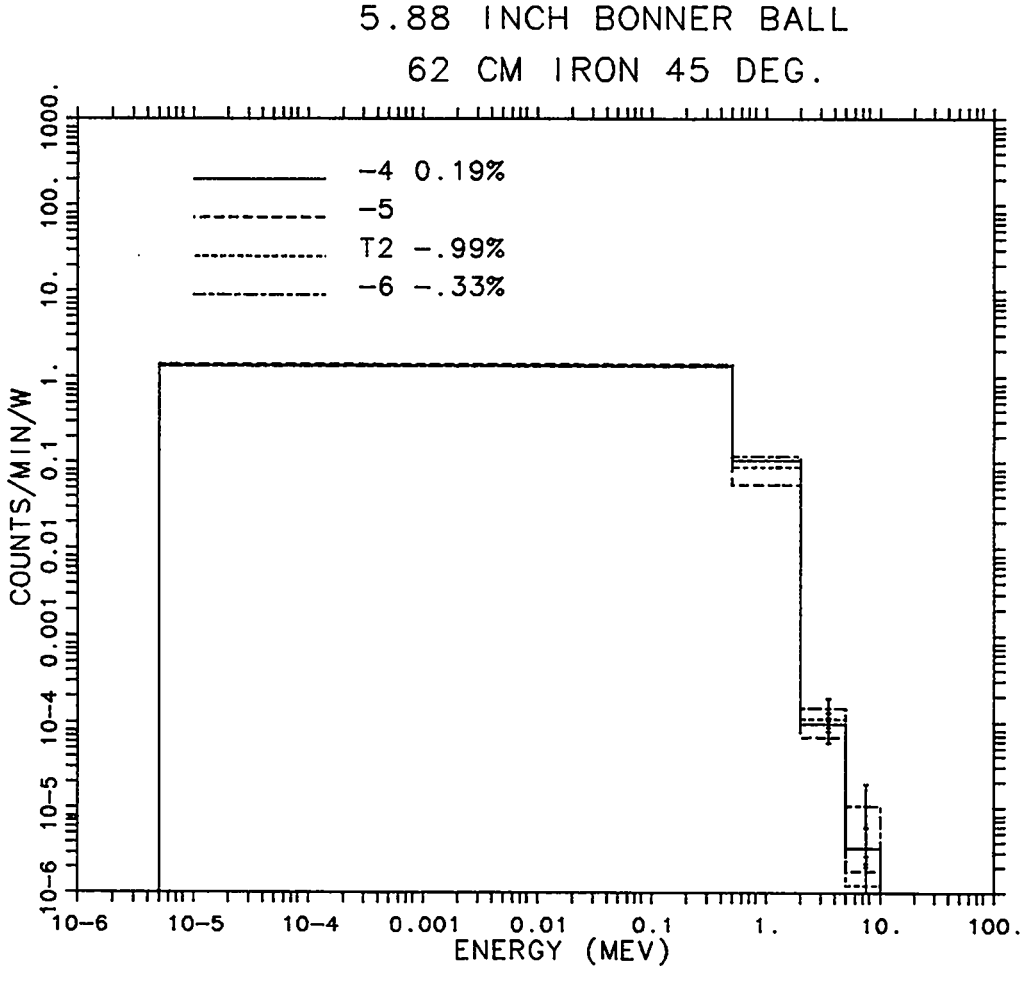

Fig. 89. Data set comparisons for the 62 cm iron slab, with the 5.88 in Bonner Ball at the 45 degree observation angle. (Normalized to ENDF/B-V)

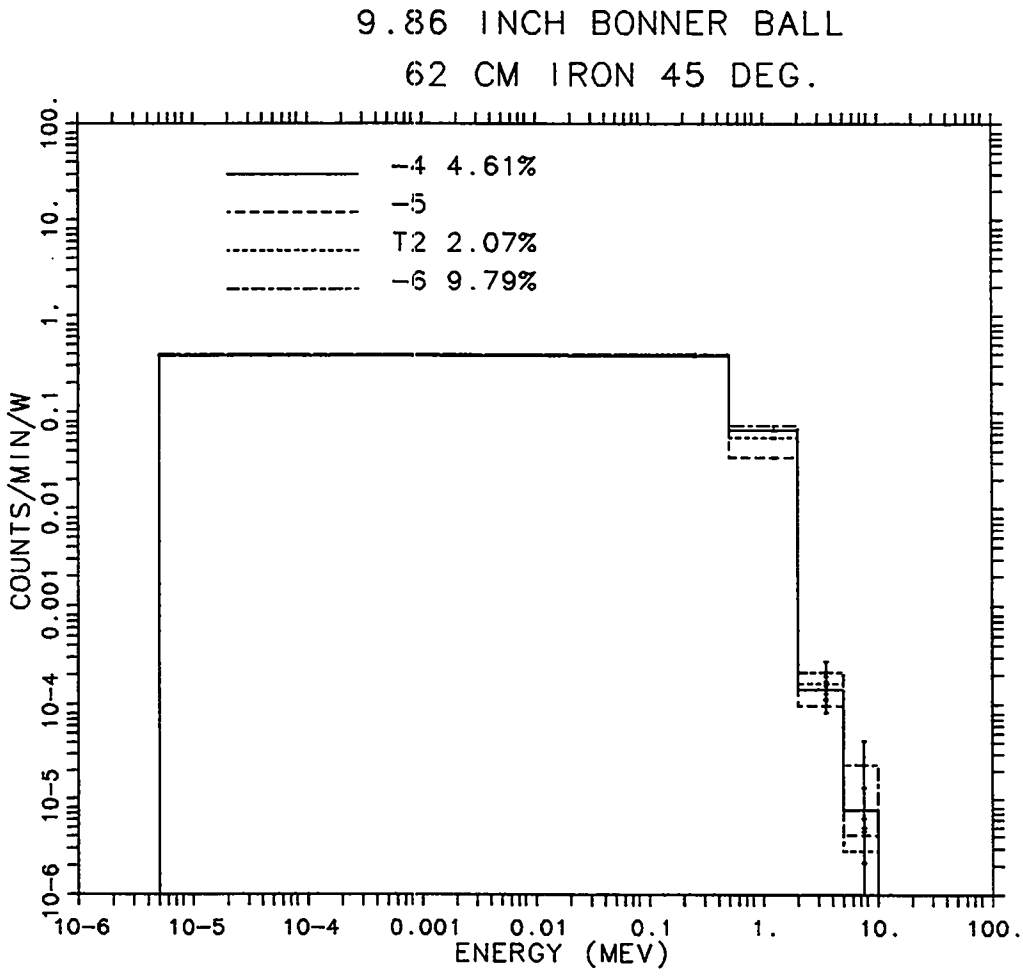

Fig. 90. Data set comparisons for the 62 cm iron slab, with the 9.86 in Bonner Ball at the 45 degree observation angle. (Normalized to ENDF/B-V)

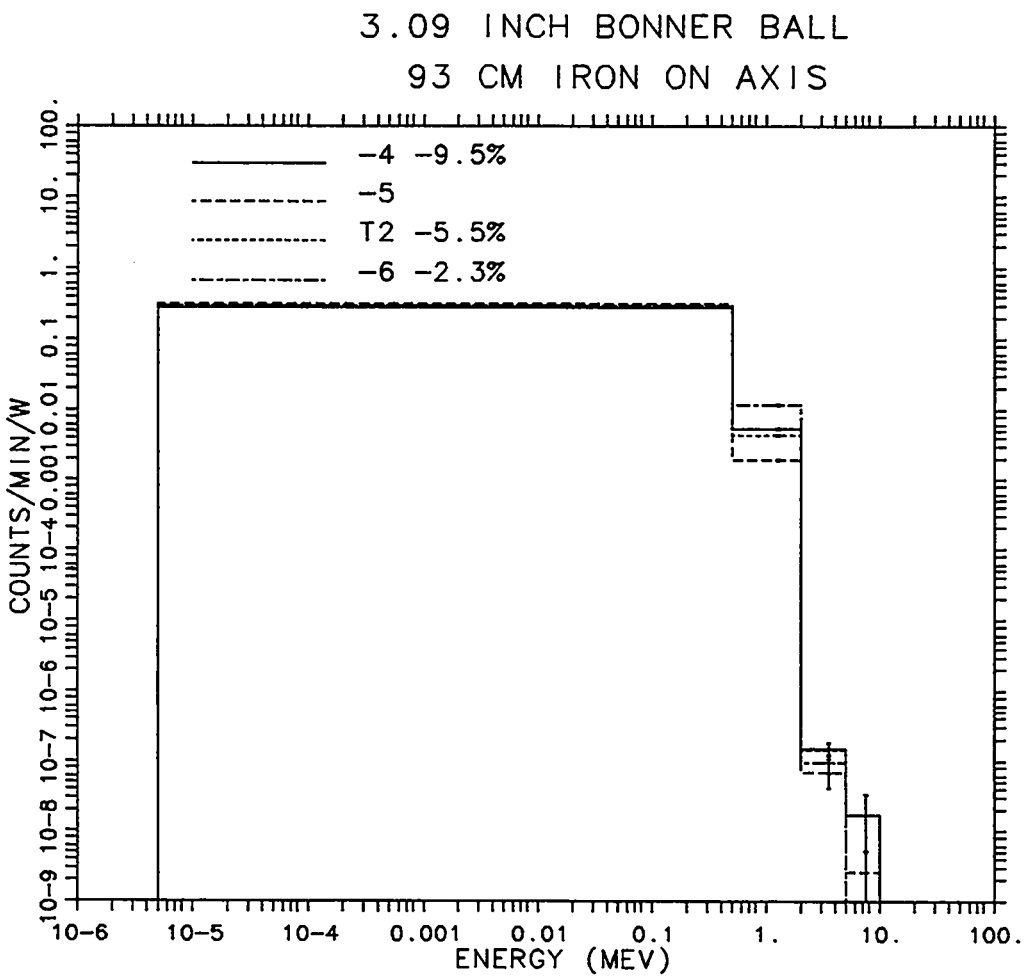

Fig. 91. Data set comparisons for the 93 cm iron slab, with the 3.09 in Bonner Ball on axis. (Normalized to ENDF/B-V)

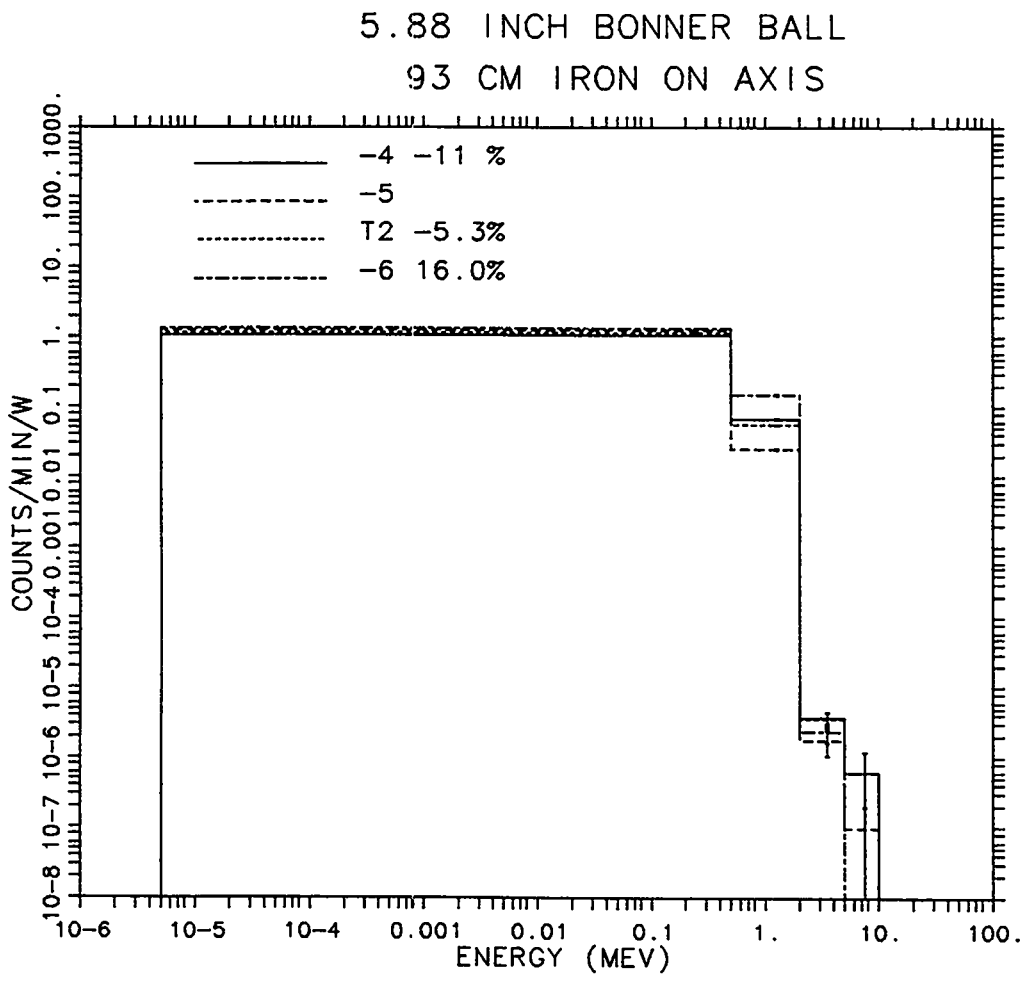

Fig. 92. Data set comparisons for the 93 cm iron slab, with the 5.88 in Bonner Ball on axis. (Normalized to ENDF/B-V)

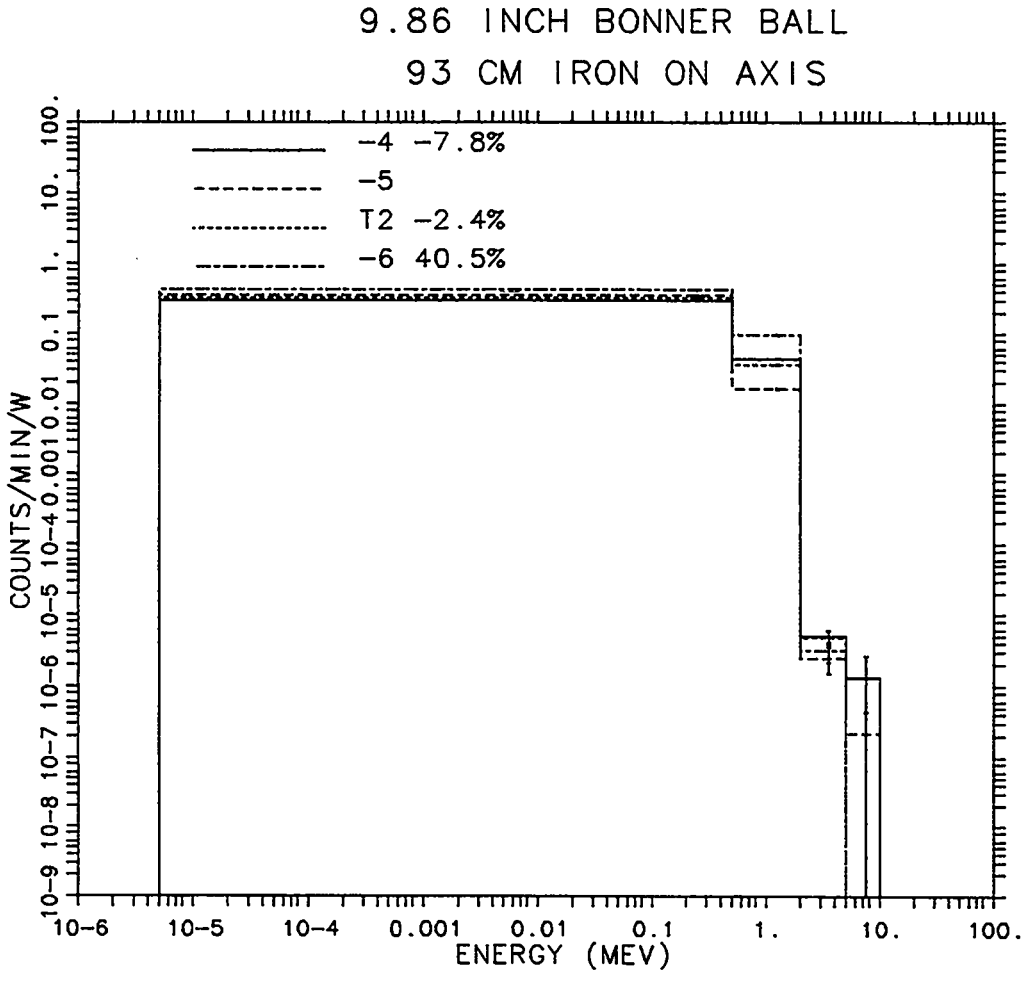

Fig. 93. Data set comparisons for the 93 cm iron slab, with the 9.86 in Bonner Ball on axis. (Normalized to ENDF/B-V)

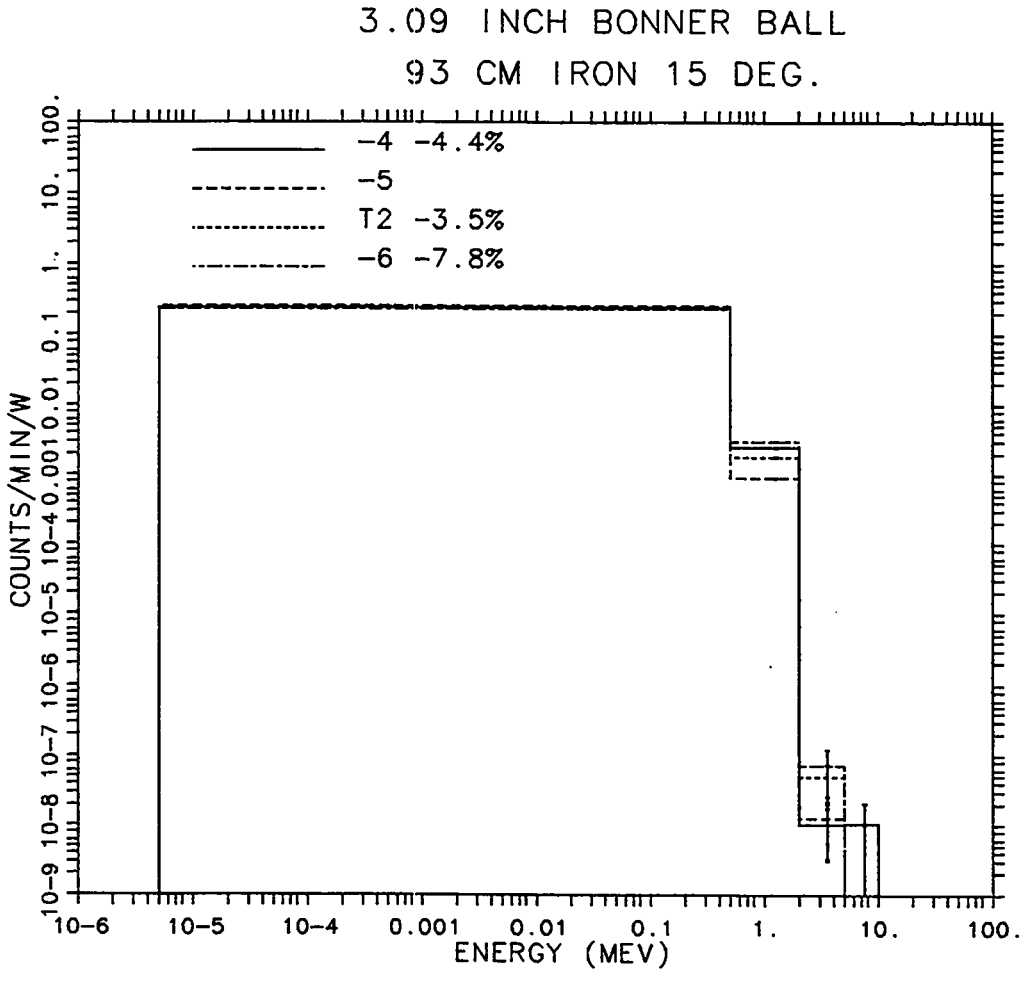

Fig. 94. Data set comparisons for the 93 cm iron slab, with the 3.09 in Bonner Ball at the 15 degree observation angle. (Normalized to ENDF/B-V)

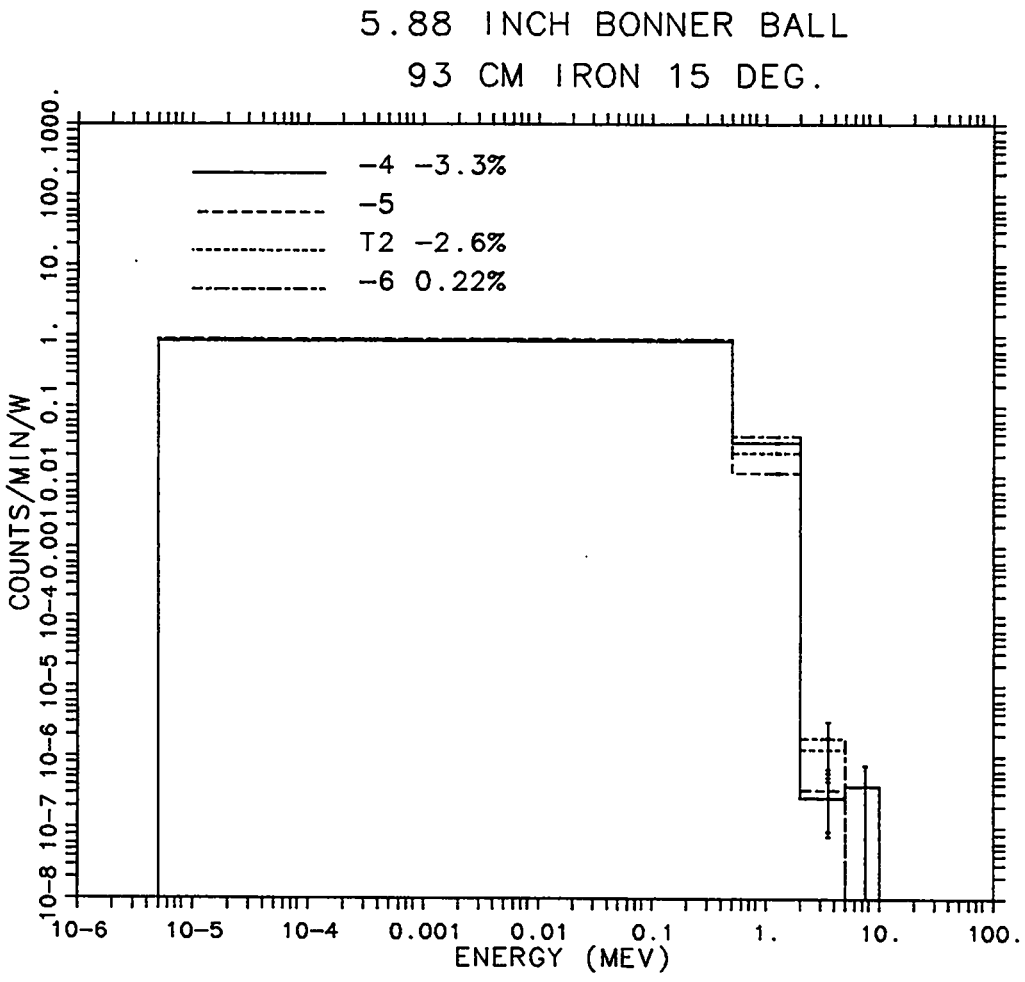

Fig. 95. Data set comparisons for the 93 cm iron slab, with the 5.88 in Bonner Ball at the 15 degree observation angle. (Normalized to ENDF/B-V)

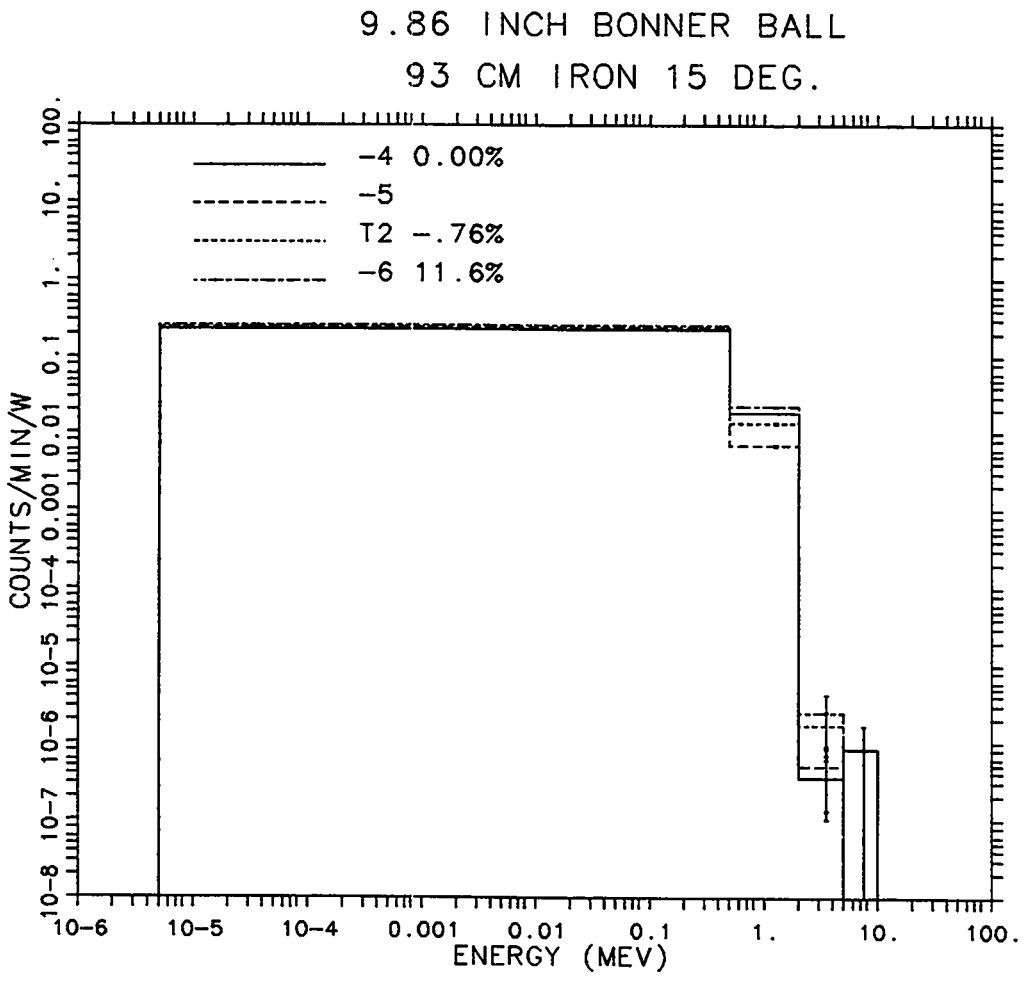

Fig. 96. Data set comparisons for the 93 cm iron slab, with the 9.86 in Bonner Ball at the 15 degree observation angle. (Normalized to ENDF/B-V)

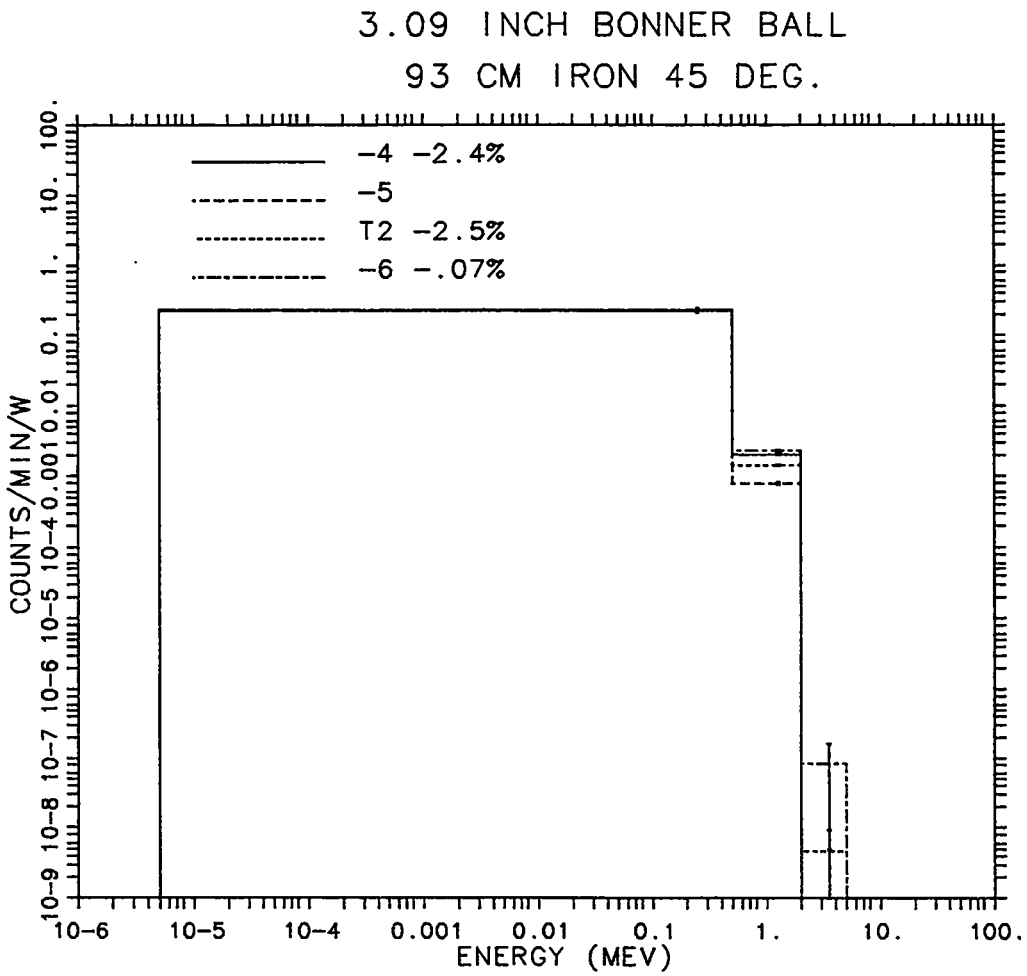

Fig. 97. Data set comparisons for the 93 cm iron slab, with the 3.09 in Bonner Ball at the 45 degree observation angle. (Normalized to ENDF/B-V)

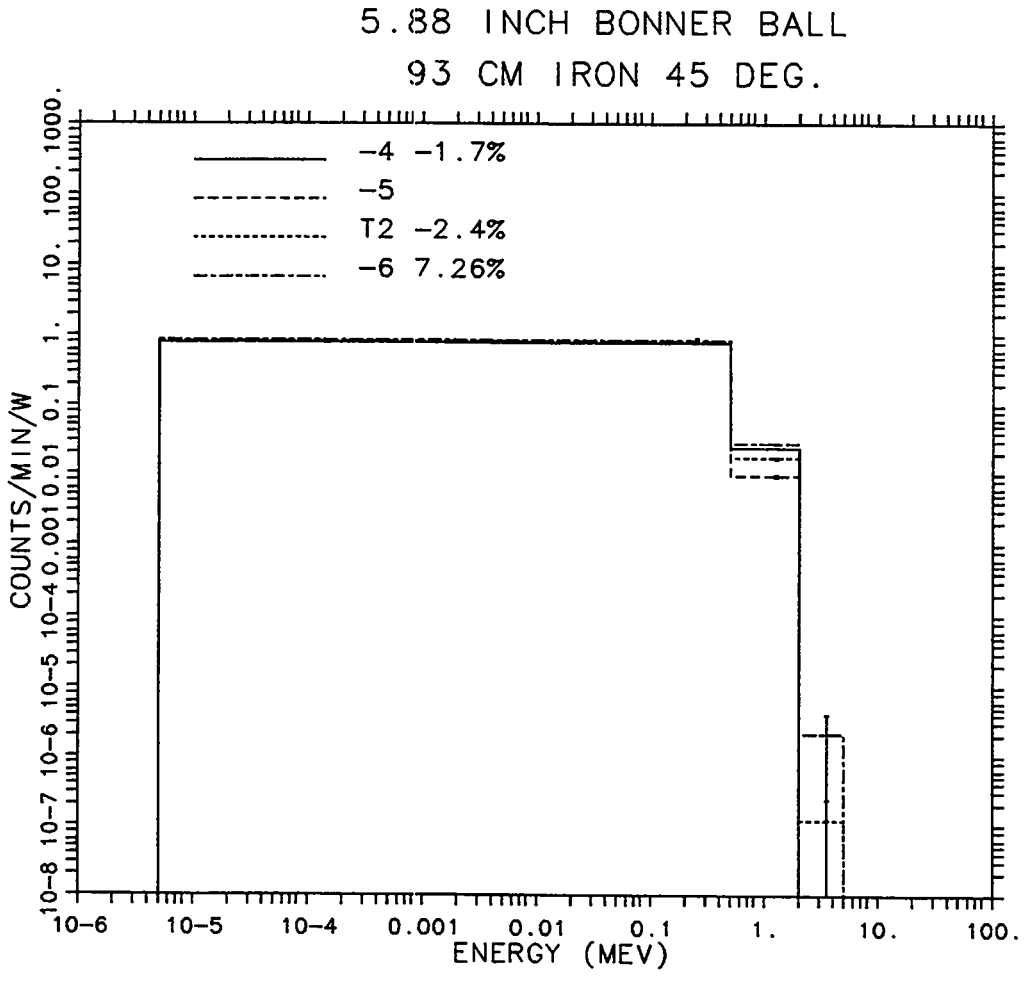

Fig. 98. Data set comparisons for the 93 cm iron slab, with the 5.88 in Bonner Ball at the 45 degree observation angle. (Normalized to ENDF/B-V)

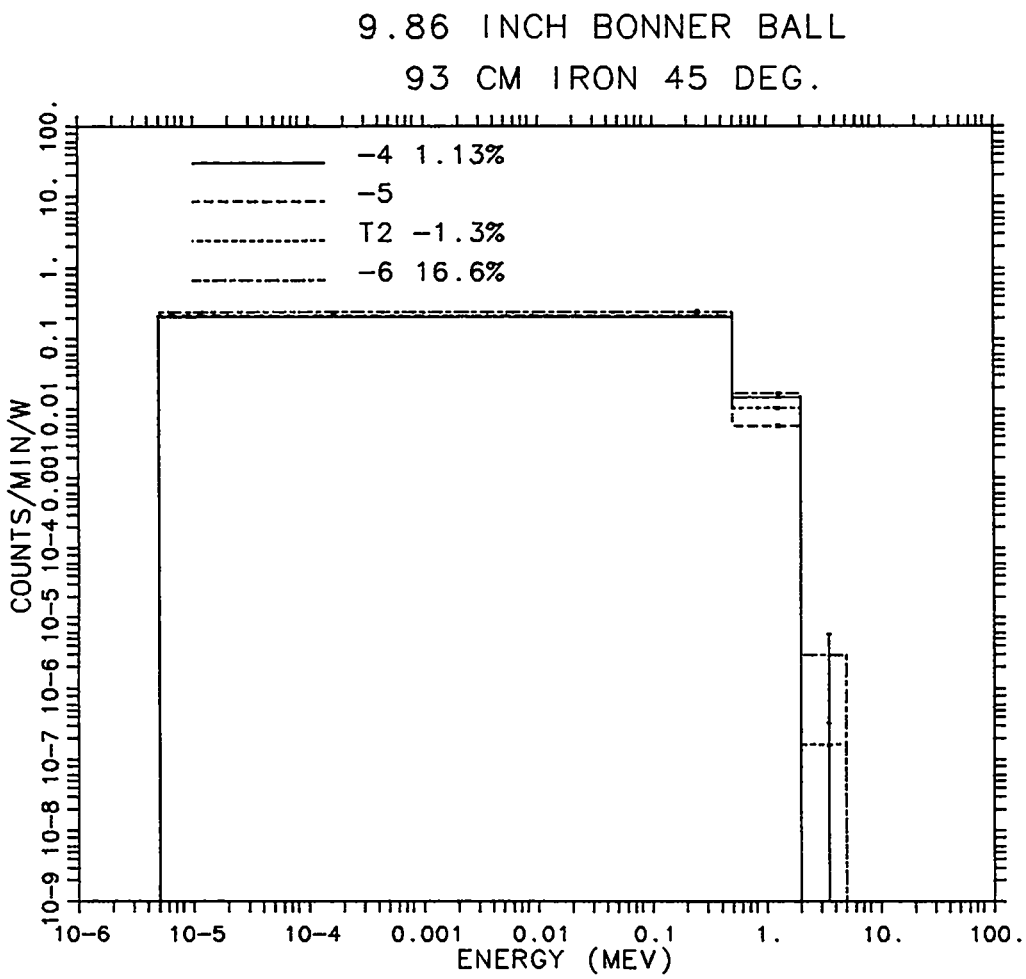

Fig. 99. Data set comparisons for the 93 cm iron slab, with the 9.86 in Bonner Ball at the 45 degree observation angle. (Normalized to ENDF/B-V)

VI. CONCLUSIONS

In general, when experimental data is available (Benchmarks 1 and 2), the MCNP Recommended Library for iron is the best, followed by ENDF/B-VI, ENDF/B-V, and ENDF/B-IV. For Benchmark 3, where experimental data was not available, and Benchmark 4, where the problem description was evidently faulty, ENDF/B-VI and the MCNP Recommended Iron Libraries tended to agree, while the ENDF/B-V and ENDF/B-IV libraries gave lower transmissions.

Therefore, we believe that the new ENDF/B-VI libraries do not provide significantly better results than the MCNP Recommended Evaluations. However, both the new ENDF/B-VI library and the MCNP Recommended Library appear better than the ENDF/B-V and ENDF/B-IV libraries. We recommend a re-evaluation of any calculations that used ENDF/B-V or ENDF/B-IV libraries with the MCNP Recommended or ENDF/B-VI libraries.

References

1. W. C. Roesch, Ed., *Final Report of the US-Japan Joint Reassessment of Atomic Bomb Radiation Dosimetry in Hiroshima and Nagasaki,* The Radiation Effects Research Foundation, Hiroshima, Japan (1987).

2. Judith F. Briesmeister, Ed., "MCNP4A–A General Monte Carlo N-Particle Transport Code," Los Alamos National Laboratory report LA-12625-M (November 1993).

3. J. S. Hendricks, S. C. Frankle, and J. D. Court, "New Data for MCNP," *Trans. Am. Nuc. Soc.* **71**, 399 (1994).

4. J. S. Hendricks, S. C. Frankle, and J. D. Court, "ENDF/B-VI Data for MCNP," Los Alamos National Laboratory report LA–12891 (December 1994).

5. Paul Whalen, "Source and Replica Calculations," *American Nuclear Society 8th International Conference on Radiation Shielding,* April 24-28, 1994, Arlington, TX., 212 (April 1994).

6. E. D. Arthur and P. G. Young, "Evaluated Neutron-Induced Cross Sections for ^{54,56}Fe to 40 MeV," Los Alamos National Laboratory report LA–8626–MS (December 1980).

7. C. Wong, J. D. Anderson, P. Brown. L. F. Hansen, J. L. Kammerdiener, C. Logan, and B. Pohl, "Livermore Pulsed Sphere Program: Program Summary Through July 1971," Lawrence Livermore National Laboratory report UCRL–51144, Rev. 1 (1972).

8. R. T. Santoro, R. G. Alsmiller, J. M. Barnes. and G. T. Chapman, "Calculation of Neuton and Gamma-Ray Spectra for Fusion Reactor Shield Design: Comparison with Experiment," *Nuclear Science and Engineering* **78**, 259-272 (1981).

9. P. F. Rose and R. W. Roussin, Ed., "Cross-Section Evaluation Working Group Benchmark Specifications Volume II," Brookhaven National Laboratory report BNL-19302-Vol.2, (December 1983).

10. R. H. Johnson, J. J. Dorning, and B. W. Wehring, "Integral Tests of Neutron Cross Sections for Iron above 1.0 MeV," *Trans. Am. Nuc. Soc.* **22**, 799 (1975).

11. R. H. Johnson, J. J. Dorning, and B. W. Wehring, "Integral Test of Cross Sections Using Neutron Leakage Spectra from Spheres of Iron, Niobium, Beryllium, and Polyethylene," *Proceedings of the Conference on Nuclear Cross Sections and Technology* **1**, 169-172 (1975).

12. R. E. Maeker and F. J. Muckenthaler, "Final Report on a Benchmark Experiment for Neutron Transport Through Iron and Stainless Steel," Oak Ridge National Laboratory report ORNL-4892 (1974).

13. L. F. Hansen, J. D. Anderson, P. S. Brown, R. J. Howerton, J. L. Kammerdiener, C. M. Logan, E. F. Plechaty, and C. Wong, "Measurements and Calculations of the Neutron Spectra from Iron Bombarded with 14-MeV Neutrons," *Nuclear Science and Engineering* **51**, 278-295 (1973).

14. D. J. Whalen, D. A. Cardon, J. L. Uhle, and J. S. Hendricks, "MCNP: Neutron Benchmark Problems," Los Alamos National Laboratory report LA–12212 (November 1991).

15. R. H. Johnson, B. W. Wehring, J. J. Dorning, and D. T. Ingersoll, "^{252}Cf Fast-Neutron Spectrum Measured to 15 MeV," *Trans. Am. Nuc. Soc.* **22**, 727 (1975).

16. R. E. Maerker, "SDT 11. The ORNL Benchmark Experiment for Neutron Transport Through Iron and Stainless Steel, Part I," Oak Ridge National Laboratory report ORNL–TM–4222 (1974).

17. J. S. Hendricks and L. L. Carter, "Computational Benchmark Problem for Deep Penetration in Iron," Los Alamos National Laboratory report LA–8193–MS (January 1980).

Appendix:
MCNP Input Decks

Table A.1 Input file for the ENDF/B-VI 4.8 mfp iron sphere for the Lawrence Livermore Pulsed Sphere Benchmark.

```
Fe Sphere with 4.8 M.F.P.  ENDF/B-VI
1    1 -7.85 -1 -3
2    1 -7.85 1 2 -3
3    2 -.001288 1 -2 -3
4    1 -7.85 -1 3 -4
5    1 -7.85 1 2 3 -4
6    2 -.001288 1 -2 3 -4
7    1 -7.85 -1 4 -5
8    1 -7.85 1 2 4 -5
9    2 -.001288 1 -2 4 -5
10   1 -7.85 -1 5 -6
11   1 -7.85 1 2 5 -6
12   2 -.001288 1 -2 5 -6
13   2 -.001288 6 -7
14   0 7

1    px -.475
2    x 0.0 1.11 22.3 2.67
3    so 6
4    so 12
5    so 18
6    so 22.3
7    so 1000
100  px 0.0

imp:n 1 1 1 2 2 2 4 4 4 8 8 8 8 0
sdef pos=0 0 0 dir=d1 erg=fdir=d2 rad=d3 vec=-1 0 0
     sur=100 tme=d4
si1  a  -1.0000 -.99619 -.98481 -.96593 -.93969
        -.90631 -.86603 -.81915 -.76604 -.70711
        -.64279 -.57358 -.50000 -.42262 -.34202
        -.25882 -.17365 -.08716  .00000  .08716
         .17365  .25882  .34202  .42262  .50000
         .57358  .64279  .70711  .76604  .81915
         .86603  .90631  .93969  .96593  .98481
         .99619  1.0000
sp1      .874 .874 .875 .876 .877
         .879 .882 .884 .888 .891
         .895 .899 .904 .909 .914
         .919 .924 .930 .935 .941
         .946 .952 .957 .962 .967
         .972 .976 .981 .985 .988
         .991 .994 .996 .998 .999
        1.0 1.0
ds2  q  -.99619 180 -.98481 175 -.96593 170 -.93962 165 -.90631 160
        -.86603 155 -.81915 150 -.76604 145 -.70711 140 -.64279 135
        -.57358 130 -.50000 125 -.42262 120 -.34202 115 -.25882 110
        -.17365 105 -.08716 100  0.0000 95   .08716 90   .17365 85
         .25882 80   .34202 75   .42262 70   .50000 65   .57358 60
         .64279 55   .70711 50   .76604 45   .81915 40   .86603 35
```

Table A.1 (cont.)

```
         .90631 30   .93969 25   .96593 20   .98481 15   .99619 10
         1.0000 5
si3  h 0 .6
sp3  d -21 1
sp4  -41 .3 0
si5  h 15.106 15.110
sp5  d 0 1
si10 h 15.095 15.106
sp10 d 0 1
si15 h 15.075 15.095
sp15 d 0 1
si20 h 15.049 15.075
sp20 d 0 1
si25 h 15.015 15.049
sp25 d 0 1
si30 h 14.974 15.015
sp30 d 0 1
si35 h 14.927 14.974
sp35 d 0 1
si40 h 14.873 14.927
sp40 d 0 1
si45 h 14.814 14.873
sp45 d 0 1
si50 h 14.750 14.814
sp50 d 0 1
si55 h 14.681 14.750
sp55 d 0 1
si60 h 14.608 14.681
sp60 d 0 1
si65 h 14.532 14.608
sp65 d 0 1
si70 h 14.453 14.532
sp70 d 0 1
si75 h 14.372 14.453
sp75 d 0 1
si80 h 14.289 14.372
sp80 d 0 1
si85 h 14.206 14.289
sp85 d 0 1
si90 h 14.123 14.206
sp90 d 0 1
si95 h 14.040 14.123
sp95 d 0 1
si100 h 13.958 14.040
sp100 d 0 1
si105 h 13.878 13.958
sp105 d 0 1
si110 h 13.800 13.878
sp110 d 0 1
si115 h 13.725 13.800
```

Table A.1 (cont.)

```
sp115 d 0 1
si120 h 13.654 13.725
sp120 d 0 1
si125 h 13.586 13.654
sp125 d 0 1
si130 h 13.522 13.586
sp130 d 0 1
si135 h 13.464 13.522
sp135 d 0 1
si140 h 13.410 13.464
sp140 d 0 1
si145 h 13.362 13.410
sp145 d 0 1
si150 h 13.320 13.362
sp150 d 0 1
si155 h 13.284 13.320
sp155 d 0 1
si160 h 13.254 13.284
sp160 d 0 1
si165 h 13.230 13.254
sp165 d 0 1
si170 h 13.214 13.230
sp170 d 0 1
si175 h 13.203 13.214
sp175 d 0 1
si180 h 13.200 13.203
sp180 d 0 1
fc5  NE213 detector response function, 766.0 cm flightpath, 30 degrees.
f5x:n -663.4 383 0
t5   1.37E+01  1.39000E+01  1.41000E+01  1.43000E+01  1.45000E+01  1.47000E+01
     1.49E+01  1.51000E+01  1.53000E+01  1.55000E+01  1.57000E+01  1.59000E+01
     1.61E+01  1.63000E+01  1.65000E+01  1.67000E+01  1.69000E+01  1.71000E+01
     1.73E+01  1.75000E+01  1.77000E+01  1.79000E+01  1.81000E+01  1.83000E+01
     1.85E+01  1.87000E+01  1.89000E+01  1.91000E+01  1.93000E+01  1.95000E+01
     1.97E+01  1.99000E+01  2.01000E+01  2.03000E+01  2.05000E+01  2.07000E+01
     2.09E+01  2.11000E+01  2.13000E+01  2.15000E+01  2.17000E+01  2.19000E+01
     2.21E+01  2.23000E+01  2.25000E+01  2.27000E+01  2.29000E+01  2.31000E+01
     2.33E+01  2.35000E+01  2.37000E+01  2.39000E+01  2.41000E+01  2.43000E+01
     2.45E+01  2.47000E+01  2.49000E+01  2.51000E+01  2.53000E+01  2.55000E+01
     2.57E+01  2.59000E+01  2.61000E+01  2.63000E+01  2.65000E+01  2.67000E+01
     2.69E+01  2.71000E+01  2.73000E+01  2.75000E+01  2.77000E+01  2.79000E+01
     2.81E+01  2.83000E+01  2.85000E+01  2.87000E+01  2.89000E+01  2.91000E+01
     2.93E+01  2.95000E+01  2.97000E+01  2.99000E+01  3.01000E+01  3.03000E+01
     3.05E+01  3.07000E+01  3.09000E+01  3.11000E+01  3.13000E+01  3.15000E+01
     3.17E+01  3.19000E+01  3.21000E+01  3.23000E+01  3.25000E+01  3.27000E+01
     3.29E+01  3.31000E+01  3.33000E+01  3.35000E+01  3.37000E+01  3.39000E+01
     3.41E+01  3.43000E+01  3.45000E+01  3.47000E+01  3.49000E+01  3.51000E+01
     3.53E+01  3.55000E+01  3.57000E+01  3.59000E+01  3.61000E+01  3.63000E+01
     3.65E+01  3.67000E+01  3.69000E+01  3.71000E+01  3.73000E+01  3.75000E+01
     3.77E+01  3.79000E+01  3.81000E+01  3.83000E+01  3.85000E+01  3.87000E+01
```

Table A.1 (cont.)

```
     3.89E+01  3.91000E+01  3.93000E+01  3.95000E+01  3.97000E+01  3.99000E+01
     4.01E+01  4.03000E+01  4.05000E+01  4.07000E+01  4.09000E+01  4.11000E+01
     4.13E+01  4.15000E+01  4.17000E+01
c    NE213 low bias response function
de5  lin 1.6 1.8 1.9 2.0 2.1 2.2 2.3 2.4 2.5 2.75
     3.0 3.5 4.0 4.5 5.0 5.5 6.0 6.4 6.6 6.8 7.0
     7.5 8.1 8.5 9.0 10.0 11.0 12.0 12.5 13.0
     13.5 14.0 15.0 16.0
df5  lin  0.00 1.46 1.86 2.26 2.58 3.00 3.29 3.42
     3.63 3.95 4.10 4.25 4.33 4.39 4.40 4.37 4.28
     4.15 4.20 4.18 4.12 3.97 3.80 3.77 3.65 3.44
     3.24 3.06 3.01 2.98 2.98 3.01 3.08 3.25
fc15 NE213 detector, low bias, 766.0 cm flightpath, 30 degrees.
f15x:n -663.4 383 0
t15   15.5 17.5 24.9 39.1
c     NE213 low bias response function
de15 lin 1.6 1.8 1.9 2.0 2.1 2.2 2.3 2.4 2.5 2.75
     3.0 3.5 4.0 4.5 5.0 5.5 6.0 6.4 6.6 6.8 7.0
     7.5 8.1 8.5 9.0 10.0 11.0 12.0 12.5 13.0
     13.5 14.0 15.0 16.0
df15 lin  0.00 1.46 1.86 2.26 2.58 3.00 3.29 3.42
     3.63 3.95 4.10 4.25 4.33 4.39 4.40 4.37 4.28
     4.15 4.20 4.18 4.12 3.97 3.80 3.77 3.65 3.44
     3.24 3.06 3.01 2.98 2.98 3.01 3.08 3.25
c
c    ENDF/B-VI
m1   26054.60c .0562600
     26056.60c .8896840
     26057.60c .0213400
     26058.60c .0027160
      6000.60c .012
     25055.60c .010
     15031.60c .007
     16032.60c .001
m2    7014.60c -.7885
      8016.60c -.2115
cut:n 39.1 1.6
print
prdmp 2j -1
nps  400000
```

Table A.2 Input file for the ENDF/B-VI Fusion Reactor Shielding Benchmark for Configuration 7, On Axis.

```
Fusion Spectra Problem ENDF/B-VI
    1 1 7.506e-2 1 -2 10 -21 -22 29 $ floor cell $
    2 1 7.506e-2 7 -8 10 -21 -22 29 $ ceiling cell $
    3 1 7.506e-2 2 -7 10 -21 -22 23 $ left wall cell $
    4 1 7.506e-2 2 -7 10 -21 -28 29 $ right wall cell $
    5 1 7.506e-2 2 -7 20 -21 -23 28 $ front wall cell $
    6 2 4.614e-5 2 -4 10 -11 -23 32 $ left door cell $
    7 2 4.614e-5 2 -4 10 -11 -33 34 $ middle door cell $
    8 2 4.614e-5 2 -4 10 -11 -35 28 $ right door cell $
    9 1 7.506e-2 4 -7 10 -11 -23 32 $ concrete above left door $
   10 1 7.506e-2 4 -7 10 -11 -33 34 $ concrete above middle door
   11 1 7.506e-2 4 -7 10 -11 -35 28 $ concrete above right door
   12 1 7.506e-2 2 -4 10 -11 -32 33 $ concrete cell betwn l/m doors
   13 1 7.506e-2 2 -4 10 -11 -34 35 $ concrete cell betwn m/r doors
   14 1 7.506e-2 4 -7 10 -11 -32 33 $ wall concrete above cell 12
   15 1 7.506e-2 4 -7 10 -11 -34 35 $ wall concrete above cell 13
   16 2 4.614e-5 2 -4 11 -12 -23 32 $ air cell betwn left door & block back
   17 2 4.614e-5 2 -4 11 -12 -33 34 $ air cell betwn middle door & block back
   18 2 4.614e-5 2 -4 11 -12 -35 28 $ air cell betwn right door & block back
   19 2 4.614e-5 2 -4 11 -12 -32 33 $ air cell betwn cell12 door & block back
   20 2 4.614e-5 2 -4 11 -12 -34 35 $ air cell betwn cell13 door & block back
   21 2 4.614e-5 4 -7 11 -12 -23 32 $ air cell betwn cell 9 door & block back
   22 2 4.614e-5 4 -7 11 -12 -33 34 $ air cell betwn cell10 door & block back
   23 2 4.614e-5 4 -7 11 -12 -35 28 $ air cell betwn cell11 door & block back
   24 2 4.614e-5 4 -7 11 -12 -32 33 $ air cell betwn cell14 door & block back
   25 2 4.614e-5 4 -7 11 -12 -34 35 $ air cell betwn cell15 door & block back
   26 2 4.614e-5 6 -7 12 -15 -23 32 $ cells 26-35: air cells abv the block
   27 2 4.614e-5 6 -7 12 -15 -32 33
   28 2 4.614e-5 6 -7 12 -15 -33 34
   29 2 4.614e-5 6 -7 12 -15 -34 35
   30 2 4.614e-5 6 -7 12 -15 -35 28
   31 2 4.614e-5 6 -7 15 -17 -23 32
   32 2 4.614e-5 6 -7 15 -17 -32 33
   33 2 4.614e-5 6 -7 15 -17 -33 34
   34 2 4.614e-5 6 -7 15 -17 -34 35
   35 2 4.614e-5 6 -7 15 -17 -35 28
   36 2 4.614e-5 2 -3 12 -15 -23 32 $ cells 36-47: air cells left of block
   37 2 4.614e-5 2 -3 12 -15 -32 24
   38 2 4.614e-5 2 -3 15 -17 -23 32
   39 2 4.614e-5 2 -3 15 -17 -32 24
   40 2 4.614e-5 3 -4 12 -15 -23 32
   41 2 4.614e-5 3 -4 12 -15 -32 24
   42 2 4.614e-5 3 -4 15 -17 -23 32
   43 2 4.614e-5 3 -4 15 -17 -32 24
   44 2 4.614e-5 4 -6 12 -15 -23 32
   45 2 4.614e-5 4 -6 12 -15 -32 24
   46 2 4.614e-5 4 -6 15 -17 -23 32
   47 2 4.614e-5 4 -6 15 -17 -32 24
   48 2 4.614e-5 2 -3 12 -15 -27 35 $ cells 48-59: air cells right of block
   49 2 4.614e-5 2 -3 12 -15 -35 28
```

Table A.2 (cont.)

```
51-          50 2 4.614e-5 2 -3 15 -17 -27 35
52-          51 2 4.614e-5 2 -3 15 -17 -35 28
53-          52 2 4.614e-5 3 -4 12 -15 -27 35
54-          53 2 4.614e-5 3 -4 12 -15 -35 28
55-          54 2 4.614e-5 3 -4 15 -17 -27 35
56-          55 2 4.614e-5 3 -4 15 -17 -35 28
57-          56 2 4.614e-5 4 -6 12 -15 -27 35
58-          57 2 4.614e-5 4 -6 12 -15 -35 28
59-          58 2 4.614e-5 4 -6 15 -17 -27 35
60-          59 2 4.614e-5 4 -6 15 -17 -35 28
61-          60 2 4.614e-5 6 -7 17 -40 -23 32 $ cells 60-69: air cells abv thermal shield
62-          61 2 4.614e-5 6 -7 17 -40 -32 33
63-          62 2 4.614e-5 6 -7 17 -40 -33 34
64-          63 2 4.614e-5 6 -7 17 -40 -34 35
65-          64 2 4.614e-5 6 -7 17 -40 -35 28
66-          65 2 4.614e-5 6 -7 40 -20 -23 32
67-          66 2 4.614e-5 6 -7 40 -20 -32 33
68-          67 2 4.614e-5 6 -7 40 -20 -33 34
69-          68 2 4.614e-5 6 -7 40 -20 -34 35
70-          69 2 4.614e-5 6 -7 40 -20 -35 28
71-          70 2 4.614e-5 2 -3 17 -40 -23 32 $ cells 70-81: air cells left of thermal shi
72-          71 2 4.614e-5 2 -3 17 -40 -32 24
73-          72 2 4.614e-5 2 -3 40 -20 -23 32
74-          73 2 4.614e-5 2 -3 40 -20 -32 24
75-          74 2 4.614e-5 3 -4 17 -40 -23 32
76-          75 2 4.614e-5 3 -4 17 -40 -32 24
77-          76 2 4.614e-5 3 -4 40 -20 -23 32
78-          77 2 4.614e-5 3 -4 40 -20 -32 24
79-          78 2 4.614e-5 4 -6 17 -40 -23 32
80-          79 2 4.614e-5 4 -6 17 -40 -32 24
81-          80 2 4.614e-5 4 -6 40 -20 -23 32
82-          81 2 4.614e-5 4 -6 40 -20 -32 24
83-          82 2 4.614e-5 2 -3 17 -40 -27 35 $ cells 82-93: air cells right of thermal sh
84-          83 2 4.614e-5 2 -3 17 -40 -35 28
85-          84 2 4.614e-5 2 -3 40 -20 -27 35
86-          85 2 4.614e-5 2 -3 40 -20 -35 28
87-          86 2 4.614e-5 3 -4 17 -40 -27 35
88-          87 2 4.614e-5 3 -4 17 -40 -35 28
89-          88 2 4.614e-5 3 -4 40 -20 -27 35
90-          89 2 4.614e-5 3 -4 40 -20 -35 28
91-          90 2 4.614e-5 4 -6 17 -40 -27 35
92-          91 2 4.614e-5 4 -6 17 -40 -35 28
93-          92 2 4.614e-5 4 -6 40 -20 -27 35
94-          93 2 4.614e-5 4 -6 40 -20 -35 28
95-          94 4 8.75e-2 3 -5 -25 26 15 -41 $ cells 94-103: air and shield cells inside
96-          95 4 8.75e-2 3 -5 -25 26 41 -42 $ the concrete box
97-          96 4 8.75e-2 3 -5 -25 26 42 -43
98-          97 4 8.75e-2 3 -5 -25 26 43 -44
99-          98 6 .11150 3 -5 -25 26 44 -45
100-         99 4 8.75e-2 3 -5 -25 26 45 -46
```

Table A.2 (cont.)

```
101-         100 6 .11150 3 -5 -25 26 46 -47
102-         101 4 8.75e-2 3 -5 -25 26 47 -48
103-        1021 2 4.614e-5 3 -5 -25 26 461 -462
104-        1022 2 4.614e-5 3 -5 -25 26 462 -463
105-        1023 2 4.614e-5 3 -5 -25 26 463 -49
106-         102 2 4.614e-5 3 -5 -25 26 48 -461
107-         103 2 4.614e-5 3 -5 -25 26 49 -17
108-         104 2 4.614e-5 3 -9 -25 26 17 -18 $ air cell betwn inner box and thermal shield
109-         105 2 4.614e-5 3 -9 -30 31 19 -40 $ cells 105-106: air cells fitting between
110-         106 2 4.614e-5 3 -9 -30 31 40 -20 $ the thermal shield and the front wall
111-         107 2 4.614e-5 9 -6 -24 27 17 -18 $ cells 107-109: air cells between the upper
112-         108 2 4.614e-5 9 -6 -24 27 18 -40 $ horizontal edge of the concrete block
113-         109 2 4.614e-5 9 -6 -24 27 40 -20 $ and the front wall
114-         110 2 4.614e-5 2 -3 -24 27 17 -18 $ cells 110-112: air cells between the
115-         111 2 4.614e-5 2 -3 -24 27 18 -40 $ lower horizontal edge of the concrete
116-         112 2 4.614e-5 2 -3 -24 27 40 -20 $ box  and the front wall
117-         113 2 4.614e-5 3 -9 -24 25 17 -18 $ cells 113-118: air cells between the
118-         114 2 4.614e-5 3 -9 -24 25 18 -40 $ right and left vertical concrete box
119-         115 2 4.614e-5 3 -9 -24 25 40 -20 $ walls and the front wall
120-         116 2 4.614e-5 3 -9 -26 27 17 -18
121-         117 2 4.614e-5 3 -9 -26 27 18 -40
122-         118 2 4.614e-5 3 -9 -26 27 40 -20
123-         119 0 -36 12 -13 $ vacuum inside beamline
124-         120 0 -36 13 -14 $ vacuum inside iron can
125-         121 0 14 -15 -38 $ vacuum inside iron pipe
126-         122 3 8.48e-2 36 -37 12 -13 $ beamline
127-         123 3 8.48e-2 36 -39 13 -14 $ iron can
128-         124 3 8.48e-2 38 -39 14 -15 $ iron pipe
129-         125 5 1.1139e-1 37 -39 12 -13
130-         126 1 7.506e-2 5 -6 12 -15 -24 33 $ cells 126-134: concrete box top cells
131-         127 1 7.506e-2 5 -6 12 -15 -33 34
132-         128 1 7.506e-2 5 -6 12 -15 -34 27
133-         129 1 7.506e-2 5 -6 15 -45 -24 33
134-         130 1 7.506e-2 5 -6 15 -45 -33 34
135-         131 1 7.506e-2 5 -6 15 -45 -34 27
136-         132 1 7.506e-2 5 -6 45 -17 -24 33
137-         133 1 7.506e-2 5 -6 45 -17 -33 34
138-         134 1 7.506e-2 5 -6 45 -17 -34 27
139-         135 1 7.506e-2 2 -3 12 -15 -24 33 $ cells 135-143: cncr box bottom cells
140-         136 1 7.506e-2 2 -3 12 -15 -33 34
141-         137 1 7.506e-2 2 -3 12 -15 -34 27
142-         138 1 7.506e-2 2 -3 15 -45 -24 33
143-         139 1 7.506e-2 2 -3 15 -45 -33 34
144-         140 1 7.506e-2 2 -3 15 -45 -34 27
145-         141 1 7.506e-2 2 -3 45 -17 -24 33
146-         142 1 7.506e-2 2 -3 45 -17 -33 34
147-         143 1 7.506e-2 2 -3 45 -17 -34 27
148-         144 1 7.506e-2 -24 25 3 -50 12 -15 $ cells 144-149: concrete box left
149-         145 1 7.506e-2 -24 25 3 -50 15 -45 $ vertical wall cells
150-         146 1 7.506e-2 -24 25 3 -50 45 -17
```

Table A.2 (cont.)

```
151-        147 1 7.506e-2 -24 25 50 -5 12 -15
152-        148 1 7.506e-2 -24 25 50 -5 15 -45
153-        149 1 7.506e-2 -24 25 50 -5 45 -17
154-        150 1 7.506e-2 -26 27 3 -50 12 -15 $ cells 150-155: concrete box right
155-        151 1 7.506e-2 -26 27 3 -50 15 -45 $ vertical wall cells
156-        152 1 7.506e-2 -26 27 3 -50 45 -17
157-        153 1 7.506e-2 -26 27 50 -5 12 -15
158-        154 1 7.506e-2 -26 27 50 -5 15 -45
159-        155 1 7.506e-2 -26 27 50 -5 45 -17
160-        156 1 7.506e-2 3 -5 -25 26 39 12 -51 $ cells 156-164: inner concrete box cells
161-        157 1 7.506e-2 3 -5 -25 26 39 51 -52
162-        158 1 7.506e-2 3 -5 -25 26 39 52 -53
163-        159 1 7.506e-2 3 -5 -25 26 39 53 -54
164-        160 1 7.506e-2 3 -5 -25 26 39 54 -55
165-        161 1 7.506e-2 3 -5 -25 26 39 55 -56
166-        162 1 7.506e-2 3 -5 -25 26 39 56 -57
167-        163 1 7.506e-2 3 -5 -25 26 39 57 -58
168-        164 1 7.506e-2 3 -5 -25 26 39 58 -15
169-      c       165 2 4.614e-5 9 -5 -25 26 18 -40 $ cells 165-170: air cells centered
170-      c       166 2 4.614e-5 9 -5 -25 26 40 -20 $ around the thermal shield
171-        167 2 4.614e-5 -25 30 3 -9 18 -40
172-        168 2 4.614e-5 -25 30 3 -9 40 -20
173-        169 2 4.614e-5 -31 26 3 -9 18 -40
174-        170 2 4.614e-5 -31 26 3 -9 40 -20
175-        171 4 8.75e-2 18 -19 3 -9 -30 31 $ thermal shield
176-        172 0 -1  $ void cell below the concrete room
177-        173 0  8 $ void cell above the concrete room
178-        174 0  1 -8 -22 29 -10 $ void cell behind the rear wall
179-        175 0  1 -8 -22 29 21  $ void cell in front of the front wall
180-        176 0  1 -8 22 $ void cell left of the room
181-        177 0  1 -8 -29 $ void cell right of the room
182-
183-          1 pz -91.44
184-          2 pz 0 $ upper floor plane
185-          3 pz 81.2 $ inner box bottom/lower thermal shield edge
186-          4 pz 218.4 $ door upper edge
187-          5 pz 253.92 $ inner box top
188-          6 pz 317.50 $ concrete box top
189-          7 pz 495.30 $ ceiling plane (lower)
190-          8 pz 586.74 $ ceiling plane (upper)
191-          9 pz 233.60 $ upper thermal shield edge
192-         10 py -29.21 $ rear wall plane (rear)
193-         11 py 0 $ rear wall plane (front)
194-         12 py 160.02 $ rear of concrete box
195-         13 py 208.28 $ end of paraffin
196-         14 py 225.56 $ rear edge of iron can
197-         15 py 253.06 $ end of iron pipe/rear of inner box
198-         16 py 232.02 $ plane of target
199-         17 py 353.06 $ front of concrete box
200-         18 py 436.52 $ front of thermal shield
```

Table A.2 (cont.)

```
201-          19 py 441.60 $ rear of thermal shield
202-          20 py 570.20 $ front wall plane (inside)
203-          21 py 661.64 $ front wall plane (outside)
204-          22 px 91.44  $ left wall plane (outside)
205-          23 px 0      $ left wall plane (inside)
206-          24 px -200.66 $ left side of concrete box
207-          25 px -278.76 $ left side of inner box
208-          26 px -434.97 $ right side of inner box
209-          27 px -513.08 $ right side of concrete box
210-          28 px -716.28 $ right wall plane (inside)
211-          29 px -807.72 $ right wall plane (outside)
212-          30 px -280.66 $ left edge of thermal shield
213-          31 px -433.06 $ right edge of thermal shield
214-          32 px -114.3  $ right edge of left door
215-          33 px -300.99 $ left edge of middle door
216-          34 px -415.29 $ right edge of middle door
217-          35 px -601.98 $ left edge of right door
218-          36 c/y -356.87 157.4 4.5   $ beamline inner surface
219-          37 c/y -356.87 157.4 5.0   $ beamline outer surface
220-          38 c/y -356.87 157.4 8.87  $ iron pipe inner surface
221-          39 c/y -356.87 157.4 16.37 $ iron pipe outer surface
222-          40 py 470
223-          41 py 263.06
224-          42 py 273.06
225-          43 py 283.54
226-          44 py 288.62
227-          45 py 293.70
228-          46 py 298.78
229-          47 py 303.86
230-          48 py 308.94
231-         461 py 313.06
232-         462 py 323.06
233-         463 py 333.06
234-          49 py 343.06
235-          50 pz 160
236-          51 py 170
237-          52 py 180
238-          53 py 190
239-          54 py 200
240-          55 py 210
241-          56 py 220
242-          57 py 230
243-          58 py 240
244-
245-       mode n
246-       wwp:n 4 3 2
247-       wwe:n  1.0000E+02
248-       wwn1:n   2.8502E-03  2.4082E-02  2.0065E-02  2.7644E-03  5.0534E-03
249-                1.0000E+00  2.3250E-01  1.0000E+00  9.3745E-02  1.1525E-01
250-                3.4394E-01  1.1440E-01  2.9391E-01  3.2889E-01  2.5248E-03
```

Table A.2 (cont.)

```
                2.4081E-02  3.3935E-02  2.6292E-02  9.5316E-02  9.7181E-02
                2.3367E-02  9.5228E-03  2.2842E-02  4.3222E-02  5.2033E-03
                2.0471E-02  2.0693E-02  2.6450E-02  2.3806E-02  2.4143E-02
                8.7829E-03  1.9774E-02  3.6164E-02  2.5231E-02  7.0119E-02
                3.2090E-02  1.3674E-01  7.2456E-03  8.3109E-03  1.0087E-02
                2.4852E-02  2.9118E-02  2.4378E-02  1.6170E-02  1.5929E-02
                3.4177E-02  1.7330E-02  4.9869E-02  1.6065E-02  1.5939E-04
                2.1902E-04  2.6421E-02  1.4780E-03  1.3265E-02  1.0118E-03
                4.9465E-04  5.9927E-04  1.4786E-02  7.8238E-03  1.1610E-02
                1.7742E-02  1.3117E-02  2.3405E-02  1.1717E-02  8.1729E-03
                2.6723E-02  7.4441E-03  5.7407E-03  2.2380E-02  1.5195E-02
                1.0032E-02  1.9793E-02  4.2505E-02  3.8536E-03  1.7791E-03
                6.7549E-03  1.9018E-03  2.8012E-03  1.2275E-02  2.8012E-03
                9.7178E-04  1.0291E-04  1.7744E-03  3.4768E-03  1.5151E-03
                4.3000E-03  5.1276E-03  1.2074E-02  1.8351E-03  6.7915E-03
                8.7327E-03  1.0296E-02  7.7935E-03  3.8375E-01  1.2152E-01
                4.0273E-02  7.9402E-03  6.5206E-03  2.3107E-03  1.2793E-03
                3.9490E-04  1.3827E-03  1.1491E-03  1.3867E-03  1.3467E-03
                1.4074E-03  5.0348E-04  2.4496E-03  5.0509E-03  2.5998E-03
                4.2980E-03  4.9403E-03  1.6865E-04  3.4768E-03  4.0966E-03
                3.0563E-03  2.5247E-03  3.4007E-03  2.1128E-04  1.3136E-02
                3.9994E-03  1.7030E+00  5.8084E+00  4.9798E-01  1.9183E+00
                1.0000E+01  1.0826E+00  3.6946E+00  5.0967E-01  3.2130E-01
                9.7112E-02  1.0000E+00  1.0000E+01  9.0891E-02  1.1782E-03
                9.0442E-04  6.3920E-04  1.0000E+01  1.0811E+01  1.0000E+00
                7.4808E-01  1.3395E+00  8.8688E-01  3.6126E-03  1.3345E-03
                1.9702E-04  4.3322E+00  1.0784E+00  2.0723E-03  5.6555E-01
                2.5977E-01  1.3386E-03  1.1988E-01  2.3554E-02  1.2882E-03
                5.0000E+00  2.2009E-01  8.6605E-04  1.3988E-01  3.0066E-01
                3.8736E+00  5.0000E+00  1.0000E+01  1.0000E+01  1.0000E+01
                5.1133E+00  2.2167E+00  3.2309E-03  3.4007E-03  8.6336E-03
                3.3759E-03  9.6020E-04 -1.0000E+00 -1.0000E+00 -1.0000E+00
               -1.0000E+00 -1.0000E+00 -1.0000E+00
     sdef pos=-356.87 232.02 157.4 dir=d1 erg=fdir=d2 rad=d3 vec=0 1 0
          sur=16
     si1  a  -1.0000 -.99619 -.98481 -.96593 -.93969
             -.90631 -.86603 -.81915 -.76604 -.70711
             -.64279 -.57358 -.50000 -.42262 -.34202
             -.25882 -.17365 -.08716  .00000  .08716
              .17365  .25882  .34202  .42262  .50000
              .57358  .64279  .70711  .76604  .81915
              .86603  .90631  .93969  .96593  .98481
              .99619  1.0000
     sp1      .874 .874 .875 .876 .877
              .879 .882 .884 .888 .891
              .895 .899 .904 .909 .914
              .919 .924 .930 .935 .941
              .946 .952 .957 .962 .967
              .972 .976 .981 .985 .988
              .991 .994 .996 .998 .999
```

Table A.2 (cont.)

```
301-              1.0 1.0
302-      ds2  q  -.99619 180 -.98481 175 -.96593 170 -.93962 165 -.90631 160
303-             -.86603 155 -.81915 150 -.76604 145 -.70711 140 -.64279 135
304-             -.57358 130 -.50000 125 -.42262 120 -.34202 115 -.25882 110
305-             -.17365 105 -.08716 100  0.0000 95   .08716 90   .17365 85
306-              .25882 80   .34202 75   .42262 70   .50000 65   .57358 60
307-              .64279 55   .70711 50   .76604 45   .81915 40   .86603 35
308-              .90631 30   .93969 25   .96593 20   .98481 15   .99619 10
309-              1.0000 5
310-      si3  h 0 .64
311-      sp3  d -21 1
312-      si5  h 15.106 15.110
313-      sp5  d 0 1
314-      si10 h 15.095 15.106
315-      sp10 d 0 1
316-      si15 h 15.075 15.095
317-      sp15 d 0 1
318-      si20 h 15.049 15.075
319-      sp20 d 0 1
320-      si25 h 15.015 15.049
321-      sp25 d 0 1
322-      si30 h 14.974 15.015
323-      sp30 d 0 1
324-      si35 h 14.927 14.974
325-      sp35 d 0 1
326-      si40 h 14.873 14.927
327-      sp40 d 0 1
328-      si45 h 14.814 14.873
329-      sp45 d 0 1
330-      si50 h 14.750 14.814
331-      sp50 d 0 1
332-      si55 h 14.681 14.750
333-      sp55 d 0 1
334-      si60 h 14.608 14.681
335-      sp60 d 0 1
336-      si65 h 14.532 14.608
337-      sp65 d 0 1
338-      si70 h 14.453 14.532
339-      sp70 d 0 1
340-      si75 h 14.372 14.453
341-      sp75 d 0 1
342-      si80 h 14.289 14.372
343-      sp80 d 0 1
344-      si85 h 14.206 14.289
345-      sp85 d 0 1
346-      si90 h 14.123 14.206
347-      sp90 d 0 1
348-      si95 h 14.040 14.123
349-      sp95 d 0 1
350-      si100 h 13.958 14.040
```

Table A.2 (cont.)

```
351-       sp100 d 0 1
352-       si105 h 13.878 13.958
353-       sp105 d 0 1
354-       si110 h 13.800 13.878
355-       sp110 d 0 1
356-       si115 h 13.725 13.800
357-       sp115 d 0 1
358-       si120 h 13.654 13.725
359-       sp120 d 0 1
360-       si125 h 13.586 13.654
361-       sp125 d 0 1
362-       si130 h 13.522 13.586
363-       sp130 d 0 1
364-       si135 h 13.464 13.522
365-       sp135 d 0 1
366-       si140 h 13.410 13.464
367-       sp140 d 0 1
368-       si145 h 13.362 13.410
369-       sp145 d 0 1
370-       si150 h 13.320 13.362
371-       sp150 d 0 1
372-       si155 h 13.284 13.320
373-       sp155 d 0 1
374-       si160 h 13.254 13.284
375-       sp160 d 0 1
376-       si165 h 13.230 13.254
377-       sp165 d 0 1
378-       si170 h 13.214 13.230
379-       sp170 d 0 1
380-       si175 h 13.203 13.214
381-       sp175 d 0 1
382-       si180 h 13.200 13.203
383-       sp180 d 0 1
384-       f5:n  -356.87 386.52 157.4 1
385-       e5      .85 .95 1.05 1.15 1.25 1.35 1.45 1.55 1.65 1.75 1.85 1.95
386-               2.15 2.35 2.55 2.75 2.95 3.15 3.35 3.55 3.75 3.95 4.15 4.45
387-               4.75 5.05 5.35 5.65 5.95 6.25 6.55 6.85 7.25 7.75 8.25 8.75
388-               9.25 9.75 10.25 10.75 11.25 11.75 12.55 13.35 14.15 14.95
389-               15.75 16.55
390-       em5     1 10 10r 5 10r 3.33 8r 2.5 2 8r 1.25 5r
391-       fq5    e d
392-       c     ft5   geb .03 .08                $ mcnp4 patch format
393-       ft5   geb 0 .282842713 .375         $ mcnp4a format
394-       prdmp  2j 1
395-       c     f15:p -356.87 386.52 157.4 1
396-       c     e15     .72 .76 .80 .84 .88 .92 .96 1.0 1.04 1.08 1.15 1.2 1.25
397-       c       1.3 1.35 1.4 1.45 1.5 1.55 1.6 1.65 1.72 1.8 1.88 1.96
398-       c       2.04 2.12 2.2 2.28 2.36 2.45 2.55 2.65 2.75 2.85 2.95 3.05
399-       c       3.15 3.25 3.35 3.45 3.55 3.66 3.79 3.93 4.06 4.19 4.32
400-       c       4.45 4.58 4.71 4.84 4.97 5.1 5.23 5.4 5.57 5.74 5.91 6.08
```

Table A.2 (cont.)

```
c      6.25 6.42 6.6 6.8 7.0 7.2 7.4 7.6 7.8 8.0 8.2 8.4 8.6 8.8 9.0
c      9.2 9.4 9.6 9.8 10
c    em15   1 25 8r 14.286 20 9r 14.286 12.5 7r 11.111 10 10r 9.0909 7.6923
c      7.1429 7.6923 9r 5.8824 6r 5.5556 5 16r
cut:n 1e33 .850 $ ignore neutrons below the detector response
wwg  5 121 0 -356.87 386.52 157.4
m1    1001.60c 7.86e-3
      8016.60c 4.39e-2
     11023.60c 1.05e-3
     12000.60c 1.40e-4
     13027.60c 2.39e-3
     14000.60c 1.58e-2
     19000.60c 6.90e-4
     20000.60c 2.92e-3
     26054.60c 1.798e-5
     26056.60c 2.843e-4
     26057.60c 6.82e-6
     26058.60c 8.68e-7
m3   26054.60c 4.918e-3
     26056.60c 7.778e-2
     26057.60c 1.866e-3
     26058.60c 2.374e-4
m4   24050.60c 7.699e-4
     24052.60c 1.483e-2
     24053.60c 1.681e-3
     24054.60c 4.177e-4
     25055.60c 1.77e-3
     26054.60c 3.492e-3
     26056.60c 5.522e-2
     26057.60c 1.324e-3
     26058.60c 1.686e-4
     28058.60c 5.346e-3
     28060.60c 2.044e-3
     28061.60c 8.848e-5
     28062.60c 2.811e-4
     28064.60c 7.125e-5
m2    7014.60c 3.64e-5
      8016.60c 9.74e-6
m5    1001.60c 5.926e-2
      6000.60c 3.338e-2
      8016.60c 1.125e-2
      3006.60c 5.565e-4
      3007.60c 6.944e-3
m6    1001.60c 7.13e-2
      6000.60c 3.41e-2
      5010.60c 4.87e-4
      5011.60c 1.97e-3
      8016.60c 3.64e-3
print
nps   1000000
```

Table A.3 Input file for the ENDF/B-VI 76 cm diameter iron sphere with a ^{252}Cf source.

```
1-      Fe Sphere with 76 cm dia  ENDF/B-VI
2-      1    2 -.001288 -3
3-      2    1 -7.85 -1 3 -4
4-      3    1 -7.85 1 2 3 -4
5-      4    2 -.001288 1 -2 3 -4
6-      5    1 -7.85 -1 4 -5
7-      6    1 -7.85 1 2 4 -5
8-      7    2 -.001288 1 -2 4 -5
9-      8    1 -7.85 -1 5 -6
10-     9    1 -7.85 1 2 5 -6
11-     10   2 -.001288 1 -2 5 -6
12-     11   2 -.001288 6 -7
13-     12   0 7
14-
15-     1    px .1
16-     2    cx 4.75
17-     3    so 7.5
18-     4    so 19
19-     5    so 28.5
20-     6    so 38
21-     7    so 1000
22-
23-     imp:n 2 2 2 2 3 3 3 6 6 6 6 0
24-     sdef pos=0 0 0 erg=d2
25-     sp2 -2 1.42
26-     fc5  NE213 detector response function, 200.0 cm flightpath, 90 degrees.
27-     fx5:n 0 200 0
28-     e5          0.75  1.0   1.25  1.50  1.75  2.00  2.25
29-          2.50  2.75  3.00  3.25  3.50  3.75  4.00  4.25
30-          4.50  4.75  5.00  5.25  5.50  5.75  6.00  6.25
31-          6.50  6.75  7.00  7.25  7.50  7.75  8.00  8.25
32-          8.50  8.75  9.00  9.25  9.50  9.75 10.00 10.25
33-          10.50 10.75 11.00 11.25 11.50 11.75 12.00 12.25
34-          12.50 12.75 13.00 13.25 13.50 13.75 14.00 14.25
35-          14.50 14.75 15.00 15.5  16    18    20
36-     c    NE213 low bias response function
37-     de0  lin 1.6 1.8 1.9 2.0 2.1 2.2 2.3 2.4 2.5 2.75
38-          3.0 3.5 4.0 4.5 5.0 5.5 6.0 6.4 6.6 6.8 7.0
39-          7.5 8.1 8.5 9.0 10.0 11.0 12.0 12.5 13.0
40-          13.5 14.0 15.0 16.0
41-     df0  lin  0.00 1.46 1.86 2.26 2.58 3.00 3.29 3.42
42-          3.63 3.95 4.10 4.25 4.33 4.39 4.40 4.37 4.28
43-          4.15 4.20 4.18 4.12 3.97 3.80 3.77 3.65 3.44
44-          3.24 3.06 3.01 2.98 2.98 3.01 3.08 3.25
45-     fc15  NE213 detector, low bias, 200.0 cm flightpath, 90 degrees.
46-     f15x:n 0 200 0
47-     e15   2 5 10 13 20
48-     c
49-     c    ENDF/B-VI
50-     m1   26054.60c .0562600
```

Table A.3 (cont.)

```
51-           26056.60c .8896840
52-           26057.60c .0213400
53-           26058.60c .0027160
54-            6000.60c .012
55-           25055.60c .010
56-           15031.60c .007
57-           16032.60c .001
58-      m2    7014.60c -.7885
59-            8016.60c -.2115
60-      cut:n j .5
61-      print
62-      prdmp 2j 1
63-      nps  400000
64-      f2:n 6
```

Table A.4 Input file for the ENDF/B-VI 93 cm iron slab of the Oak Ridge National Laboratory Benchmark For Neutron Transport through Iron.

```
1-      ORNL Iron Benchmark 93 cm slab ENDF/B-VI
2-      1 0 -1 3 -4 5 -6
3-      2 0 2 3 -4 5 -6
4-      3 0 -3
5-      4 0 4
6-      5 0 -5
7-      6 0 6
8-      7 2 4.614e-5 1 -7 9 -10 19 -20
9-      8 2 4.614e-5 1 -8 9 -10 13 -19
10-     9 2 4.614e-5 1 -8 9 -10 20 -14
11-     10 2 4.614e-5 1 -8 11 -9 13 -14
12-     11 2 4.614e-5 1 -8 10 -12 13 -14
13-     12 2 4.614e-5 1 -2 3 -11 5 -6
14-     13 2 4.614e-5 1 -2 12 -4 5 -6
15-     14 2 4.614e-5 1 -2 11 -12 5 -13
16-     15 2 4.614e-5 1 -2 11 -12 14 -6
17-     16 1 -7.79 -8 -24
18-     17 1 -7.79 8 -15 11 -12 13 -14 16
19-     18 2 4.614e-5 8 -15 -16
20-     19 3 -1.0 15 -17 11 -12 13 -14 16
21-     20 3 -1.0 15 -17 18 -16
22-     21 2 4.614e-5 15 -17 -18
23-     22 4 0.11139 17 -21 11 -12 13 -14 16
24-     23 3 -1.0 17 -21 22 -16
25-     24 2 4.614e-5 17 -2 -22
26-     25 2 4.614e-5 21 -23 11 -12 13 -14 22
27-     26 3 -1.0 23 -2 22 -16
28-     27 2 4.614e-5 23 -2 11 -12 13 -14 16
29-     28 1 -7.79 -8 24 -25
30-     29 1 -7.79 -8 25 -26
31-     30 1 -7.79 -8 26 -27
32-     31 1 -7.79 -8 27 -28
33-     32 1 -7.79 -8 28 -29
34-     33 1 -7.79 -8 29 -30
35-     34 1 -7.79 -8 30 -31
36-     35 1 -7.79 -8 31 -32 9 -10 19 -20
37-     36 1 -7.79 -8 32 -33 9 -10 19 -20
38-     37 1 -7.79 -8 33 -34 9 -10 19 -20
39-     38 1 -7.79 -8 34 -35 9 -10 19 -20
40-     39 1 -7.79 -8 35 -36 9 -10 19 -20
41-     40 1 -7.79 -8 36 -37 9 -10 19 -20
42-     41 1 -7.79 -8 37 -38 9 -10 19 -20
43-     42 1 -7.79 -8 38 -39 9 -10 19 -20
44-     43 1 -7.79 -8 39 -40 9 -10 19 -20
45-     44 1 -7.79 -8 40 -41 9 -10 19 -20
46-     45 1 -7.79 -8 41 -42 9 -10 19 -20
47-     46 1 -7.79 -8 42 -43 9 -10 19 -20
48-     47 1 -7.79 -8 43 -44 9 -10 19 -20
49-     48 1 -7.79 -8 44 -45 9 -10 19 -20
50-     49 1 -7.79 -8 45 -46 9 -10 19 -20
```

Table A.4 (cont.)

```
51-      50 1 -7.79 7 -8 46 -47 9 -10 19 -20
52-      51 1 -7.79 7 -8 47 9 -10 19 -20
53-
54-      1 px -750
55-      2 px  200
56-      3 py -500
57-      4 py  500
58-      5 pz -500
59-      6 pz  500
60-      7 px -265.58
61-      8 px -172.72
62-      9 py  -76.2
63-      10 py   76.2
64-      11 py -200
65-      12 py  200
66-      13 pz -200
67-      14 pz  200
68-      15 px -161.93
69-      16 cx   18.9
70-      17 px -107.95
71-      18 x  -161.93 18.9 -107.95 5.3975
72-      19 pz  -76.2
73-      20 pz   76.2
74-      21 px  -51.435
75-      22 cx    5.3975
76-      23 px  -35.56
77-      24 sx -170.22      6.5
78-      25 sx -166.1575   14.5625
79-      26 sx -160.345    24.375
80-      27 sx -152.595    36.125
81-      28 sx -142.72     50
82-      29 sx -130.5325   66.1875
83-      30 sx -115.845    84.875
84-      31 sx  -98.47    106.25
85-      32 sx  -78.22    130.5
86-      33 sx  -54.9075  157.8125
87-      34 sx  -28.345   188.375
88-      35 sx    1.655   222.375
89-      36 sx   35.28    260
90-      37 sx   72.7175  301.4375
91-      38 sx  114.155   346.875
92-      39 sx  159.78    396.5
93-      40 sx  209.78    450.5
94-      41 sx  264.3425  509.0625
95-      42 sx  323.655   572.375
96-      43 sx  387.905   640.625
97-      44 sx  457.28    714
98-      45 sx  531.9675  792.6875
99-      46 sx  612.155   876.875
100-     47 sx  698.03    966.75
```

Table A.4 (cont.)

```
101-
102-      mode n
103-      wwp:n 5 3 5
104-      wwe:n  1.0000E+02
105-      wwn1:n  -1.0000E+00 -1.0000E+00 -1.0000E+00 -1.0000E+00 -1.0000E+00
106-             -1.0000E+00  0           0           0           0
107-              0           0           0           0           0
108-              2.5178E+06  2.6000E+06  0           1.7736E+07  3.5959E+07
109-              0           1.2338E+07  2.7810E+07  0           0
110-              0.0000E+00  0           2.2719E+06  1.4306E+06  1.2553E+06
111-              1.0407E+06  8.9104E+05  7.8092E+05  6.9713E+05  6.0664E+05
112-              5.6081E+05  5.2478E+05  4.7667E+05  4.3861E+05  4.1295E+05
113-              3.8066E+05  3.5304E+05  3.2650E+05  2.9641E+05  2.6759E+05
114-              2.2474E+05  2.1117E+05  1.7605E+05  1.2906E+05  1.5248E+05
115-              1.6280E+05
116-      sdef dir=d1 vec=-1 0 0 erg=d2 wgt=6.821e6 pos=0 0 0 cel=24
117-      c    Calculation for the source weight.
118-      c         The tabulated value for total intensity for the source from
119-      c    ORNL-4892, Table III. is 3.186e4 neutrons/cm^2/min/W/Group.
120-      c    The values in Table III. are taken from
121-      c    a circular surface area with diameter of 6.5 inches, giving an
122-      c    area of 2.141e2 cm^2.  Normalizing to 1 Watt and multiplying by
123-      c    this area gives 6.821e6 neutrons/min/Group.
124-      si1  0.99886 1
125-      sp1  0 1
126-      si2  0         1.45e-7  5.24e-7   1.89e-6  6.79e-6  2.44e-5  8.8e-5
127-           3.167e-4  1.14e-3  1.16e-3   3.7e-3   4.3e-3   5.8e-3   6.7e-3
128-           8.2e-3    8.8e-3   1.0e-2    1.5e-2   1.9e-2   2.2e-2   2.325e-2
129-           2.375e-2  2.45e-2  2.52e-2   2.57e-2  2.7e-2   3.1e-2   3.8e-2
130-           6.2e-2    6.8e-2   7.2e-2    7.7e-2   8.0e-2   8.14e-2  8.24e-2
131-           8.27e-2   8.3e-2   8.7e-2    1.1e-1   1.275e-1 1.292e-1 1.3e-1
132-           1.34e-1   1.362e-1 1.383e-1  1.395e-1 1.44e-1  1.55e-1  1.64e-1
133-           1.675e-1  1.685e-1 1.75e-1   1.82e-1  1.852e-1 2.e-1    2.08e-1
134-           2.186e-1  2.198e-1 2.32e-1   2.432e-1 2.44e-1  2.448e-1 2.62e-1
135-           2.67e-1   2.71e-1  2.75e-1   3.00e-1  3.095e-1 3.14e-1  3.307e-1
136-           3.314e-1  3.482e-1 3.505e-1  3.545e-1 3.573e-1 3.578e-1 3.588e-1
137-           3.593e-1  3.735e-1 3.75e-1   3.772e-1 3.78e-1  4.33e-1  4.365e-1
138-           4.377e-1  4.64e-1  4.675e-1  4.691e-1 4.93e-1  4.98e-1  5.03e-1
139-           5.105e-1  5.15e-1  5.34e-1   5.36e-1  5.40e-1  5.43e-1  5.465e-1
140-           5.525e-1  5.575e-1 5.59e-1   5.605e-1 5.695e-1 5.76e-1  5.80e-1
141-           5.905e-1  6.075e-1 6.125e-1  6.165e-1 6.20e-1  6.38e-1  6.44e-1
142-           6.48e-1   6.525e-1 6.59e-1   6.63e-1  6.91e-1  6.93e-1  6.97e-1
143-           7.00e-1   7.10e-1  7.32e-1   7.39e-1  7.41e-1  7.51e-1  7.525e-1
144-           7.67e-1   7.69e-1  8.20e-1   8.25e-1  8.30e-1  8.34e-1  8.36e-1
145-           8.39e-1   8.465e-1 8.525e-1  8.555e-1 8.78e-1  8.82e-1  8.91e-1
146-           8.985e-1  9.17e-1  9.19e-1   9.27e-1  9.32e-1  9.36e-1  9.395e-1
147-           9.415e-1  9.44e-1  9.46e-1   9.51e-1  9.57e-1  9.60e-1  9.74e-1
148-           9.82e-1   9.92e-1  9.98e-1   1.013    1.020    1.023    1.029
149-           1.084     1.090    1.098     1.107    1.1135   1.1165   1.1195
150-           1.130     1.136    1.155     1.169    1.192    1.197    1.205
```

Table A.4 (cont.)

```
151-          1.211    1.217    1.221     1.244    1.251    1.285    1.291
152-          1.306    1.313    1.339     1.363    1.382    1.392    1.401
153-          1.405    1.411    1.442     1.472    1.497    1.506    1.522
154-          1.567    1.587    1.638     1.6465   1.680    1.686    1.722
155-          1.747    1.783    1.81      1.82     1.889    1.90     1.943
156-          2.232    2.262    2.35      2.38     2.59     3.00     4.00
157-          5.00     6.00     8.00      1.00e1
158-      c   No-norm probability distribution (multiplied by bin width)
159-      c sp2  0        9.541e-4 5.844e-4 7.868e-4  2.72e-3  9.756e-3 3.302e-2
160-      c      1.292e-1 5.072e-1 1.796e-4 1.626     5.196e-2 2.61e-1  7.884e-2
161-      c      1.89e-1  2.658e-2 9.756e-2 1.32      6.32e-1  3.0e-1   4.788e-2
162-      c      7.4e-3   1.613e-2 1.393e-2 6.85e-3   4.459e-2 3.896e-1 1.001
163-      c      8.496    4.344e-1 1.764e-1 2.55e-1   8.76e-2  1.862e-2 9.49e-3
164-      c      8.55e-4  8.55e-4  1.484e-1 4.439     2.223    1.921e-2 4.232e-3
165-      c      1.044e-1 3.08e-2  2.793e-2 8.94e-3   1.233e-1 7.029e-1 4.464e-1
166-      c      6.615e-2 5.38e-3  2.243e-1 2.548e-1  5.376e-2 1.157    3.376e-1
167-      c      5.936e-1 7.608e-3 7.991e-1 6.922e-1  3.528e-3 3.528e-3 1.629
168-      c      1.375e-1 8.76e-2  8.76e-2  3.375     4.769e-1 1.067e-1 1.458
169-      c      2.562e-3 1.435    2.645e-2 8.04e-2   3.864e-2 7.17e-4  4.81e-3
170-      c      1.21e-3  9.699e-1 1.047e-2 2.244e-2  2.984e-3 1.26e1   4.725e-2
171-      c      5.424e-3 2.609    4.62e-2  9.584e-3  2.165    9.5e-2   9.75e-2
172-      c      2.22e-1  8.1e-2   1.465    1.624e-2  6.56e-2  3.81e-2  4.97e-2
173-      c      1.488e-1 1.055e-1 9.51e-3  9.51e-3   3.42e-1  1.788e-1 6.76e-2
174-      c      4.82e-1  1.284    1.11e-1  7.2e-2    5.53e-2  1.492    1.68e-1
175-      c      7.4e-2   9.495e-2 1.989e-1 7.6e-2    3.752    1.898e-2 7.8e-2
176-      c      4.44e-2  4.86e-1  2.354    2.366e-1  1.898e-2 4.75e-1  1.028e-2
177-      c      9.802e-1 1.796e-2 1.102e1  1.03e-1   1.005e-1 6.32e-2  1.586e-2
178-      c      3.63e-2  2.22e-1  1.392e-1 3.48e-2   1.924    5.92e-2  2.997e-1
179-      c      2.063e-1 1.212    1.478e-2 2.24e-1   8.7e-2   5.48e-2  4.235e-2
180-      c      1.37e-2  2.11e-2  1.37e-2  8.45e-2   1.206e-1 3.0e-2   6.51e-1
181-      c      2.112e-1 3.28e-1  1.17e-1  7.44e-1   1.666e-1 3.0e-2   1.206e-1
182-      c      9.735    1.206e-1 2.08e-1  2.664e-1  1.547e-1 3.0e-2   3.0e-2
183-      c      3.602e-1 1.206e-1 1.235    6.804e-1  1.822    8.85e-2  2.272e-1
184-      c      1.272e-1 1.278e-1 5.68e-2  1.944     1.813e-1 4.25     1.35e-1
185-      c      8.52e-1  1.813e-1 2.553    2.244     1.416    4.01e-1  3.186e-1
186-      c      6.64e-2  1.428e-1 3.844    3.75      2.6      3.42e-1  1.082
187-      c      8.55     1.7      1.117e1  3.324e-1  4.791    1.554e-1 5.508
188-      c      2.725    5.508    3.186    4.38e-1   2.077e1  5.225e-1 8.17
189-      c      3.662e2  3.9      3.379e1  3.9       1.863e2  6.064e2  2.186e3
190-      c      1.426e3  8.4e2    1.33e3   3.8e2
191-      c   Source energy probabilities directly from Table III, ORNL-4892
192-      sp2   0    6580    1542     576    555    554    554    565    616
193-            8.98 640      86.6   174    87.6   126    44.3   81.3   264
194-            158  100      38.3   14.8   21.5   19.9   13.7   34.3   97.4
195-            143  354      72.4   44.1   51.0   29.2   13.3   9.49   2.85
196-            2.85 37.1     193    127    11.3   5.29   26.1   14.0   13.3
197-            7.45 27.4     63.9   49.6   18.9   5.38   34.5   36.4   16.8
198-            78.2 42.2     56.0   6.34   65.5   61.8   4.41   4.41   94.7
199-            27.5 21.9     21.9   135    50.2   23.7   87.3   3.66   85.4
200-            11.5 20.1     13.8   2.39   4.81   2.42   68.3   6.98   10.2
```

Table A.4 (cont.)

```
201-          3.73  229      13.5     4.52  99.2   13.2    5.99  90.6    19.0
202-          19.5   29.6    18.0    77.1    8.12  16.4   12.7   14.2    24.8
203-          21.1    6.34    6.34   38.0   27.5   16.9   45.9   75.5    22.2
204-          18.0   15.8    82.9    28.0   18.5   21.1   30.6   19.0   134
205-          9.49   19.5    14.8    48.6  107     33.8    9.49  47.5     6.85
206-          67.6    8.98  216      20.6   20.1   15.8    7.93  12.1    29.6
207-          23.2   11.6    85.5    14.8   33.3   27.5   65.5    7.39   28.0
208-          17.4   13.7    12.1     6.85   8.44   6.85  16.9   20.1    10.0
209-          46.5   26.4    32.8    19.5   49.6   23.8   10.0   20.1   177
210-          20.1   26.0    29.6    23.8   10.0   10.0   34.3   20.1    65.0
211-          48.6   79.2    17.7    28.4   21.2   21.3   14.2   84.5    25.9
212-          125    22.5    56.8    25.9   98.2   93.5   74.5   40.1    35.4
213-          16.6   23.8   124     125    104     38.0   67.6  190      85.0
214-          219    39.1   143      25.9  153    109    153    118      43.8
215-          301    47.5   190    1267    130    384    130    887    1479
216-          2186 1426     840     665    190
217-     f5:n -548.68 0 0 0
218-     f15:n -548.68 0 0 0
219-     f25:n -548.68 0 0 0
220-     f35:n -538.52 76.2 0 0
221-     f45:n -538.52 76.2 0 0
222-     f55:n -538.52 76.2 0 0
223-     f65:n -463.59 207.01 0 0
224-     f75:n -463.59 207.01 0 0
225-     f85:n -463.59 207.01 0 0
226-     pd0    1 17r 0.1 0.1 1 1 0.1 1 27r
227-     e0       0.5     2     5     10     13     20
228-     de0  lin 3.839e-7 4.73e-7  6.07e-7  7.79e-7  1.e-6    1.285e-6 1.65e-6
229-              2.12e-6  2.72e-6  3.49e-6  4.49e-6  5.76e-6  7.40e-6  9.50e-6
230-              1.219e-5 1.566e-5 2.01e-5  2.58e-5  3.31e-5  4.26e-5  5.46e-5
231-              7.02e-5  9.01e-5  1.157e-4 1.485e-4 1.907e-4 2.45e-4  3.14e-4
232-              4.04e-4  5.18e-4  6.66e-4  8.55e-4  1.098e-3 1.409e-3 1.810e-3
233-              2.32e-3  2.98e-3  3.83e-3  4.92e-3  6.32e-3  8.11e-3  1.041e-2
234-              1.337e-2 1.717e-2 2.20e-2  2.83e-2  3.63e-2  4.67e-2  5.99e-2
235-              7.69e-2  9.88e-2  1.169e-1 1.292e-1 1.428e-1 1.578e-1 1.744e-1
236-              1.928e-1 2.13e-1  2.35e-1  2.60e-1  2.88e-1  3.18e-1  3.51e-1
237-              3.88e-1  4.29e-1  4.74e-1  5.24e-1  5.79e-1  6.40e-1  7.07e-1
238-              7.82e-1  8.64e-1  9.54e-1  1.055    1.166    1.289    1.425
239-              1.574    1.740    1.923    2.13     2.35     2.60     2.87
240-              3.17     3.50     3.87     4.28     4.73     5.23     5.78
241-              6.38     7.06     7.80     8.62     9.52     1.053e1  1.163e1
242-              1.286e1  1.421e1
243-     df5  lin 0        6.01e-1  1.004    1.244    1.391    1.464    1.491
244-              1.492    1.479    1.452    1.423    1.390    1.355    1.316
245-              1.277    1.237    1.193    1.092    1.109    1.072    1.031
246-              9.65e-1  8.47e-1  8.35e-1  8.69e-1  8.41e-1  8.02e-1  7.72e-1
247-              7.43e-1  7.01e-1  6.82e-1  6.54e-1  6.26e-1  6.00e-1  5.73e-1
248-              5.48e-1  5.25e-1  5.02e-1  4.81e-1  4.61e-1  4.41e-1  4.22e-1
249-              4.02e-1  3.84e-1  3.66e-1  3.48e-1  3.30e-1  3.12e-1  2.94e-1
250-              2.76e-1  2.57e-1  2.44e-1  2.36e-1  2.28e-1  2.20e-1  2.11e-1
```

Table A.4 (cont.)

```
251-                2.03e-1  1.947e-1 1.863e-1 1.778e-1 1.694e-1 1.609e-1 1.525e-1
252-                1.443e-1 1.359e-1 1.278e-1 1.198e-1 1.120e-1 1.044e-1 9.71e-2
253-                9.01e-2  8.34e-2  7.69e-2  7.08e-2  6.50e-2  5.95e-2  5.44e-2
254-                4.96e-2  4.51e-2  4.09e-2  3.71e-2  3.35e-2  3.01e-2  2.71e-2
255-                2.43e-2  2.18e-2  1.951e-2 1.732e-2 1.534e-2 1.476e-2 1.340e-2
256-                1.193e-2 9.83e-3  9.03e-3  7.95e-3  7.12e-3  6.35e-3  5.57e-3
257-                4.98e-3  4.40e-3
258-       df15 lin 0        1.892e-1 3.38e-1  4.45e-1  5.28e-1  5.89e-1  6.36e-1
259-                6.75e-1  7.09e-1  7.39e-1  7.67e-1  7.92e-1  8.17e-1  8.39e-1
260-                8.61e-1  8.81e-1  8.98e-1  8.69e-1  9.31e-1  9.49e-1  9.63e-1
261-                9.51e-1  8.81e-1  9.12e-1  9.99e-1  1.018    1.020    1.034
262-                1.045    1.036    1.060    1.068    1.073    1.079    1.082
263-                1.086    1.089    1.092    1.096    1.102    1.107    1.111
264-                1.115    1.123    1.131    1.140    1.151    1.164    1.180
265-                1.199    1.219    1.233    1.243    1.252    1.260    1.269
266-                1.277    1.285    1.292    1.298    1.304    1.307    1.307
267-                1.311    1.308    1.304    1.299    1.289    1.278    1.264
268-                1.246    1.227    1.203    1.176    1.146    1.114    1.078
269-                1.040    9.99e-1  9.56e-1  9.06e-1  8.65e-1  8.14e-1  7.55e-1
270-                7.17e-1  6.57e-1  6.20e-1  5.84e-1  5.39e-1  5.09e-1  4.81e-1
271-                4.52e-1  3.96e-1  3.69e-1  3.28e-1  2.94e-1  2.62e-1  2.28e-1
272-                2.02e-1  1.795e-1
273-       df25 lin 0        2.43e-2  4.36e-2  5.76e-2  6.85e-2  7.66e-2  8.28e-2
274-                8.81e-2  9.29e-2  9.72e-2  1.013e-1 1.052e-1 1.091e-1 1.127e-1
275-                1.165e-1 1.201e-1 1.233e-1 1.201e-1 1.299e-1 1.338e-1 1.371e-1
276-                1.367e-1 1.278e-1 1.339e-1 1.486e-1 1.534e-1 1.557e-1 1.598e-1
277-                1.639e-1 1.647e-1 1.711e-1 1.751e-1 1.786e-1 1.826e-1 1.862e-1
278-                1.900e-1 1.937e-1 1.978e-1 2.02e-1  2.07e-1  2.12e-1  2.18e-1
279-                2.23e-1  2.30e-1  2.38e-1  2.47e-1  2.57e-1  2.69e-1  2.84e-1
280-                3.03e-1  3.26e-1  3.44e-1  3.57e-1  3.71e-1  3.86e-1  4.02e-1
281-                4.20e-1  4.39e-1  4.61e-1  4.84e-1  5.10e-1  5.35e-1  5.63e-1
282-                5.97e-1  6.29e-1  6.65e-1  7.03e-1  7.42e-1  7.82e-1  8.25e-1
283-                8.68e-1  9.12e-1  9.56e-1  9.98e-1  1.040    1.080    1.117
284-                1.150    1.179    1.201    1.198    1.224    1.215    1.161
285-                1.185    1.105    1.111    1.139    1.120    1.095    1.064
286-                1.027    9.81e-1  9.13e-1  8.74e-1  8.05e-1  7.40e-1  6.61e-1
287-                6.05e-1  5.52e-1
288-       df35 lin 0        6.01e-1  1.004    1.244    1.391    1.464    1.491
289-                1.492    1.479    1.452    1.423    1.390    1.355    1.316
290-                1.277    1.237    1.193    1.092    1.109    1.072    1.031
291-                9.65e-1  8.47e-1  8.35e-1  8.69e-1  8.41e-1  8.02e-1  7.72e-1
292-                7.43e-1  7.01e-1  6.82e-1  6.54e-1  6.26e-1  6.00e-1  5.73e-1
293-                5.48e-1  5.25e-1  5.02e-1  4.81e-1  4.61e-1  4.41e-1  4.22e-1
294-                4.02e-1  3.84e-1  3.66e-1  3.48e-1  3.30e-1  3.12e-1  2.94e-1
295-                2.76e-1  2.57e-1  2.44e-1  2.36e-1  2.28e-1  2.20e-1  2.11e-1
296-                2.03e-1  1.947e-1 1.863e-1 1.778e-1 1.694e-1 1.609e-1 1.525e-1
297-                1.443e-1 1.359e-1 1.278e-1 1.198e-1 1.120e-1 1.044e-1 9.71e-2
298-                9.01e-2  8.34e-2  7.69e-2  7.08e-2  6.50e-2  5.95e-2  5.44e-2
299-                4.96e-2  4.51e-2  4.09e-2  3.71e-2  3.35e-2  3.01e-2  2.71e-2
300-                2.43e-2  2.18e-2  1.951e-2 1.732e-2 1.534e-2 1.476e-2 1.340e-2
```

Table A.4 (cont.)

```
301-              1.193e-2 9.83e-3  9.03e-3  7.95e-3  7.12e-3  6.35e-3  5.57e-3
302-              4.98e-3  4.40e-3
303-       df45 lin 0        1.892e-1 3.38e-1  4.45e-1  5.28e-1  5.89e-1  6.36e-1
304-              6.75e-1  7.09e-1  7.39e-1  7.67e-1  7.92e-1  8.17e-1  8.39e-1
305-              8.61e-1  8.81e-1  8.98e-1  8.69e-1  9.31e-1  9.49e-1  9.63e-1
306-              9.51e-1  8.81e-1  9.12e-1  9.99e-1  1.018    1.020    1.034
307-              1.045    1.036    1.060    1.068    1.073    1.079    1.082
308-              1.086    1.089    1.092    1.096    1.102    1.107    1.111
309-              1.115    1.123    1.131    1.140    1.151    1.164    1.180
310-              1.199    1.219    1.233    1.243    1.252    1.260    1.269
311-              1.277    1.285    1.292    1.298    1.304    1.307    1.307
312-              1.311    1.308    1.304    1.299    1.289    1.278    1.264
313-              1.246    1.227    1.203    1.176    1.146    1.114    1.078
314-              1.040    9.99e-1  9.56e-1  9.06e-1  8.65e-1  8.14e-1  7.55e-1
315-              7.17e-1  6.57e-1  6.20e-1  5.84e-1  5.39e-1  5.09e-1  4.81e-1
316-              4.52e-1  3.96e-1  3.69e-1  3.28e-1  2.94e-1  2.62e-1  2.28e-1
317-              2.02e-1  1.795e-1
318-       df55 lin 0        2.43e-2  4.36e-2  5.76e-2  6.85e-2  7.66e-2  8.28e-2
319-              8.81e-2  9.29e-2  9.72e-2  1.013e-1 1.052e-1 1.091e-1 1.127e-1
320-              1.165e-1 1.201e-1 1.233e-1 1.201e-1 1.299e-1 1.338e-1 1.371e-1
321-              1.367e-1 1.278e-1 1.339e-1 1.486e-1 1.534e-1 1.557e-1 1.598e-1
322-              1.639e-1 1.647e-1 1.711e-1 1.751e-1 1.786e-1 1.826e-1 1.862e-1
323-              1.900e-1 1.937e-1 1.978e-1 2.02e-1  2.07e-1  2.12e-1  2.18e-1
324-              2.23e-1  2.30e-1  2.38e-1  2.47e-1  2.57e-1  2.69e-1  2.84e-1
325-              3.03e-1  3.26e-1  3.44e-1  3.57e-1  3.71e-1  3.86e-1  4.02e-1
326-              4.20e-1  4.39e-1  4.61e-1  4.84e-1  5.10e-1  5.35e-1  5.63e-1
327-              5.97e-1  6.29e-1  6.65e-1  7.03e-1  7.42e-1  7.82e-1  8.25e-1
328-              8.68e-1  9.12e-1  9.56e-1  9.98e-1  1.040    1.080    1.117
329-              1.150    1.179    1.201    1.198    1.224    1.215    1.161
330-              1.185    1.105    1.111    1.139    1.120    1.095    1.064
331-              1.027    9.81e-1  9.13e-1  8.74e-1  8.05e-1  7.40e-1  6.61e-1
332-              6.05e-1  5.52e-1
333-       df65 lin 0        6.01e-1  1.004    1.244    1.391    1.464    1.491
334-              1.492    1.479    1.452    1.423    1.390    1.355    1.316
335-              1.277    1.237    1.193    1.092    1.109    1.072    1.031
336-              9.65e-1  8.47e-1  8.35e-1  8.69e-1  8.41e-1  8.02e-1  7.72e-1
337-              7.43e-1  7.01e-1  6.82e-1  6.54e-1  6.26e-1  6.00e-1  5.73e-1
338-              5.48e-1  5.25e-1  5.02e-1  4.81e-1  4.61e-1  4.41e-1  4.22e-1
339-              4.02e-1  3.84e-1  3.66e-1  3.48e-1  3.30e-1  3.12e-1  2.94e-1
340-              2.76e-1  2.57e-1  2.44e-1  2.36e-1  2.28e-1  2.20e-1  2.11e-1
341-              2.03e-1  1.947e-1 1.863e-1 1.778e-1 1.694e-1 1.609e-1 1.525e-1
342-              1.443e-1 1.359e-1 1.278e-1 1.198e-1 1.120e-1 1.044e-1 9.71e-2
343-              9.01e-2  8.34e-2  7.69e-2  7.08e-2  6.50e-2  5.95e-2  5.44e-2
344-              4.96e-2  4.51e-2  4.09e-2  3.71e-2  3.35e-2  3.01e-2  2.71e-2
345-              2.43e-2  2.18e-2  1.951e-2 1.732e-2 1.534e-2 1.476e-2 1.340e-2
346-              1.193e-2 9.83e-3  9.03e-3  7.95e-3  7.12e-3  6.35e-3  5.57e-3
347-              4.98e-3  4.40e-3
348-       df75 lin 0        1.892e-1 3.38e-1  4.45e-1  5.28e-1  5.89e-1  6.36e-1
349-              6.75e-1  7.09e-1  7.39e-1  7.67e-1  7.92e-1  8.17e-1  8.39e-1
350-              8.61e-1  8.81e-1  8.98e-1  8.69e-1  9.31e-1  9.49e-1  9.63e-1
```

Table A.4 (cont.)

```
351-              9.51e-1  8.81e-1  9.12e-1  9.99e-1  1.018    1.020    1.034
352-              1.045    1.036    1.060    1.068    1.073    1.079    1.082
353-              1.086    1.089    1.092    1.096    1.102    1.107    1.111
354-              1.115    1.123    1.131    1.140    1.151    1.164    1.180
355-              1.199    1.219    1.233    1.243    1.252    1.260    1.269
356-              1.277    1.285    1.292    1.298    1.304    1.307    1.307
357-              1.311    1.308    1.304    1.299    1.289    1.278    1.264
358-              1.246    1.227    1.203    1.176    1.146    1.114    1.078
359-              1.040    9.99e-1  9.56e-1  9.06e-1  8.65e-1  8.14e-1  7.55e-1
360-              7.17e-1  6.57e-1  6.20e-1  5.84e-1  5.39e-1  5.09e-1  4.81e-1
361-              4.52e-1  3.96e-1  3.69e-1  3.28e-1  2.94e-1  2.62e-1  2.28e-1
362-              2.02e-1  1.795e-1
363-      df85 lin 0        2.43e-2  4.36e-2  5.76e-2  6.85e-2  7.66e-2  8.28e-2
364-              8.81e-2  9.29e-2  9.72e-2  1.013e-1 1.052e-1 1.091e-1 1.127e-1
365-              1.165e-1 1.201e-1 1.233e-1 1.201e-1 1.299e-1 1.338e-1 1.371e-1
366-              1.367e-1 1.278e-1 1.339e-1 1.486e-1 1.534e-1 1.557e-1 1.598e-1
367-              1.639e-1 1.647e-1 1.711e-1 1.751e-1 1.786e-1 1.826e-1 1.862e-1
368-              1.900e-1 1.937e-1 1.978e-1 2.02e-1  2.07e-1  2.12e-1  2.18e-1
369-              2.23e-1  2.30e-1  2.38e-1  2.47e-1  2.57e-1  2.69e-1  2.84e-1
370-              3.03e-1  3.26e-1  3.44e-1  3.57e-1  3.71e-1  3.86e-1  4.02e-1
371-              4.20e-1  4.39e-1  4.61e-1  4.84e-1  5.10e-1  5.35e-1  5.63e-1
372-              5.97e-1  6.29e-1  6.65e-1  7.03e-1  7.42e-1  7.82e-1  8.25e-1
373-              8.68e-1  9.12e-1  9.56e-1  9.98e-1  1.040    1.080    1.117
374-              1.150    1.179    1.201    1.198    1.224    1.215    1.161
375-              1.185    1.105    1.111    1.139    1.120    1.095    1.064
376-              1.027    9.81e-1  9.13e-1  8.74e-1  8.05e-1  7.40e-1  6.61e-1
377-              6.05e-1  5.52e-1
378-      prdmp 2j 1
379-          m1    6000.60c  9.815e-4
380-                25055.60c  5.150e-4
381-                26054.60c  4.939e-3
382-                26056.60c  7.679e-2
383-                26057.60c  1.758e-3
384-                26058.60c  2.344e-4
385-          m2    7014.60c  3.640e-5
386-                8016.60c  9.740e-6
387-          m3    1001.60c  .667
388-                8016.60c  .333
389-          m4    1001.60c  5.926e-2
390-                6000.60c  3.338e-2
391-                8016.60c  1.125e-2
392-                3006.60c  5.565e-4
393-                3007.60c  6.944e-3
394-      print
395-      wwg 65 24 0 -463.59 207.01 0
396-      cut:n j 3.839e-7 -1.e-6 -1.e-7
397-      mt3 lwtr.01t
398-      mt4 poly.01t
399-      nps 500000
```

Los Alamos
NATIONAL LABORATORY
Los Alamos, New Mexico 87545